THE OCCURRENCE OF DRY PERIODS AND WET PERIODS IN THE NORTHEASTERN UNITED STATES

A Thesis

Presented to the Faculty of the Graduate School

of Cornell University

in Partial Fulfillment of the Requirements for the Degree of

Master of Science

by

Marcus Dean Walter

May 2013

ABSTRACT

This goal of this research was to understand the occurrence of dry periods and wet periods in the northeastern United States over a 48 year period, from 1961 to 2008. An index that took into account daily precipitation and evaporation was developed and extreme value theory, a branch of statistics used to study extreme events, was used. Results from this work suggest that there has been a slight wetting trend across the Northeast over the period of study. Results also show that the extreme value theory's statistical distributions fit well to the maxima of the data but not the minima (max duration, max value in wet periods, etc.). Further work in this area would involve better analyzing the minima of the index data, as well as fitting the maxima data to more complicated trend lines and anomalies like the El Nino Southern Oscillation and North Atlantic Oscillation Indices.

BIOGRAPHICAL SKETCH

Marcus D. Walter graduated with honors from the Pennsylvania State University, earning a bachelors degree in meteorology focused in weather forecasting and communications in the spring of 2008. During his undergraduate and graduate career, he participated in the Significant Opportunities in Atmospheric Research and Science (SOARS) program at the National Center for Atmospheric Research (NCAR) in Boulder, Colorado, and the Summer Research Opportunities Program (SROP) at Penn State. He has had an interest in weather ever since age 12.

ACKNOWLEDGEMENTS

This thesis is dedicated first to my family and friends for their help and support with completing my master's degree. Its also dedicated to my amazing advisors and mentors from all parts of Cornell, Penn State, SOARS, NCAR and other organizations who have helped in this process. I send a special thank you to the Cornell University Department of Earth and Atmospheric Science and my advisors Art DeGaetano, Todd Walter. I also send a special thank you to the atmospheric science department administrator Pam Vitale and atmospheric science doctoral student Michael Kelleher for all their help and support. I would not have been able to successfully navigate this journey without any of them. Thank you.

TABLE OF CONTENTS

LIST OF TABLES

LIST OF FIGURES

CHAPTER 1

INTRODUCTION

Dry periods and wet periods, analogous to droughts and flooding, can have devastating impacts on society. Droughts, in particular, are among the world's costliest events and affect large numbers of people each year (Wilhite, 2000). Drought impacts can be felt across a wide spectrum of societal activities including agriculture, water supply and hydropower generation, to name a few (Woodhouse and Overpeck, 1998). In 1995, the U.S. Federal Emergency Management Agency (FEMA) estimated that the annual cost of U.S. drought was in the range of $6 to $8 billion (Richards et al. 1995). According to the National Climatic Data Center (NCDC) the United States drought of 1988 cost nearly $62 billion (Andreadis et al. 2005).

Flooding or wet periods can be just as devastating. These phenomena can be thought of as exact opposites of drought and dry periods. Wet periods can interrupt planting and harvest practices. Prolonged periods of above average wetness can ruin harvests, cause fields to over saturate and even lead to river flooding, all of which can have devastating impacts on society. Flooding damages rank among the top weather-caused losses in the United States, with annual losses ranging from $1 billion per year in the 1940s to $6 billion per year during the 1980s and 1990s (Andreadis et al. 2005), (Easterling et al. 2000).

Because wet periods and dry periods have such a wide range of impacts, there is no unique way these events have been defined or measured. The most well known index used to define and measure wet and dry periods is the Palmer Drought Severity Index (PDSI). This index was the first comprehensive drought index developed in the United States and is still used today by many U.S. gov-

ernment agencies to assess dry periods and wet periods. Other indices used to assess dry and wet periods include the Standardized Precipitation Index (SPI), the Crop Moisture Index (CMI), the Surface Water Supply Index (SWSI), and Reclamation Drought Index, to name a few (Heim, 2002).

For the northeastern United States, increases in wet and dry periods could negatively impact the more than 54 million people living in the region. There is concern for how wet periods and dry periods will be impacted by climate change and inter-annual variations in the precipitation patterns (Groisman et al. 2005), (Sun and Groisman, 2004) in this region. Some studies have pointed to increased frequency of both extreme wet and dry events.

Groisman and Knight (2008) investigated whether prolonged dry periods in the United States have already started to increase over the past 40 years (1967 - 2006), due to changes in the intensity of precipitation but not total precipitation. They analyzed dry periods during the warm season (warm season defined as air temperature consistently above 5 degrees C), defining a dry day as a day with less than 1 mm of precipitation, and a dry period as a sequence of these days. Their results showed that over the past 4 decades the mean duration of dry periods in the U.S. have increased significantly. According to Groisman and Knight (2008) a return period for a 1-month dry period has decreased from 15 years to approximately 6-7 years in the eastern United States. More pronounced changes in dry periods were observed in the west and southwest U.S.

The results obtained from Groisman and Knight (2008) only took into account temperature and precipitation, and in essence observed dry periods from a narrow meteorological view. Their results were also too conservative. For instance, a mid summer period in which 1 mm of precipitation fell per day would

not be considered dry, when in fact, such an instance would be considered among the worst droughts in many locations. One way to improve upon the work of Groisman and Knight (2008) could be to perform analysis of dry conditions using the Palmer Drought Severity Index (PSDI). Studies using PDSI have been useful in assessing dry conditions on weekly and monthly scales (Dai et al. 2004). However, often a finer temporal resolution is needed to assess changes in dry periods that are associated with changes in precipitation frequency. PDSI would not be useful in this type of assessment.

Groisman and Knight (2008) neglected several factors during their analysis, including evapotranspiration and soil water content. These two factors are key to defining dry and wet periods beyond a meteorological sense and hence assessing the climate change impacts associated with an altered hydrologic cycle. In this work we define dry and wet periods accounting for evaporation and soil water content, beyond a meteorological sense, to better characterize these events and their impacts.

CHAPTER 2

METHODS

The goal of this research was to assess the occurrence and characteristics of dry and wet periods in the northeastern United States and improve upon the work of Groisman and Knight (2008). Interest lies in gaining a better understanding of the climatology for these events in this region and to learn if this region has become drier over the past forty to fifty years. These events, dry periods and wet periods, depending on how they are defined, can be classified as extreme events. Extreme events are events that are rare in nature, but can carry with them severe impacts to regions and locations where they occur. For the northeastern United States, the occurrence of dry periods or wet periods can significantly impact the water resources of the region and the region's agricultural practices, as examples.

In this study, a water bucket model utilized daily precipitation, evaporation estimates, and available water content (AWC, is a measure of how much water is available within the soil) to analyze wet periods and dry periods. With this model, the bucket was analogous to the soil, with the top of the bucket set even with the surface of the soil and the depth of the bucket set equal to the AWC value for the location of interest. For example, if the AWC for a location were 10 cm, the bucket depth would be 10 cm. There was an initial assumption that the bucket was filled to capacity for the start of each year for which data was analyzed.

The model was used to keep track of the water level anomalies, also referred to as the soil water anomalies (SWA), in the bucket through accounting for the daily cumulative sum of precipitation and evaporation. Each day the evapora-

tion would be subtracted from the precipitation and this sum would be added to the bucket. If there was no precipitation or evaporation on a particular day, either because the data was missing , only the value present was incorporated with the water level anomaly for that day. If both precipitation and evaporation were missing, meaning the data were unavailable or that there was no evaporation or precipitation on a day, then the water level would not change for that day.

If the bucket was full, any positive sum of precipitation and evaporation would be recorded for that day and considered to be run-off because the bucket would not be able to hold more than its filled capacity. An empty bucket would correspond to a water level anomaly of the negative of the AWC value for the location of interest (i.e. -10 cm from the example mentioned above). Daily water level anomalies were not allowed to go below the negative of the AWC value for the locations of interest. If the bucket was empty and there was only evaporation for that day, the evaporation was ignored and the water level anomaly for that day was set to the negative of the AWC value.

Once the SWA were obtained for the period and station of interest, the first and third quartiles of the SWA were used to define wet periods and dry periods explicitly. If the SWA exceeded the third quartile for at least one day, a wet period began. It would end once the SWA fell below the third quartile threshold. If the SWA fell below the first quartile, a dry period would begin. It would end once the values rose above the first quartile threshold. Wet periods and dry periods were not allowed to cross years. With these rules, wet periods and dry periods could be obtained and their characteristics analyzed.

Daily precipitation and evaporation estimates from an 8-month period

(March 1 to October 31) from years 1961 to 2008, and available water content values were obtained from various sources for 30 International Civil Aviation Organization (ICAO)/National Weather Service Cooperative Observer Program (NWS COOP) weather stations from across the region. These stations were located at airports or within close proximity to an airport (see Figure 2.1) and had precipitation records starting in or before 1961.

Daily precipitation data were obtained from the NWS Cooperative network. Of the 30 stations selected, precipitation data from the period of interest for the Syracuse Hancock International Airport (KSYR), Willow Grove Naval Air Station (KNXX), Newark International Airport (NEWR), and the Baltimore-Washington International Airport (KBWI) were not available at the time this study was undertaken. These stations data were replaced with precipitation data from Brewerton Locks 23, NY; Neshammy, PA; Canoe Brook, NJ; and Laurel, MD, respectively, which are in close proximity to the original stations.

Daily evapotranspiration (evaporation) estimates were obtained for the period of interest for each station from an evapotranspiration model developed by the Northeast Regional Climate Center (NRCC) at Cornell University in Ithaca, NY. This model is based on the Penman-Montieth equation, is an extension of the British Meteorological Office Rainfall and Evaporation Calculation System (MORECS), and was validated for use in the Northeast United States by the NRCC (DeGaetano et al. 1994). According to the NRCC, it is very difficult to obtain daily evaporation measurements because they are not measured routinely in the region.

AWC values were obtained from the work of Miller and White (1998). According to Miller and White (1998), in part because of soil information being

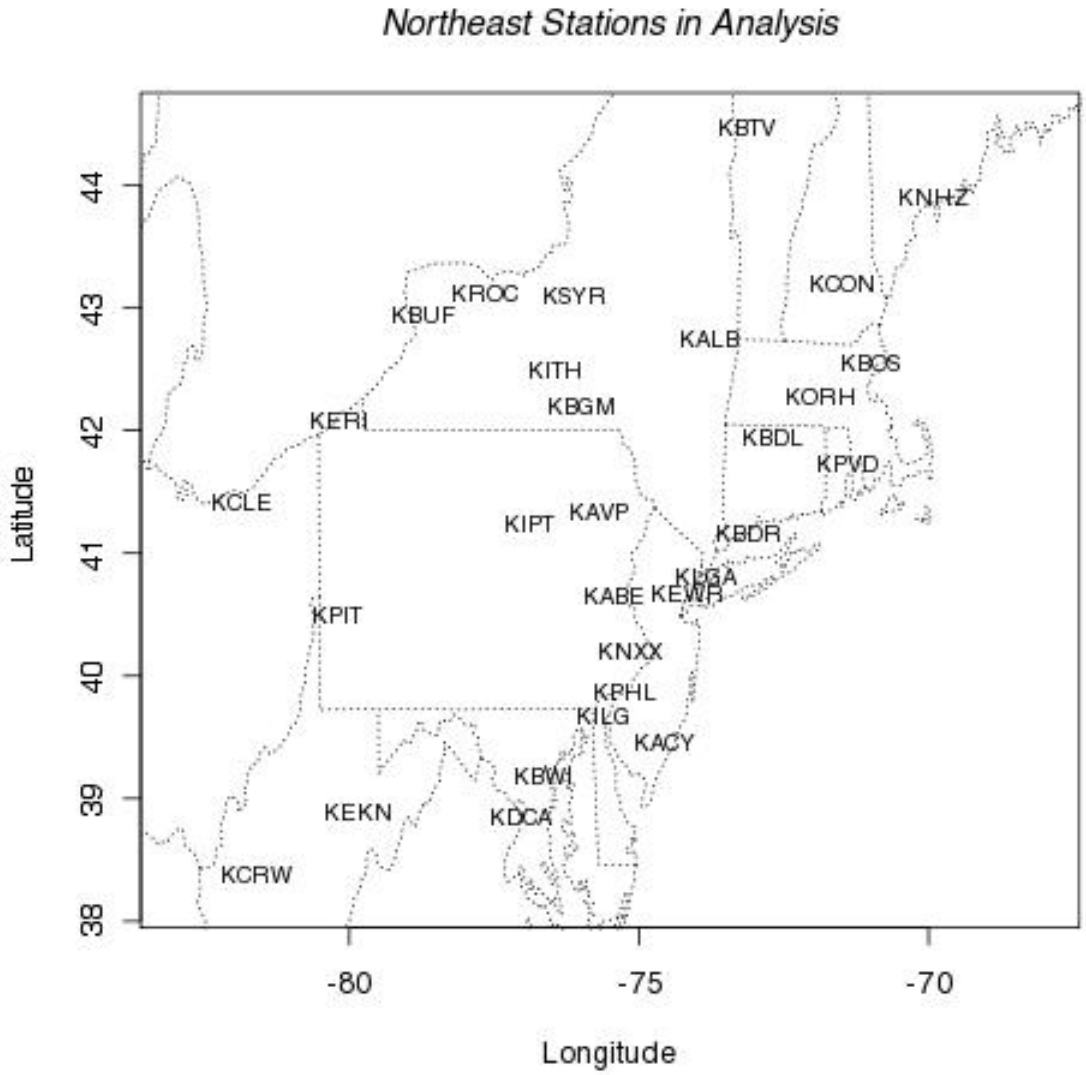

Figure 2.1: A plot of the 30 ICAO/NWS COOP weather stations selected for the study. Precipitation, evaporation estimates, and available water content values were obtained for each station and were used to analyze the occurrence of dry and wet periods in this region.

widely required for climate and hydrological modeling, they developed a multilayer soil characteristics data set for the continental United States that specifically addressed the need for soil physical and hydraulic property information over large areas. From this dataset, three types of AWC were available and were dependent on the profile depth observed, with profile depth being defined as the distance between the surface and some point below the surface. For this study, AWC values were obtained for a profile depth of 100 cm. This profile depth was selected because this was depth to which water would be most likely available to the surface. The available water content values at this profile depth across the Northeast are shown in Figure 2.2.

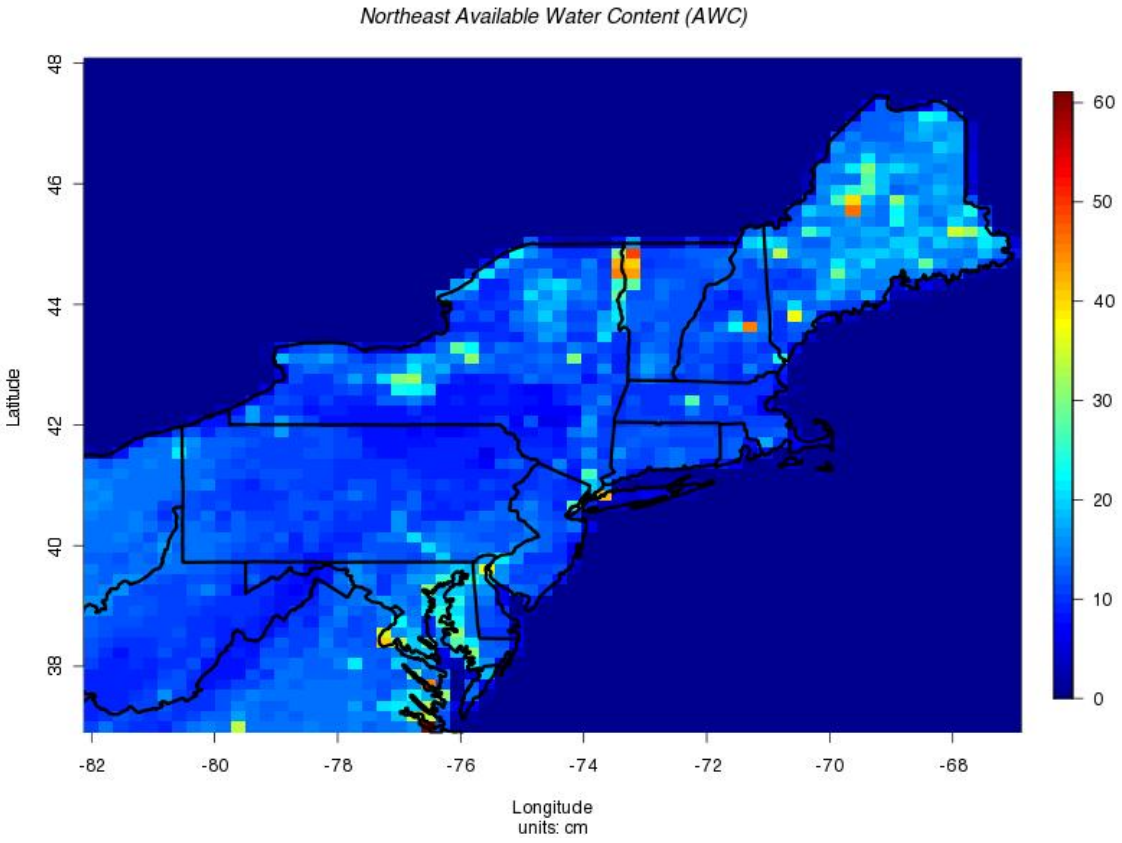

Figure 2.2: A spatial plot of the available water content (AWC) values within the first 100 cm of the surface for the Northeastern United States. The AWC values have been measured in units of centimeters.

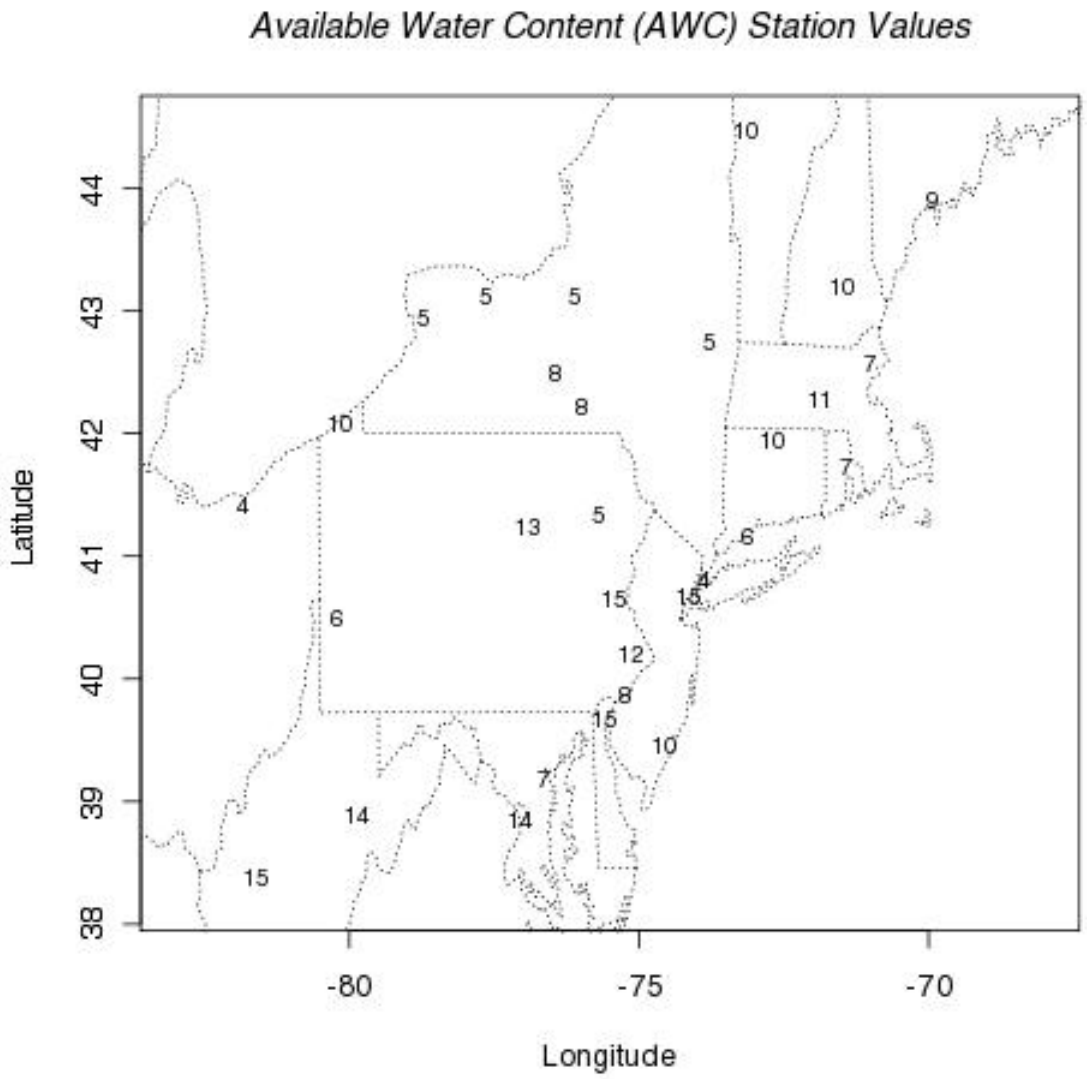

Figure 2.3: A spatial plot of the available water content (AWC) values for the stations used in the analysis. Newark's AWC value was adjusted from 23 cm to 15 cm due to concern the original value may have been unreasonably high.

Most of this the region had an available water content value of 10 cm within the first 100 meters of the surface. Locations along the coast and closest to lakes and other water bodies tended to have higher available water content values, in particular across the Finger Lakes region of Central New York, the Northern border between New York and Vermont, and the Delaware Maryland Virginia area, even around the New York City area. Actual water bodies were excluded from this data. Figure 2.3 shows the AWC value used for each station in this analysis spatially. The value as Newark was originally 23 cm, but due concern with this value being unreasonably high, possibly due to its proximity to the coast, we set this value equal to 15 cm, the highest value among the stations in the analysis.

CHAPTER 3

EXTREME VALUE THEORY

In this study, extreme value theory (EVT) was used to quantify the frequency and intensity of wet periods and dry periods that have occurred in the north-eastern United States over the past 48 years. Two approaches derived from EVT were used and are described below and in Coles (2001).

3.1 Block Maxima Approach

The first approach used was the Block Maxima approach. Theory behind this approach states that the maximum of a sequence of observations, under very general conditions, is approximately distributed as the generalized extreme value (GEV) distribution. The GEV distribution has three parameters, location (μ), scale (σ), and shape (ξ), and its distribution function (G(z)) is shown below:

$$G(z) = exp[-[1 + \xi(\frac{z-\mu}{\sigma})]^{-1/\xi}] \tag{3.1}$$

For this function, z represents the maximum of a sequence of observations that satisfy the following conditions: $1 + [\xi]((z - \mu)/\sigma) > 0$, $-\infty < \mu < \infty$, $\sigma > 0$, and $-\infty < \xi < \infty$.

For this approach, a series of observations – usually values of a process measured on a regular time-scale, such as hourly or daily [2] – are blocked into same-length sequences. Once blocked, the maximum value from each block is used to generate another series, a block maxima series. A stationary generalized extreme value (GEV) distribution is then fit to the block maxima series, as-

suming the statistical characteristic of the maxima don't change systematically through time. This approach can also be used for block minima series, with a GEV distribution being fit to the negative of the block minima. By the changing the sign of the minima, the values that were once the smallest become the largest and can be treated as block maxima (Coles, 2001).

Often the blocks are chosen to correspond to a time period of length one year (Coles, 2001), but can be any length of time. Still, the choice of block size can be critical. Blocks that are too small can lead to bias in the GEV parameter estimates (μ, σ, ξ). Bias, in this case, caused by too much sample data being used to obtain parameter estimates, possibly pulling the parameter estimates away from the true parameter values. Blocks that are too large generate too few block maxima, while could lead to too small of sample data analyzed. This would lead to large estimation variance (Coles, 2001).

The figures below show an example of the Block Maxima approach being used for the Pittsburgh International Airport (KPIT) soil water anomalies (SWA). The SWA were calculated in centimeters (cm) for an 8-month period (245 days) starting March 1 (Day 1) and ending October 31 (Day 245), 1961; these values are shown in Figure 3.1. The circled point in the figure marks the maxima during the period. This value and maxima from the KPIT SWA spanning the same 8-month period, from years 1962 to 2008, are shown in Figure 3.2. A GEV distribution was then fit to these maxima, shown in Figure 3.3.

For this study, the Block Maxima approach was used to analyze the SWA, over the March 1 to October 31 period, from 1961 to 2008, for each station. The SWA block maxima for each station were obtained and stationary GEV distributions were fit to each stations data. The values for parameters μ, σ, and ξ for

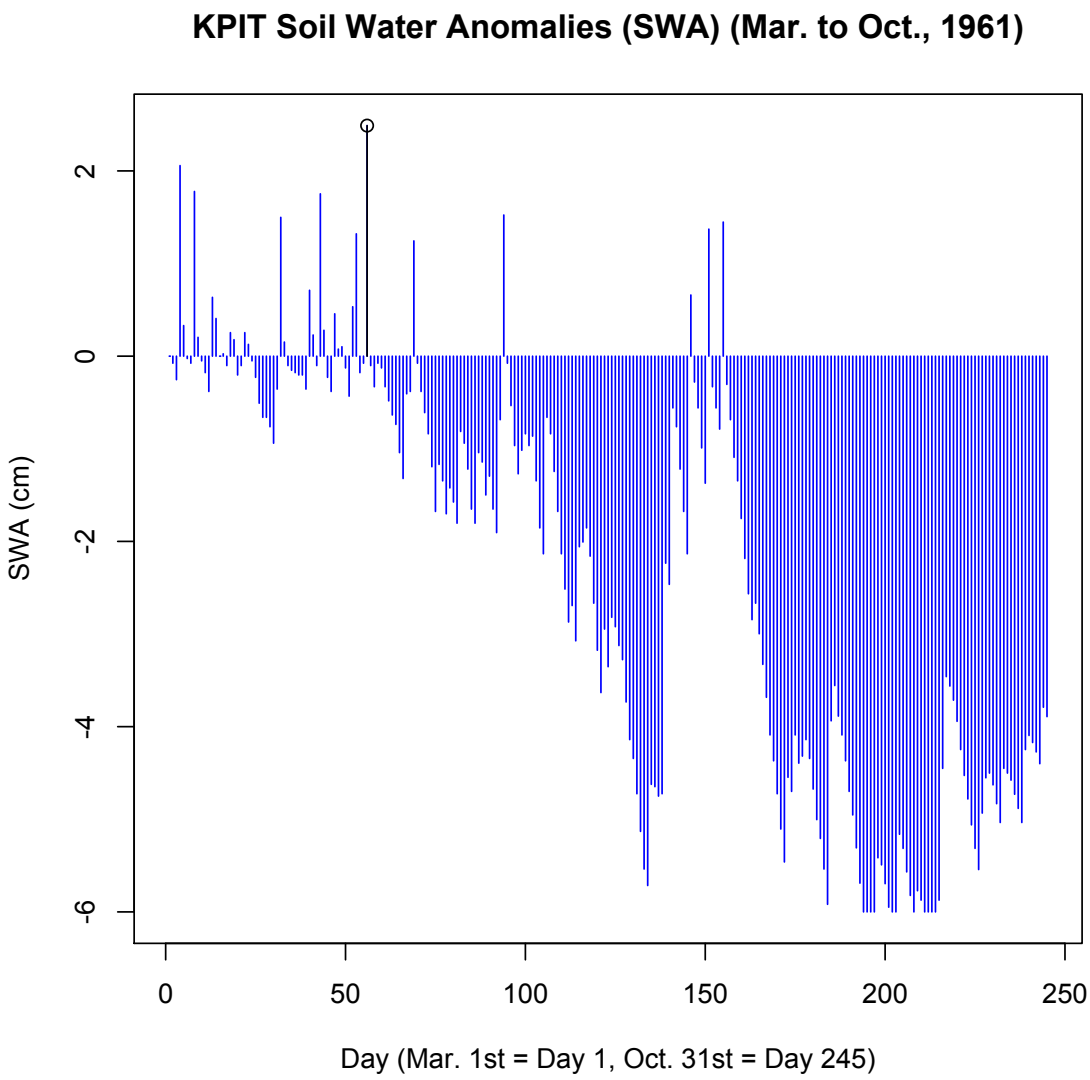

Figure 3.1: Block Maxima example for soil water anomalies (SWA) calculated from March 1 to October 31, 1961 at the Pittsburgh International Airport (KPIT). The maximum of the SWA for this period was 2.49 cm, marked by the circled point.

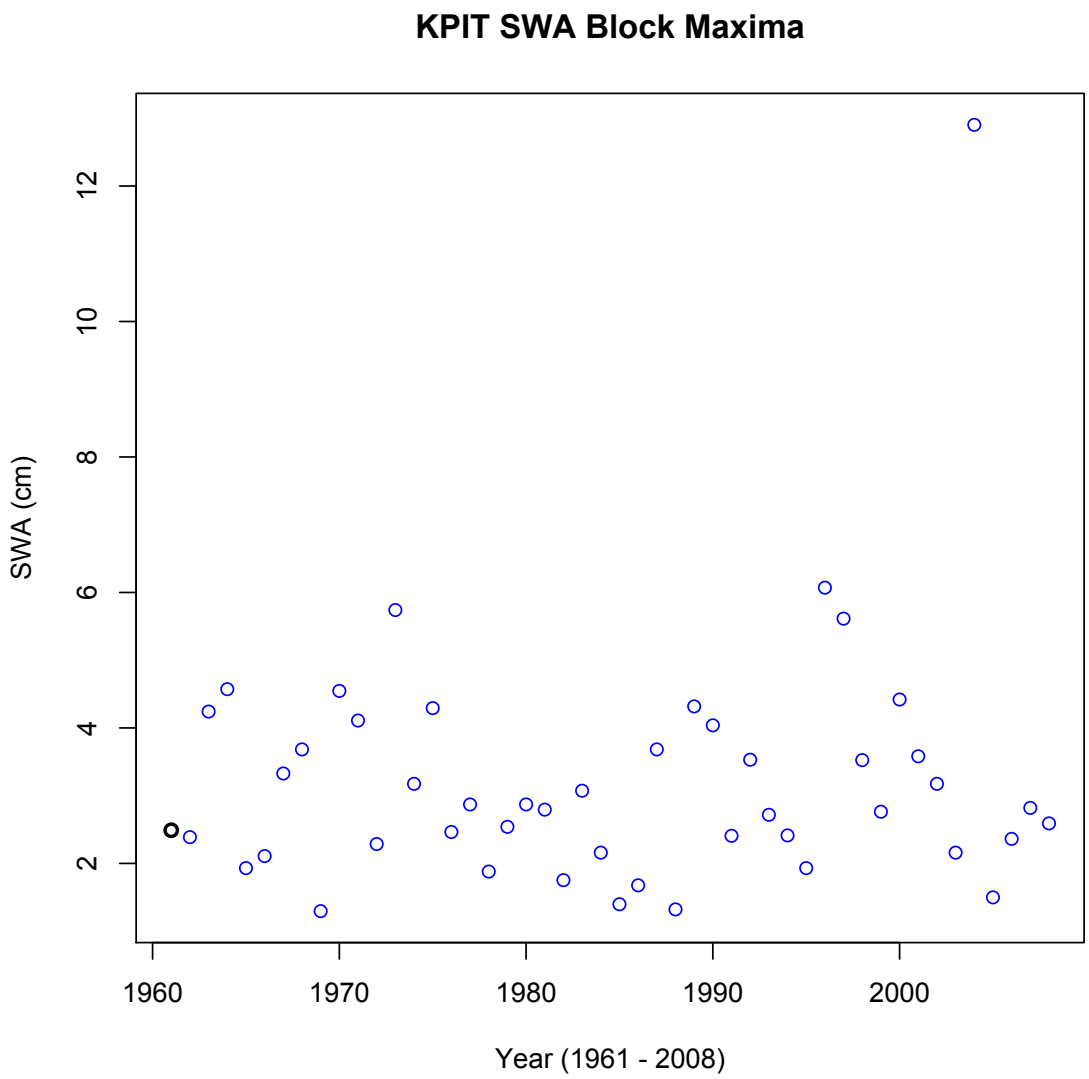

Figure 3.2: A plot of SWA block maxima from 1961 to 2008 at the Pittsburgh International Airport. The first point in this figure corresponds to the maximum of the Pittsburgh SWA in 1961, which was 2.49 cm.

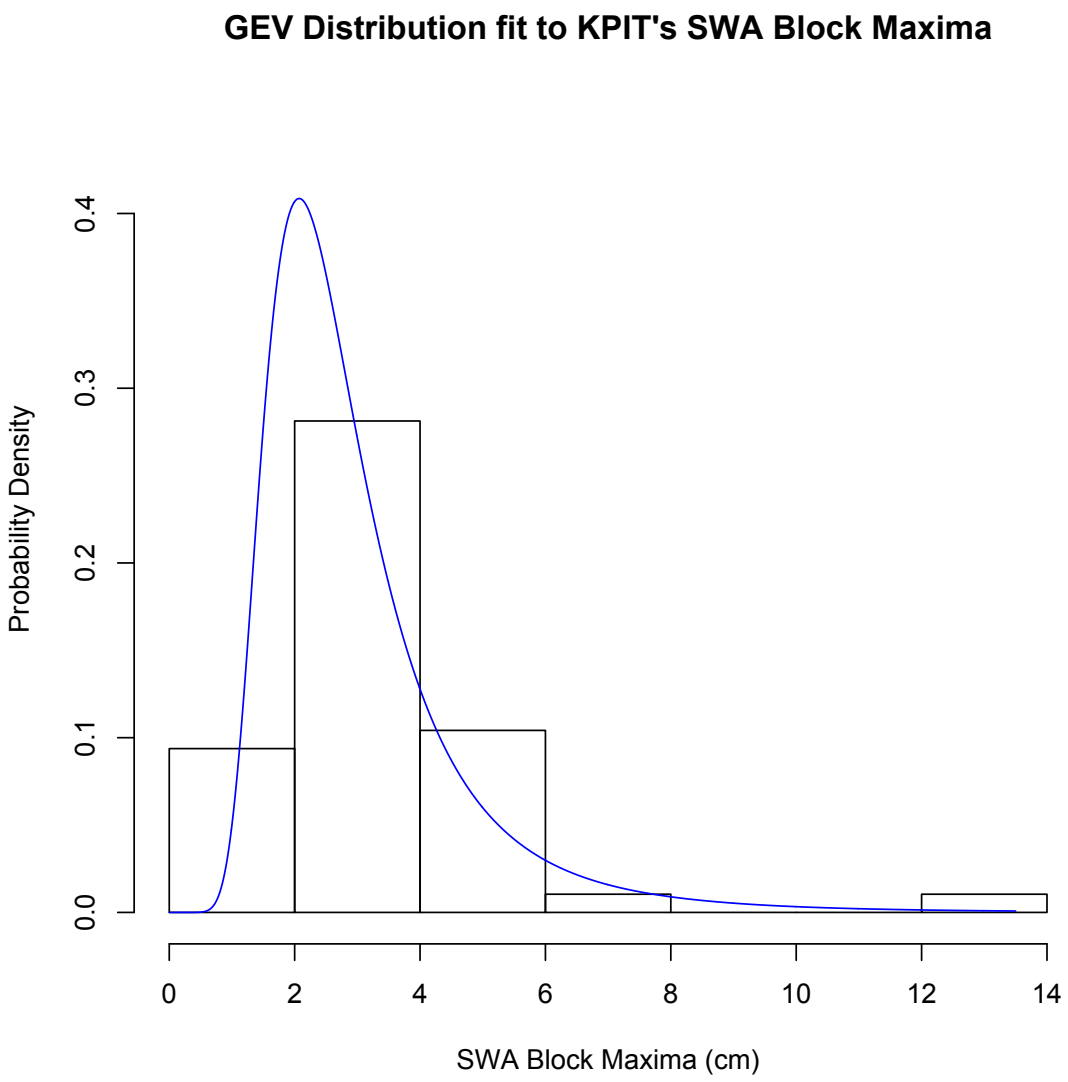

Figure 3.3: A density estimate plot of Pittsburgh's SWA block maxima histogram and fitted GEV distribution.

each stations GEV distribution fit were obtained by maximum likelihood estimation (MLE) through the R programming environment and extRemes Toolkit (See Maximum Likelihood Estimation, Chapter 9). MLE, in general, is used to adopt the model, or in this case, the parameters, for a given distribution family that assign the highest likelihood (probability) to the observed data. In other words, MLE is used to find the parameters for a particular distribution that give the best distribution fit to the observed data.

Diagnostic plots were used to observe how well the GEV distributions fit to the block maxima for each station. Figure 3.4 shows the diagnostics plots from a GEV distribution fit to Pittsburgh's block maxima. The diagnostic plots consist of a probability plot, a quantile plot, a return-level plot, and a density estimate plot.

The quantile plot compares the model (i.e. the fitted GEV distribution) quantiles against the data (empirical) quantiles. The probability plot compares the model probabilities against the data (empirical) probabilities. For a perfect fit, the data would line up on the diagonal of the probability and quantile plots. Significant departures from linearity, or a quantile or probability plot that deviates greatly from a straight line, suggest that the model assumptions may be invalid for the data plotted (i.e. the GEV distribution may not be a good fit to the data). Figure 3.4 shows that the GEV distribution is a reasonable fit for Pittsburgh's block maxima.

The return level plot shows the model estimated return periods against the (empirical) return levels, with an estimated 95 percent confidence interval. The return period is the expected time interval between exceedences of a particular return level. The return level is the level (water level in the case of Figure 3.4)

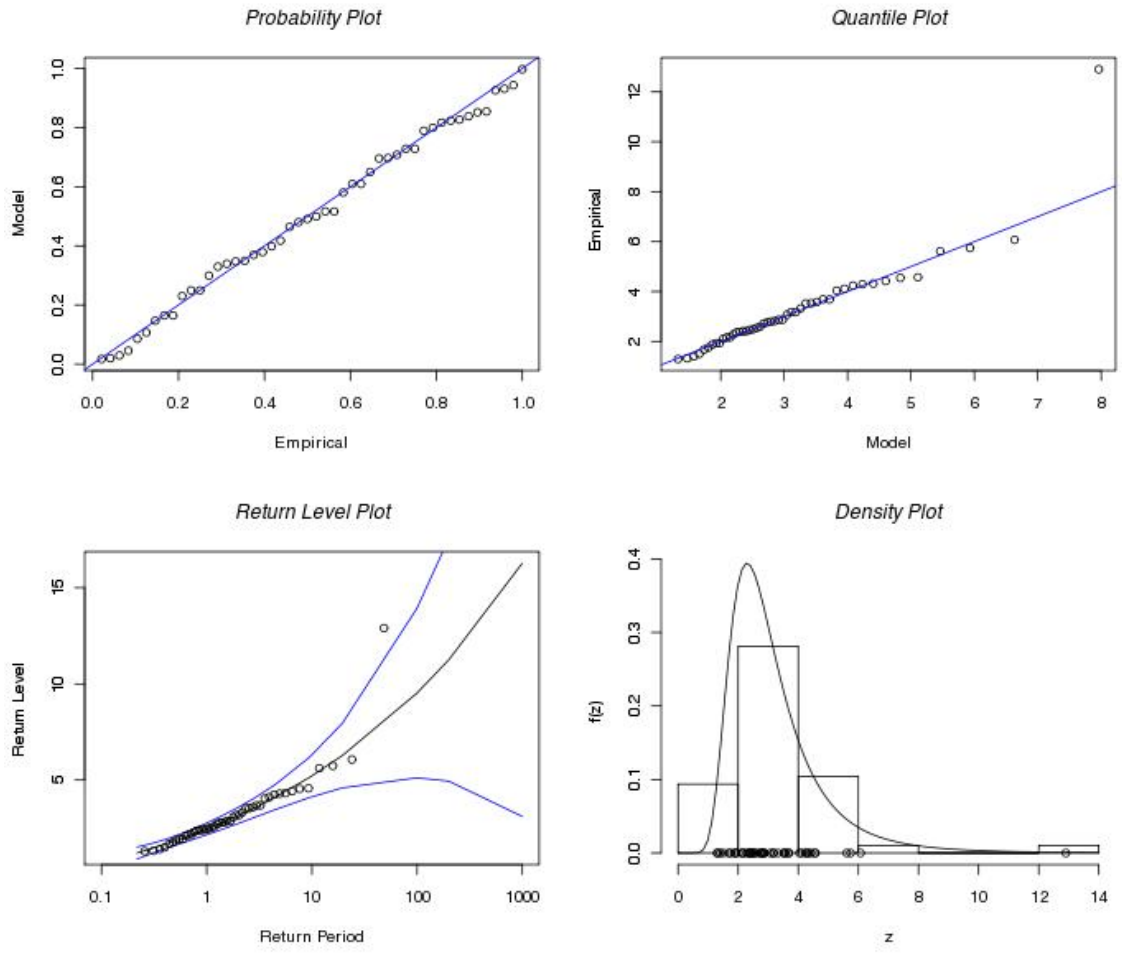

Figure 3.4: A diagnostic plot of a GEV distribution fit to Pittsburgh's block maxima produced by the R programming environment and extRemes Toolkit.

that is expected to be exceeded, on average, once every equal number of time points (years in the case of Figure 3.4). Lastly, the density estimate plot shows a histogram of the data, the observed data plotted along the bottom of the histogram, and the estimated distribution for the data. In the case of Figure 3.4, it is a histogram of Pittsburgh's block maxima and the estimated GEV distribution for the data. For each stations block maxima, if the GEV distributions fit well to the data, these distributions can be used to describe the station's data

statistically.

3.2 Block Maxima Approach and Non-Stationarity

The Block Maxima approach can also be extended to analyze non-stationarity or trending in block maxima. Non-stationary processes have characteristics that change systematically through time, possibly due to climate change, or a number of other factors (Coles, 2001). Observing non-stationarity in the data may help to infer what is happening with the climate of the maxima, and subsequently, dry periods and wet periods in the northeastern United States.

To investigate non-stationarity in the block maxima, a GEV distribution must be fit to the data with a parameter that is, or parameters that are, modeled to change as a function of time (days, months, years, etc.). This is represented in equation 3.2, where parameters μ, σ, and ξ where replaced with parameters μ(t), σ(t), ξ(t) in the GEV distribution function:

$$G(z) = exp[-[1 + \xi(t)(\frac{z_t - \mu(t)}{\sigma(t)})]^{-1/\xi(t)}] \tag{3.2}$$

z_t represents the maximum of a sequence observation at a certain time point such that:

$1 + \xi$(t)[(z - μ(t))/σ(t)] > 0, $-\infty < \mu(t) < \infty$, σ(t) > 0, and $-\infty < \xi(t) < \infty$. The diagnostic plot of a non-stationary GEV distribution fit to Pittsburgh's block maxima is shown in Figure 3.5.

The residual probability and quantile plots in Figure 3.5 were used to diag-

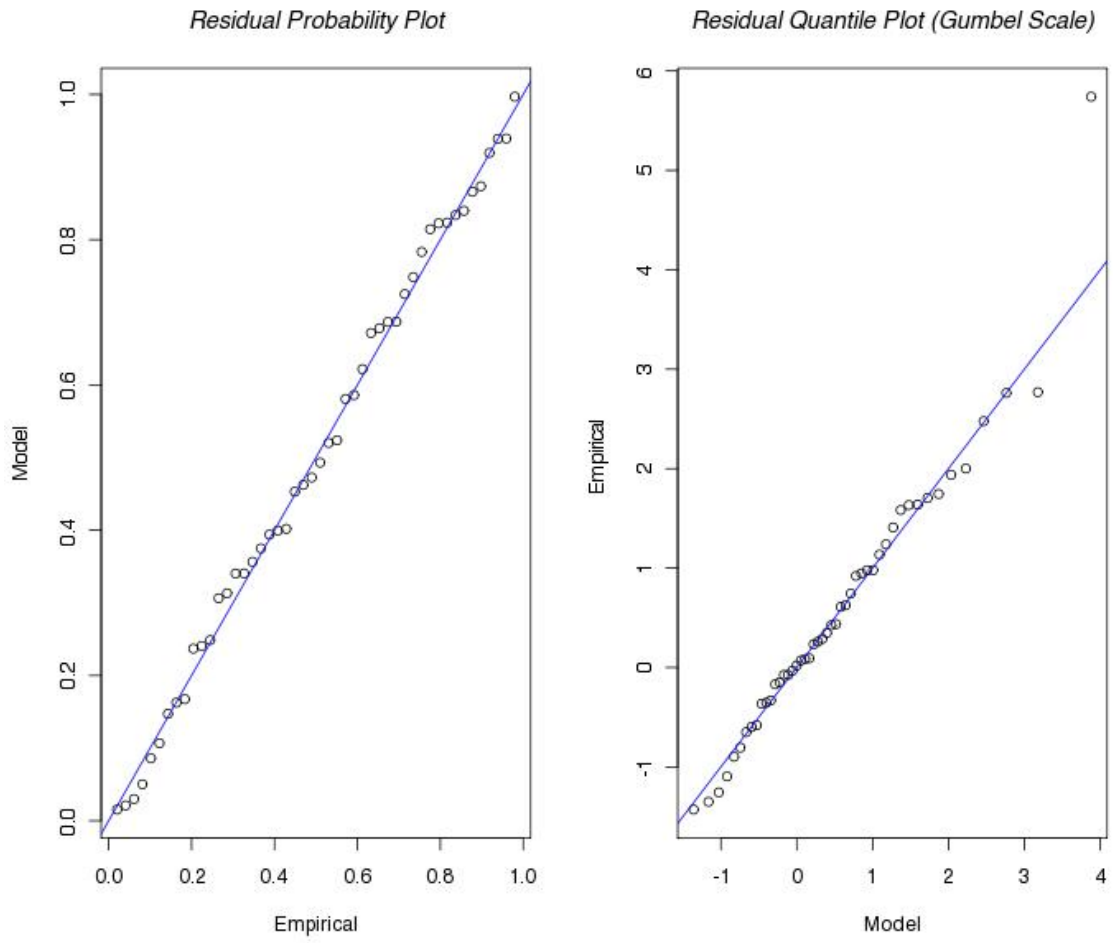

Figure 3.5: A diagnostic plot for a non-stationary GEV distribution fit to Pittsburgh's block maxima data produced by the R programming environment and extRemes Toolkit.

nose how well the non-stationary GEV distribution fit to the block maxima. The closer the points on both plots are to linearity, the better the distribution fit is for the data. From this diagnostic plot, in particularly from the probability and quantile plots, the non-stationary GEV distribution fit well to Pittsburgh's block maxima.

The first step to fitting a non-stationary GEV distribution to the Pittsburgh

block maxima was to develop a time series to which the GEV parameters could be modeled. Since the data spans a 48-year period from 1961 to 2008, a year list from 1 to 48 was developed, where 1 corresponded to 1961 and 48 corresponded to 2008. This was done so that the parameters could be modeled as a function of time and as a function of the corresponding years for the data. For this non-stationary GEV distribution fit, the shape parameter was assumed to be constant, and only the location and scale changed linearly and log-normally, respectively, as a function of time (i.e. μ(t), ln(σ(t)), ξ). Then, as in the case of the stationary GEV distribution fit, MLE was used to estimate the constant shape parameter and two additional terms (b_0, b_1) for the location and two terms (c_0, c_1) for the scale parameters. The two additional time-dependence terms for both parameters account for these parameters changing as a function of time, i.e. μ(t) = $b_0 + b_1$(t) and ln(σ(t)) = $c_0 + c_1$(t) . The terms b_1 and c_1 represented the yearly rate of change in the location and scale parameter values.

There are not set rules to deciding which parameter or parameters to choose to model with time or how they should vary with time (linearly, log-normally, etc.). This depends on prior hypotheses about the statistical characteristics of the data. It also depends on how well the estimated distribution fits to the data from an initial guess. Because of the many choices in which the parameters can be modeled, selecting the appropriate parameters to model and how to model them becomes an important issue. The goal is to model the parameters in the simplest way as possible to produce a distribution fit that explains as much of the variation in the data as possible. In general, it is more difficult to estimate the shape parameter for the GEV distribution, and because of this, it is normally assumed to be stationary with time (Coles, 2001). With the other parameters and how they are modeled with time, each would have to be tested for the best

results.

The same methods for fitting a non-stationary GEV distribution to Pittsburgh's block maxima were used to fit a non-stationary GEV distribution to the block maxima for every station. Depending on how well the non-stationary GEV distributions fit to the data, judging from diagnostic plots similar to Figure 3.5, this information was used to estimate how the GEV distributions and the connecting return levels and return periods to these distributions changed overtime for each station.

Once a stationary and non-stationary GEV distribution were fit to the maxima for each station, a likelihood ratio test (LRT) was performed to test the statistical significance of the non-stationary GEV distribution fit over the stationary one. A LRT consists of comparing a sub-model (stationary GEV distribution, m_0) to a higher ordered model (non-stationary GEV distribution, m_1) of the same distribution. A test of the validity of the sub-model to the higher ordered model at some level of significance α is to reject the sub-model in favor of the higher ordered model if the deviance statistic D is greater than c_α, where c_α is the (1 - α) quantile of the Chi-Squared (χ^2_d) distribution. The subscript d is degrees of freedom and α is some predetermined significance level. Because there were a total of 3 parameters for the stationary GEV distribution and 5 parameters for the non-stationary GEV distribution for each station, the degrees of freedom were calculated to be 2 ($5 - 3 = 2$). For this study, α was selected to be 0.05. The deviance statistic is the following:

$$D = 2[l_1(m_1) - l_0(m_0)] \tag{3.3}$$

where $l_1(m_1)$ represents the maximized log-likelihood of the higher ordered model and $l_0(m_0)$ represents the maximized log-likelihood for the sub-model. Based on the results of the LRT, it will be known whether the non-stationary GEV distributions are a statistical improvement and if they should be selected over the stationary ones for the purpose of statistically describing each stations data.

3.3 Peaks-Over-Threshold Approach

The second method used in this research was the Peaks-Over-Threshold (POT) approach. The theory behind this approach states that individual excesses (peaks) over a high threshold are approximately distributed as a generalized Pareto (GP) distribution. The GP distribution has two parameters: a scale parameter (σ*) and a shape parameter (ξ). The GP distribution function is as follows:

$$H(y) = 1 - (1 + \frac{\xi y}{\sigma *})^{-1/\xi} \tag{3.4}$$

y represents a threshold excess defined on y: y > 0 and $(1 + \xi y/\sigma^*) > 0$, $\sigma^* = \sigma + \xi(u - \mu)$, with u being the high threshold and μ being the mean. σ in the above equation represents that scale value calculated from the GEV distribution fit.

Generally, threshold exceedences occur in clusters (i.e. groups), not individually. With the POT approach, the maximum from each cluster is identified. These data, called cluster maxima, are assumed to be independent and a GP

distribution is fit to them.

An empirical rule is used to define clusters for this approach. This empirical rule, for example, could be a simple temperature or water gauge threshold u. Once the temperature or water flow exceeds the threshold, a cluster begins. The cluster ends once the temperature or water level falls back below the threshold.

This approach improves upon the Block Maxima approach because it allows for the use of more data in the analysis, helping to give more statistical information about the data being analyzed. Still, this approach is sensitive to the empirical rule used. If the empirical rule for cluster determination is too restrictive or too loose, this will directly impact how many clusters are observed and how much of the available data is utilized. This will in turn impact how well the GP distribution fits to the data being analyzed. An example of the POT approach being applied to Pittsburghs daily SWA is shown below in Figure 3.6 and Figure 3.7.

For the Pittsburgh SWA from March 1 to October 31, 1961, a threshold of -0.53 cm, the third quartile for the entire Pittsburgh SWA dataset, was used to define clusters. Based on this threshold, there were seven clusters during the 1961 period, marked by the groupings of circled points in Figure 3.6. The maxima for each cluster, including the single day clusters, for the same period, from years 1961 to 2008, for the Pittsburgh data were identified and a GP distribution were fit to them.

Figure 3.7, as with Figure 3.4, is a diagnostic plot but for a GP distribution fit to Pittsburgh's cluster maxima. From this figure, in particular from the probability plot, the GP distribution may not fit well to the cluster maxima because

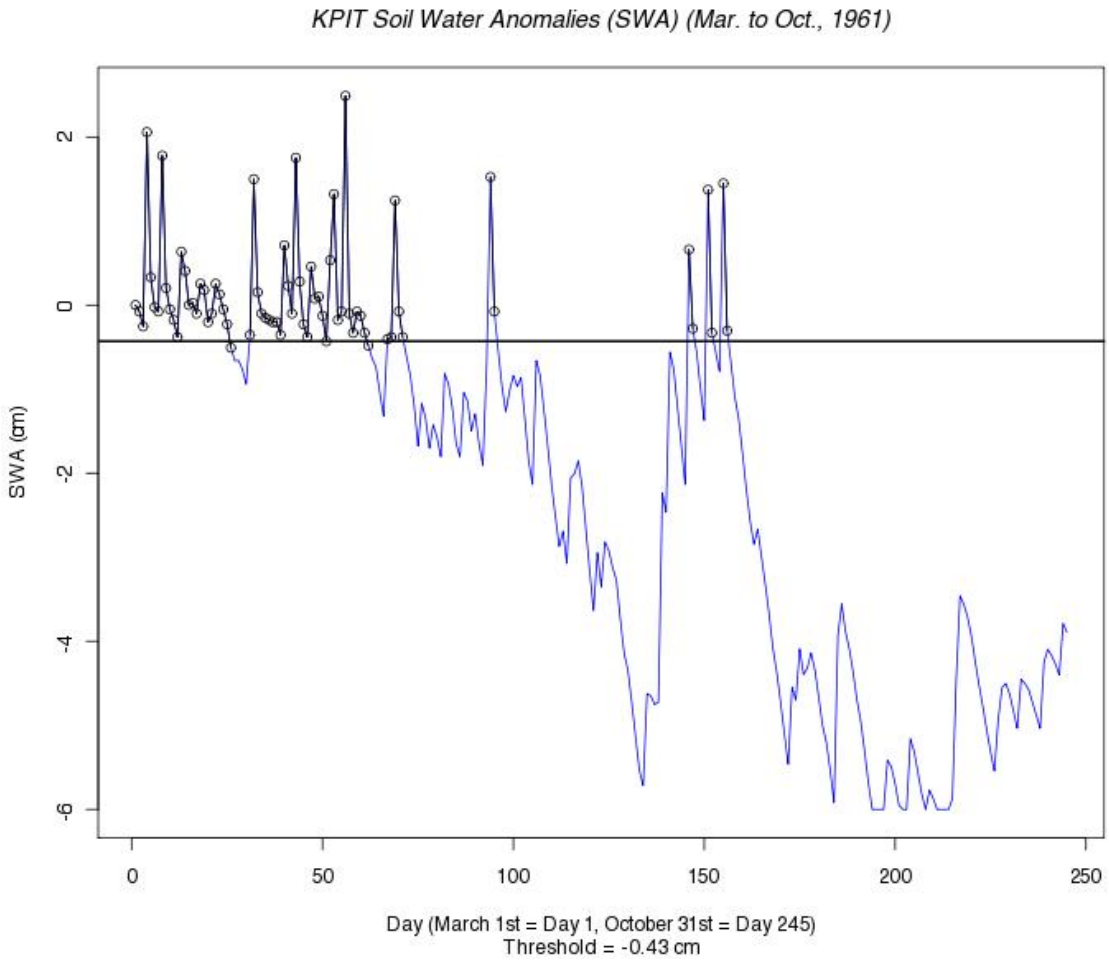

Figure 3.6: Example of the POT approach being applied to the Pittsburgh SWA. The clusters in the figure, marked by the groupings of circled points, were based on a threshold of -0.53 cm, which is the third quartile of Pittsburgh's SWA entire dataset. Based on this threshold, there were seven clusters from March 1 to October 31, 1961.

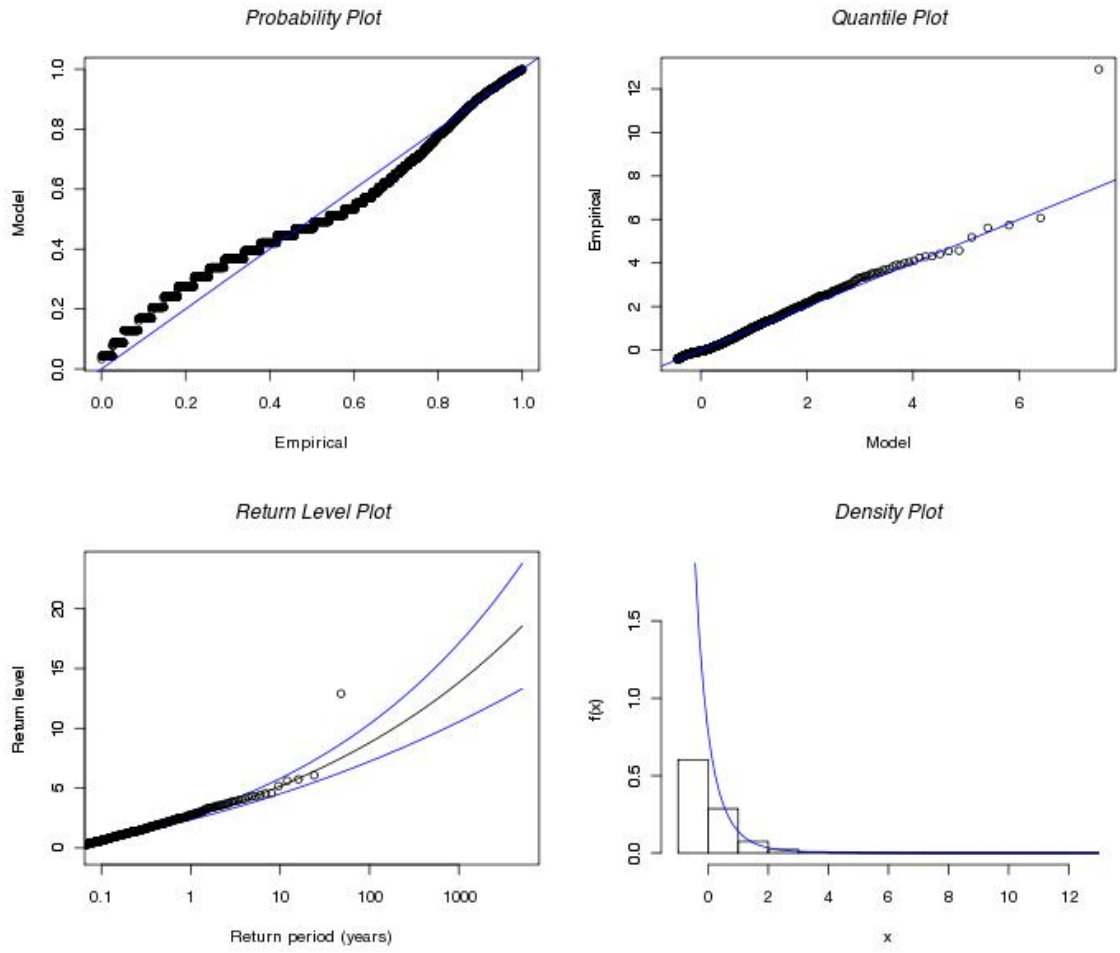

Figure 3.7: Diagnostic plot for a stationary GP distribution fit to Pittsburgh's cluster maxima.

they are likely not independent, one of the GP model requirements.

The POT approach was used to analyze the wet periods and dry periods in more detail in this study. To define wet periods in this study, the third quartile of a station's SWA was used. To define dry periods, the first quartile of a stations SWA was used. The minimum possible length of a wet period or dry period in this study was 1 day. The maximum possible length of a wet period or dry period was 245 days, the number of days from March 1 to October 31.

No wet periods or dry periods crossed from one year to another. A wet period started when the daily SWA value exceeded the specified threshold. A wet period ended when the daily SWA value fell to or below the specified threshold. A dry period began when the daily SWA fell below the specified threshold and ended when it reached or exceeded the specified threshold. The POT approach was then used to fit a stationary GP distribution to the maxima from each wet period (i.e. cluster maxima) for each station.

Similar to how the block maxima were fit to GEV distributions using MLE in R and the extRemes Toolkit, the cluster maxima for each station were used to estimate parameters (scale and shape) for the respective GP distributions that best fit the data. Based on how well the distributions fit, the fit information was used to describe the data statistically.

3.4 POT Approach and Non-stationarity

The POT approach was used to investigate any non-stationarity in the cluster maxima for each station. Observing non-stationarity in the cluster maxima could help give understanding to how the distributions of the cluster maxima, and subsequently wet and dry periods, for each station may have changed through time. Figure 3.8 shows example results of the POT approach applied to the Pittsburgh's cluster maxima for a non-stationary case.

Similar to fitting a non-stationary GEV distribution to the block maxima, to investigate non-stationarity in the cluster maxima, a GP distribution can be fit to the data with parameters that are modeled to change as a function of time, substituting σ(t), ξ(t)) for σ and ξ in equation 3.4, as shown in equation 3.5

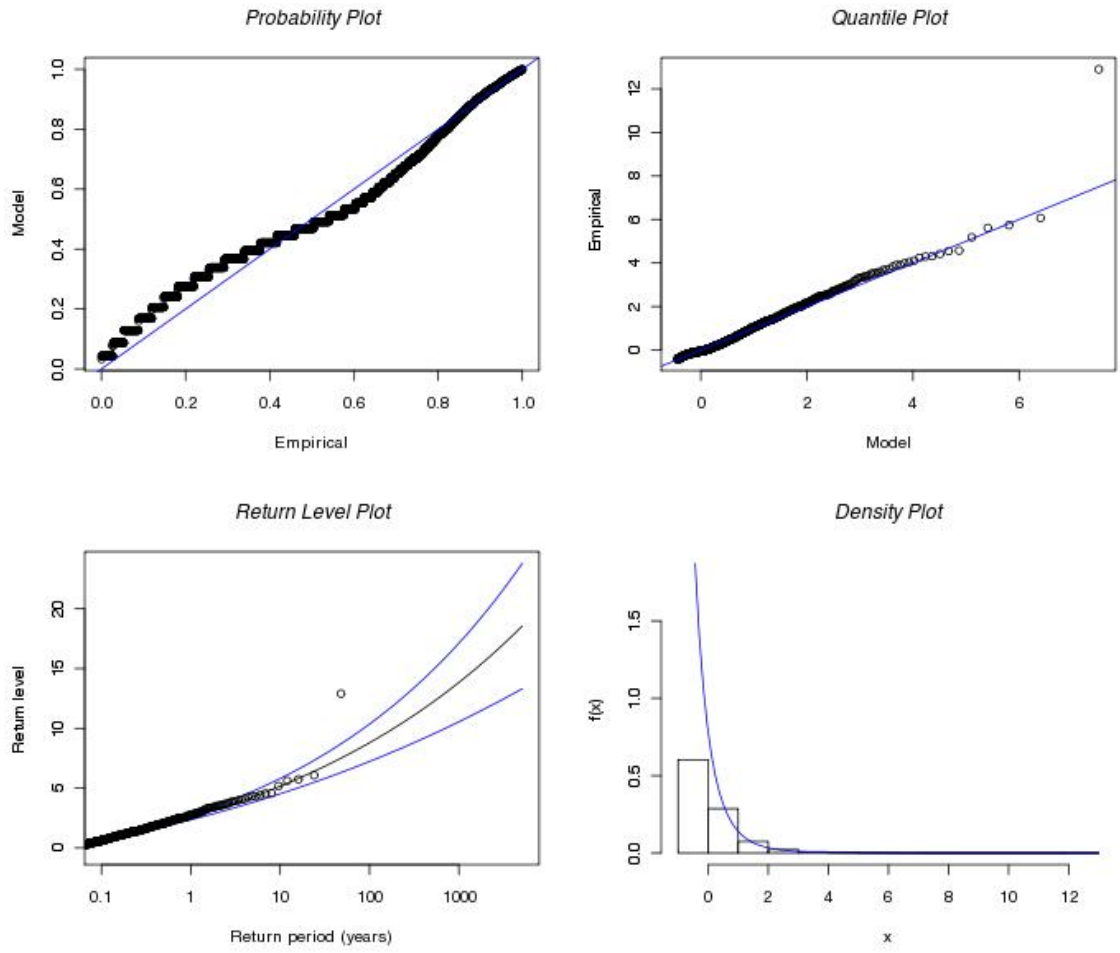

Figure 3.8: A diagnostic plot for a non-stationary GP distribution fit to Pittsburgh's cluster maxima.

below:

$$H(y_t) = 1 - (1 + \frac{\xi(t)y_t}{\sigma(t)*})^{-1/\xi(t)} \tag{3.5}$$

where y_t represent a threshold excess at certain time defined on y_t: $y_t > 0$ and $(1 + \xi(t)y_t/\sigma(t)^*) > 0$, $\sigma(t)^* = \sigma(t) + \xi(t)[u - \mu(t)]$, with u being the high threshold.

Figure 3.8 is a diagnostic plot of a non-stationary GP distribution fit to

Pittsburgh's cluster maxima. The probability and quantile plots in this figure were used to diagnose how well the model, in this case, the non-stationary GP distribution, fits to the cluster maxima. From this diagnostic plot, there is weak support for this particular model as a reasonable fit to Pittsburgh's cluster maxima because both the quantile and probability plots from the diagnostic plots were not linear.

The first step to fitting non-stationary GP distributions to the cluster maxima for Pittsburgh and the other stations was to develop a time series to which the GP distribution parameters can be modeled. Since the data is daily, spanning 245 days, every year, for a 48-year period, a day list from day 1 (March 1, 1961) to day 11760 (October 31, 2008) was assembled. This day list corresponds to the days of the data used for the parameters to be modeled.

For non-stationary GP distribution fits, the shape parameter was assumed to be constant and the scale parameter to change linearly as a function of time in days (i.e. $\sigma(t), \xi$). Then, as in the case of the stationary GP distribution fits, MLE was used to estimate the constant shape parameter and two additional time-dependent terms (d_0, d_1) for the scale parameter that account for the change in the scale parameter over time (i.e. $\sigma(t) = d_0 + d_1(t)$). For the cluster minima, GP distributions were fit to the negative of the minima for each station, with both the scale and shape parameters changing linearly as a function of time using MLE. The results from these fits would be used to estimate how the GP distributions and connecting return levels and return periods for each station changed during the period of the data, from 1961 to 2008.

As in the case of the GEV distribution fits, there are not set rules to deciding which parameter or parameters to choose to model with time or how they

should vary with time (linearly, log-normally, etc.). From initial tests of the stations data, the ”best distributions fits” for the cluster maxima were obtained through a linear change in the scale parameter, and linear changes in both the scale and shape parameters for the cluster minima, as observed from diagnostic plots.

Once a stationary and non-stationary GP distribution were fit to the maxima and minima for each station, a likelihood ratio test (LRT) was performed to test the statistical significance of the non-stationary distribution over the stationary distribution. Based on the results of the LRT, it will be known whether the non-stationary GP distributions are a statistical improvement over the stationary ones.

3.5 Maximum Wet Period and Dry Period Annual Durations Analyses

The block maxima approach was used to analyze maximum annual duration of the wet periods and dry periods for each station. Similar to what was done for the annual maximum SWA, stationary and non-stationary GEV distributions were fit to each stations annual maximum wet period and dry period duration. For the non-stationary GEV distribution fits, from an initial guess, the location parameter assumed to be constant and the scale parameter was assumed to change log-normally with time. Diagnostic plots were produced for these analyses and used to measure how well the distributions fit to the data. Return level and return period plots were produced, and likelihood ratio tests were performed to understand whether the non-stationary GEV distribution fits were a

statistically significant improvement over the stationary ones.

CHAPTER 4

GEV RESULTS

4.1 Stationary GEV distribution fit to block maxima

As mentioned in the methods section, stationary GEV distributions were fit to the block maxima of each station. Table 4.1 shows the estimated GEV location, scale and shape parameters with standard errors (in parentheses) for each stations GEV distribution fit. These parameters are also shown spatially in Figures 4.1, 4.2, and 4.3 .

The ranges of values for the location, scale and shape parameters were 2.40 cm to 4.96 cm, 0.95 cm to 2.29 cm and -0.19 to 0.36, respectively. The medians of the location, scale and shape parameters were 3.32 cm, 1.67 cm and 0.07, respectively. The means for the location, scale and shape parameters were 3.51 cm, 1.63 cm and 0.08, respectively. When observing the location, scale and shape parameter values, it was hard to discern a clear spatial pattern for the values. For the location and scale parameter values, the highest values were generally located along the eastern seaboard. The lowest values were located further inland toward the great lakes. There was no clear or recognizable pattern for the shape parameter values other than the values being mostly positive. Specifically, there were 8 stations with negative shape parameters (KLGA, KACY, KBOS, KORH, KBTV, KPVD, KCLE, KIPT). This would suggest that the GEV distributions for these stations would be bounded at the tail.

Generally, the stationary GEV distributions fit well to the each stations block maxima. Diagnostic plots produced from the stationary GEV distribution fits

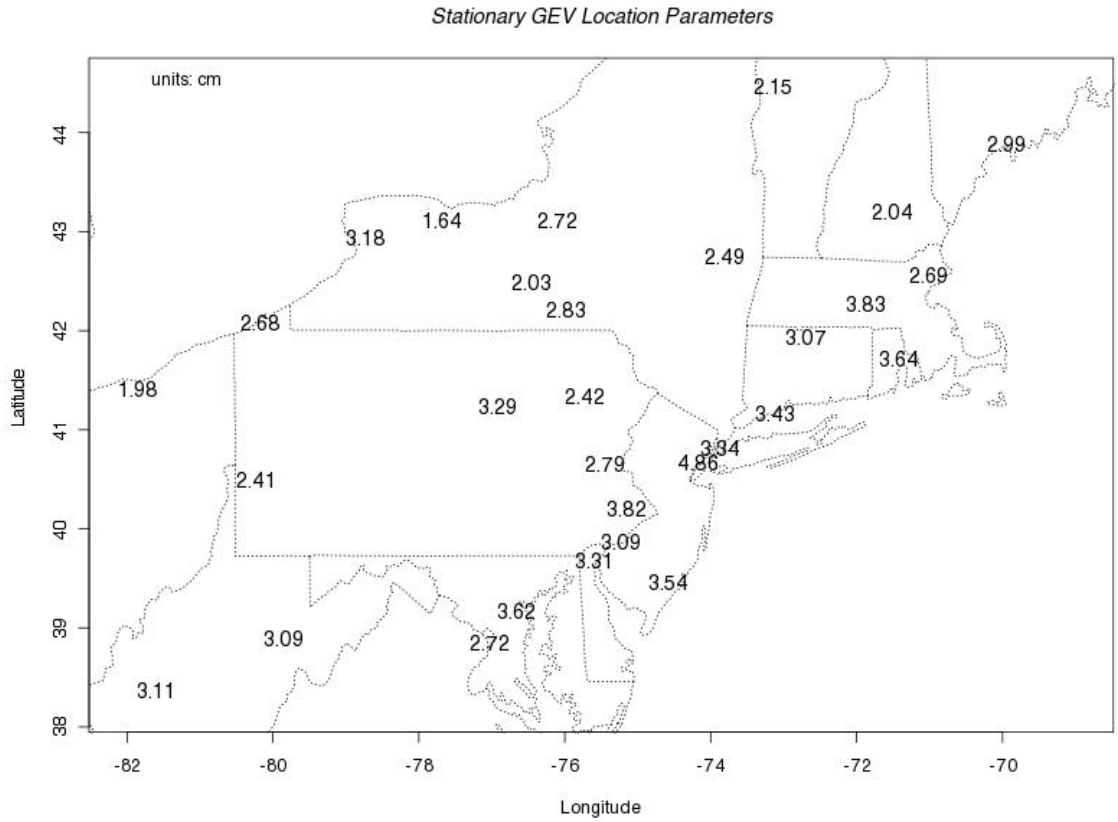

Figure 4.1: Stationary GEV location parameters spatial plot.

for KABE, KACY, KEKN and KCLE are shown in Figures 4.4, 4.5, 4.6 and 4.7 as examples of this. KABE and KACY are located closer to the east coast and KEKN and KCLE are located further inland. The probability and quantile plots in Figures 4.4, 4.5, 4.6 and 4.7 for these stations were very linear, with only a few outliers. This was the case for the rest of the stations in the block maxima analysis.

The stationary GEV distribution fit information was used to estimate return levels for each station. Table 4.2 shows the 2-year, 10-year and 20-year return levels for each stations block maxima. The ranges of values for the 2-year, 10-

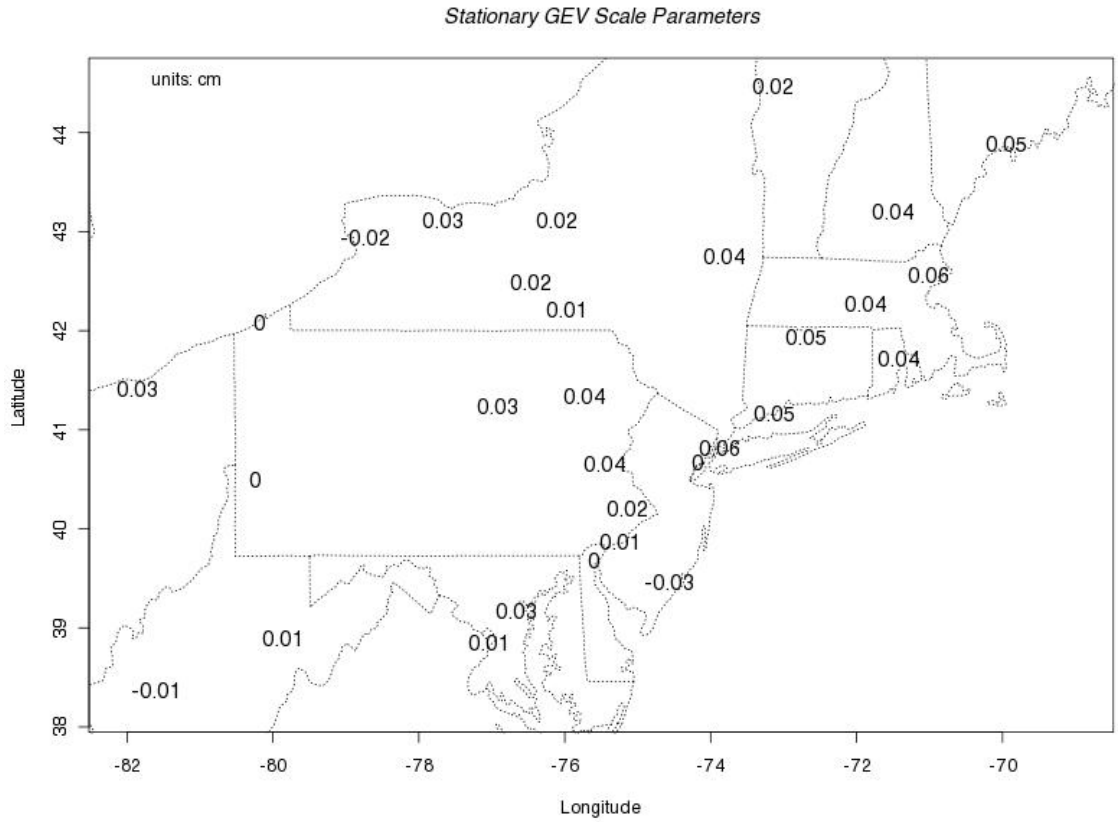

Figure 4.2: Stationary GEV scale parameters spatial plot.

year and 20-year return levels were 2.82 cm to 5.66 cm, 4.62 cm to 11.14 cm and 5.24 cm to 14.43 cm, respectively. The medians for the 2-year, 10-year and 20-year return levels were 3.88 cm, 7.60 cm and 9.03 cm, respectively. The means for these return levels were 4.12 cm, 7.57 cm and 9.09 cm, respectively. The 2-year, 10-year and 20-year return levels are shown spatially in Figures 4.8, 4.9 and 4.10. From observing the return levels spatially, it is apparent that the highest values for the 2-year, 10-year and 20-year return levels are located along the eastern seaboard. This corresponds to where the largest location and scale parameter values were observed, along the eastern seaboard, as shown in Figures 4.1 and 4.2.

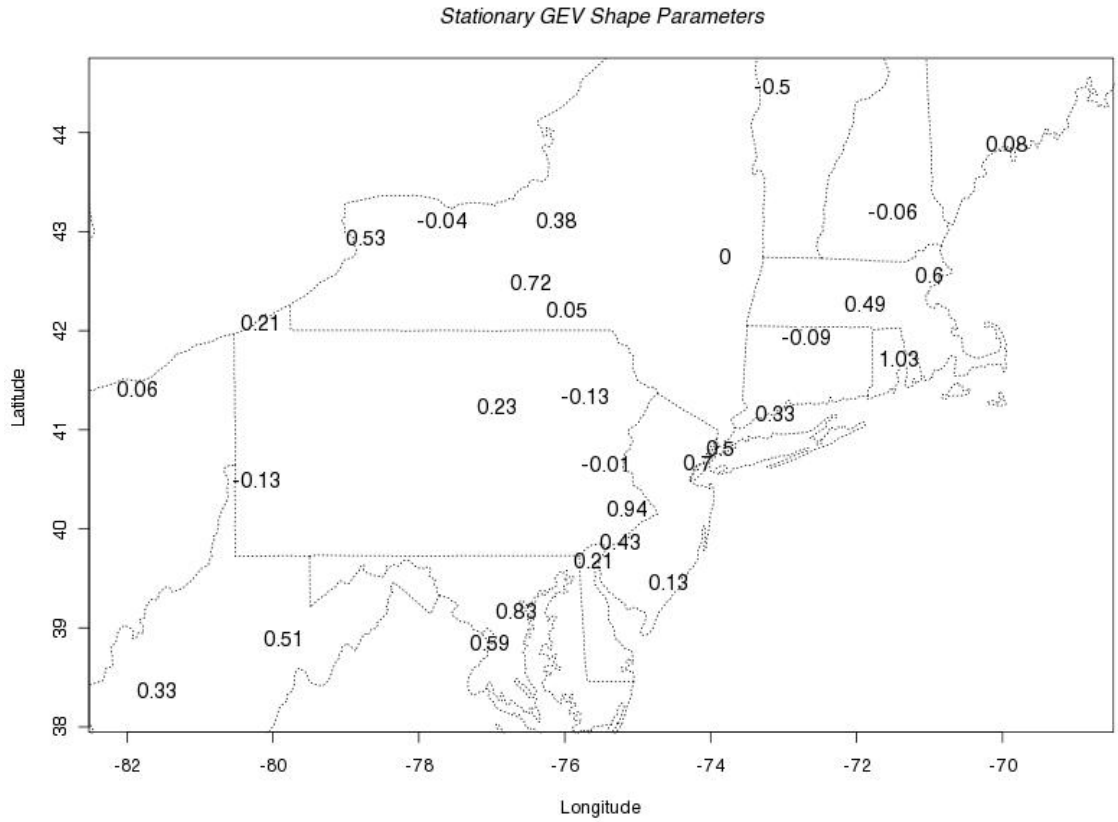

Figure 4.3: Stationary GEV shape parameters spatial plot.

4.2 Non-Stationary GEV distribution fit to block maxima

Non-stationary GEV distributions were also fit to each station's block maxima and the parameter results of these analyses are shown in Table 4.3. For the non-stationary GEV distributions, the location parameter was modeled to change linearly with time ($\mu(t) = b_0 + b_1 t$) and the scale parameter was modeled to change log-normally with time ($\ln \sigma(t) = c_0 + c_1 t$). Specifically, the estimated location intercept (b_0) and its slope (b_1), the log-normally transformed scale intercept (c_0) and its slope (c_1), and the shape parameters with standard errors are shown for each station. Table 4.3 also shows the p-value results from a

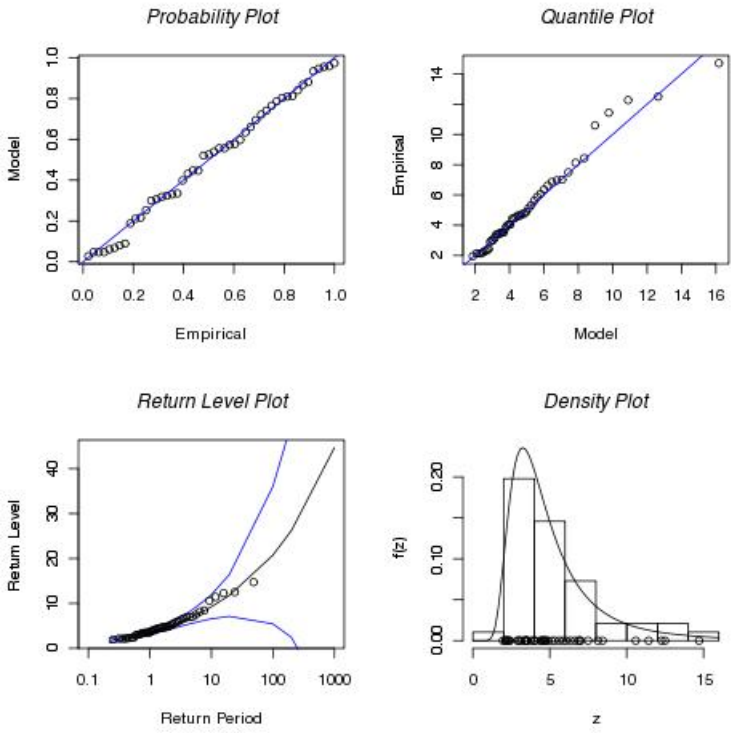

Figure 4.4: Stationary GEV distribution diagnostic plots for KABE.

likelihood ratio test (LRT) performed to test the statistical significance of the non-stationary GEV distribution fit over the stationary GEV fit for each station.

From Table 4.3, it appears that the highest b_0 values are located along the coastal areas and the lowest values located farthest inland. The values for b_0 ranged from 1.64 cm to 4.86 cm, with a median value of 3.03 cm and a mean value of 2.96 cm. The highest b_1 values were generally located along the east coast as well. The values for b_1 ranged from -0.03 cm per year to 0.06 cm per year, with median of 0.03 cm per year and a mean of 0.02 cm per year. There were only three stations with negative b_1 values (KACY, KBUF, KCRW). Table 4.3 also shows that there were 7 stations with negative c_0 values (KPIT, KROC, KAVP, KCON, KBTV, KBDL, KABE), with these stations spread out across the Northeast. The values for c_0 range from -0.50 cm to 1.03 cm, with a median and

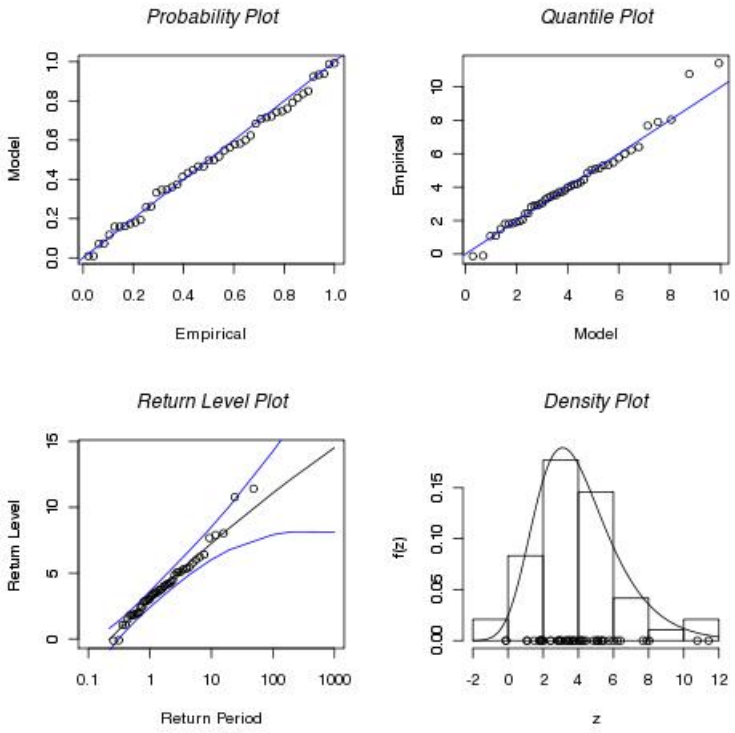

Figure 4.5: Stationary GEV distribution diagnostic plots for KACY

mean 0.03 cm and 0.30 cm, respectively. The values c_1 ranged from -0.02 cm to 0.02 cm, with a median and mean of 0.004 and 0.005, respectively. As well, Table 4.3 shows that there were 7 stations with negative c_1 values (KLGA, KBOS, KORH, KCON, KBTV, KPVD, KIPT), all of which were located on along the east coast. The shape parameter values ranged from -0.20 to 0.41, with a median and mean of 0.07 and 0.08, respectively, and there was no clear spatial pattern for this parameter.

The non-stationary GEV distribution fit very well to each stations block maxima. Diagnostic plots produced from the non-stationary GEV distribution fits to KABE, KACY, KBUF and KCRW are shown in Figures 4.11, 4.12, 4.13 and 4.14. The residual probability and quantile plots were very linear for these and the other stations in the analysis. There were 10 stations where non-stationary GEV

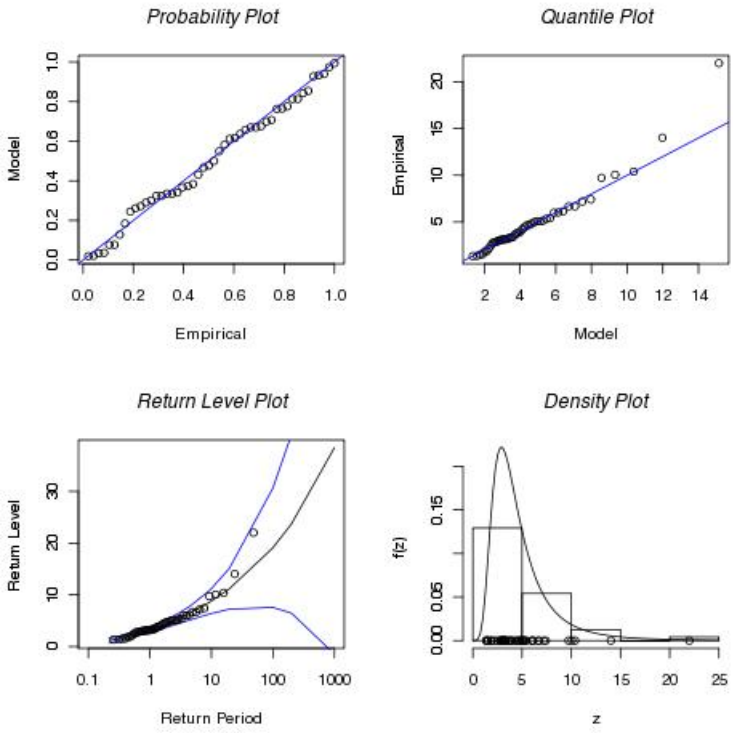

Figure 4.6: Stationary GEV distribution diagnostic plots for KEKN.

fits were a statistically significant improvement over the stationary fits (KALB, KLGA, KAVP, KBOS, KCON, KBTV, KBDL, KNHZ, KSYR and KCLE).

The non-stationary GEV distribution fit information was used to estimate 2 sets of the 2-year, 10-year and 20-year return levels; the first set produced from the stations' 1961 estimated GEV parameters, and the second produced from the stations' 2008 estimated GEV parameters. This was done to observe how the estimated return levels changed through time and is shown in Table 4.4. The differences in the 2-year, 10-year and 20-year return levels for each station were plotted spatially in Figures 4.15, 4.16, and 4.17. Of all the stations, there were only 4 stations (KACY, KBUF, KCRW, KEWR) that showed decreases in the return levels over time. Several of the stations with a statistically significant improvement of the non-stationary GEV distribution fit over the stationary GEV

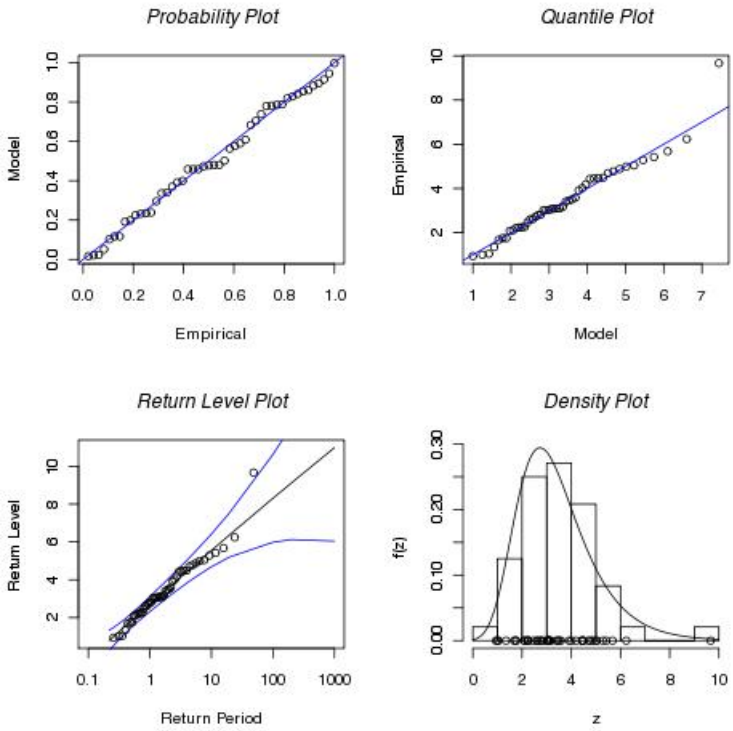

Figure 4.7: Stationary GEV distribution diagnostic plots for KCLE.

distribution also were some of the stations with the largest differences in the return periods from 1961 to 2008. For example, KNHZ had the largest changes in the 2-year, 10-year and 20-year return levels of 3.24 cm, 7.22 cm and 8.79 cm, respectively, from 1961 to 2008.

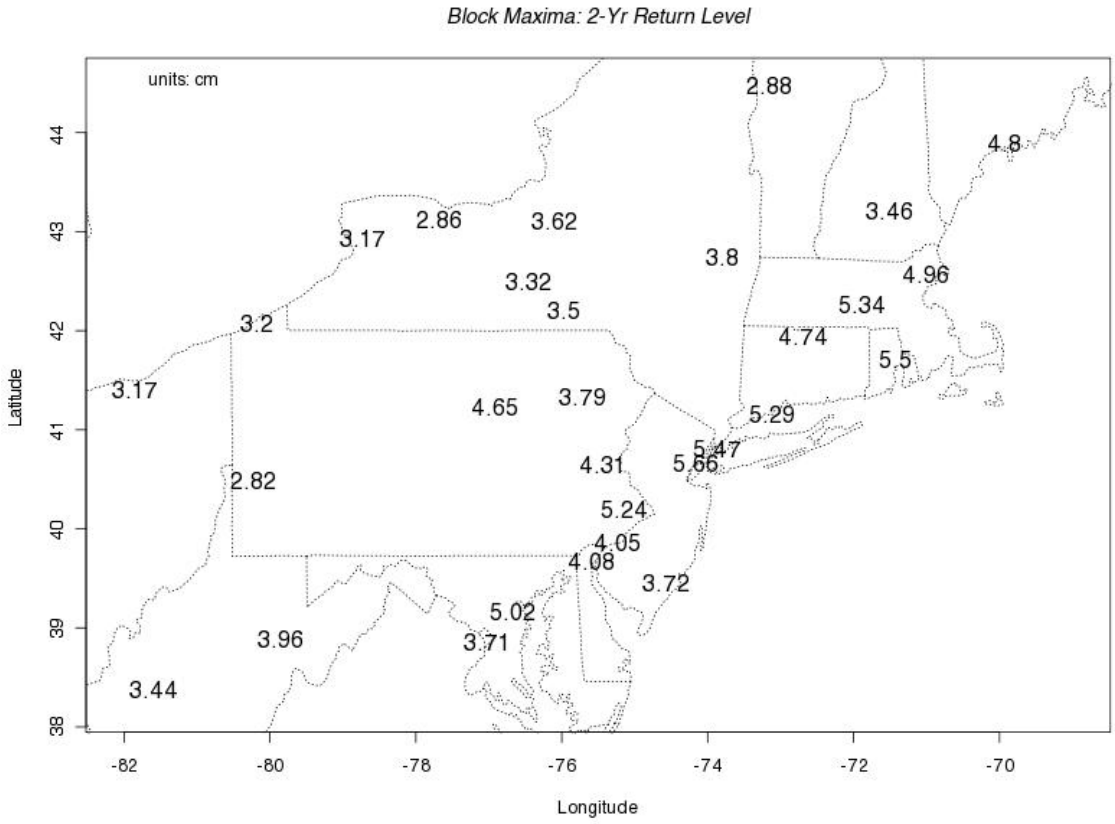

Figure 4.8: A spatial map of the 2-year return levels estimated from each station's GEV distribution fit.

Table 4.1: The estimated GEV distribution parameters with standard errors (in parentheses) from the stationary GEV distributions fit to each station's block maxima. Values in the table were rounded to 2 decimals.

Station	Location	Scale	Shape
KPIT	2.46 (0.16)	0.95 (0.12)	0.19 (0.11)
KALB	3.33 (0.2)	1.27 (0.15)	0.07 (0.09)
KBGM	3.05 (0.2)	1.16 (0.16)	0.24 (0.15)
KITH	2.65 (0.3)	1.81 (0.23)	0.07 (0.13)
KLGA	4.7 (0.33)	2.09 (0.23)	−0.02 (0.08)
KPHL	3.44 (0.27)	1.63 (0.2)	0.12 (0.11)
KROC	2.4 (0.21)	1.26 (0.15)	0.01 (0.12)
KACY	3.01 (0.31)	1.94 (0.22)	−0.05 (0.09)
KAVP	3.19 (0.26)	1.61 (0.2)	0.14 (0.12)
KBOS	4.15 (0.36)	2.21 (0.26)	−0.03 (0.1)
KBUF	2.74 (0.18)	1.12 (0.14)	0.19 (0.11)
KERI	2.76 (0.19)	1.16 (0.15)	0.18 (0.12)
KORH	4.69 (0.3)	1.82 (0.22)	−0.19 (0.12)
KCON	2.95 (0.22)	1.38 (0.16)	0 (0.1)
KBTV	2.53 (0.16)	0.99 (0.11)	−0.05 (0.09)
KBDL	4.13 (0.27)	1.61 (0.21)	0.23 (0.12)
KILG	3.38 (0.3)	1.85 (0.24)	0.21 (0.12)
KCRW	2.91 (0.23)	1.43 (0.18)	0.13 (0.11)
KNXX	4.44 (0.35)	2.18 (0.25)	0 (0.1)
KNHZ	4.08 (0.31)	1.92 (0.24)	0.11 (0.11)
KPVD	4.67 (0.37)	2.29 (0.26)	−0.1 (0.11)
KSYR	3.19 (0.18)	1.15 (0.13)	0 (0.08)
KABE	3.67 (0.28)	1.63 (0.24)	0.32 (0.16)
KBDR	4.56 (0.32)	1.92 (0.25)	0.14 (0.13)
KCLE	2.71 (0.2)	1.25 (0.14)	−0.01 (0.09)
KDCA	3.01 (0.31)	1.89 (0.23)	0.05 (0.11)
KEKN	3.3 (0.28)	1.71 (0.23)	0.27 (0.13)
KIPT	4.02 (0.28)	1.74 (0.2)	−0.03 (0.1)
KEWR	4.96 (0.3)	1.79 (0.27)	0.36 (0.15)
KBWI	4.28 (0.33)	2.01 (0.24)	0.01 (0.11)

Table 4.2: The 2-year, 10-year and 20-year return levels estimated from the GEV distribution fit to each station's block maxima

	Return Level (cm)		
Station	2-yr	10-yr	20-yr
KPIT	2.82	5.14	6.28
KALB	3.8	6.4	7.48
KBGM	3.5	6.53	8.1
KITH	3.32	7.05	8.6
KLGA	5.47	9.32	10.76
KPHL	4.05	7.67	9.3
KROC	2.86	5.28	6.23
KACY	3.72	7.17	8.41
KAVP	3.79	7.42	9.08
KBOS	4.96	8.94	10.4
KBUF	3.17	5.88	7.19
KERI	3.2	5.97	7.3
KORH	5.34	8.03	8.83
KCON	3.46	6.08	7.08
KBTV	2.88	4.62	5.24
KBDL	4.74	8.85	10.94
KILG	4.08	8.68	10.98
KCRW	3.44	6.62	8.06
KNXX	5.24	9.34	10.91
KNHZ	4.8	8.98	10.82
KPVD	5.5	9.28	10.54
KSYR	3.62	5.78	6.6
KABE	4.31	9.04	11.74
KBDR	5.29	9.65	11.65
KCLE	3.17	5.49	6.36
KDCA	3.71	7.52	9.08
KEKN	3.96	8.63	11.15
KIPT	4.65	7.8	8.97
KEWR	5.66	11.14	14.43
KBWI	5.02	8.84	10.31

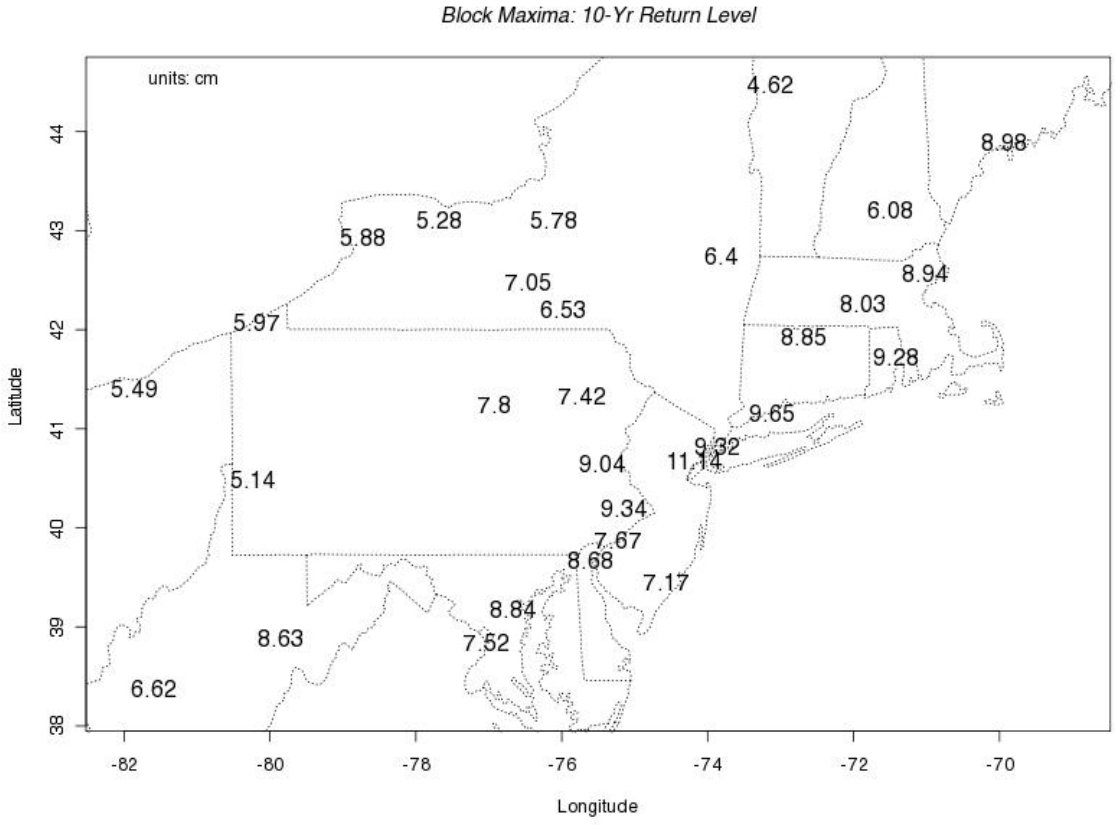

Figure 4.9: A spatial map of the 10-year return levels estimated from each station's stationary GEV distribution fit.

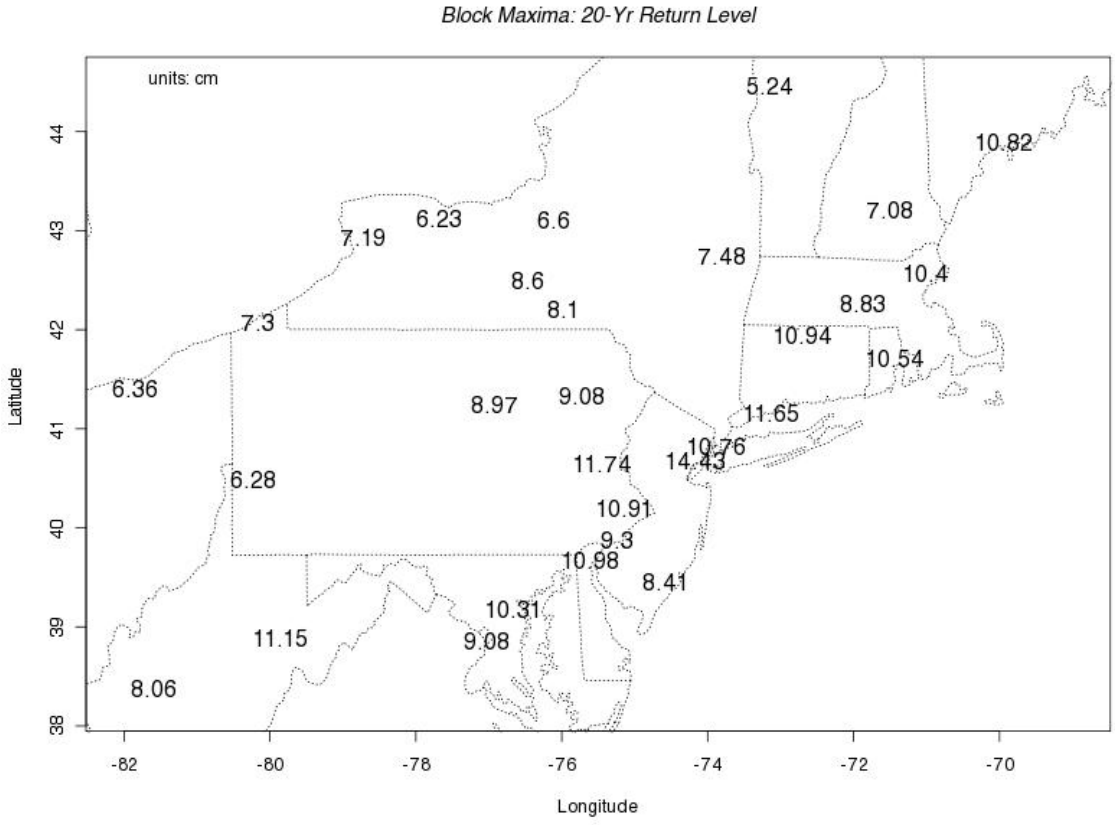

Figure 4.10: A spatial map of the 20-year return levels estimated from each station's stationary GEV distribution fit.

Table 4.3: The estimated non-stationary GEV distribution parameters with standard errors in parentheses. (* - statistically significant)

Station	b_0	b_1	c_0	c_1	ξ	α
KPIT	2.41 (0.29)	0 (0.01)	−0.13 (0.26)	0 (0.01)	0.18 (0.12)	0.939
KALB	2.49 (0.33)	0.04 (0.01)	0 (0.27)	0.01 (0.01)	0.09 (0.1)	0.02∗
KBGM	2.83 (0.37)	0.01 (0.01)	0.05 (0.27)	0 (0.01)	0.24 (0.15)	0.786
KITH	2.03 (0.6)	0.02 (0.02)	0.72 (0.3)	−0.01 (0.01)	0.12 (0.15)	0.144
KLGA	3.34 (0.56)	0.06 (0.02)	0.5 (0.23)	0.01 (0.01)	−0.05 (0.15)	0.026∗
KPHL	3.09 (0.51)	0.01 (0.02)	0.43 (0.24)	0 (0.01)	0.12 (0.11)	0.734
KROC	1.64 (0.34)	0.03 (0.01)	−0.04 (0.25)	0.01 (0.01)	0.03 (0.12)	0.058
KACY	3.54 (0.44)	−0.03 (0.02)	0.13 (0.37)	0.02 (0.01)	0.05 (0.13)	0.27
KAVP	2.42 (0.35)	0.04 (0.02)	−0.13 (0.26)	0.02 (0.01)	0.07 (0.12)	0.031∗
KBOS	2.69 (0.61)	0.06 (0.02)	0.6 (0.23)	0 (0.01)	−0.02 (0.12)	0.028∗
KBUF	3.18 (0.45)	−0.02 (0.01)	0.53 (0.26)	−0.02 (0.01)	0.22 (0.14)	0.124
KERI	2.68 (0.37)	0 (0.01)	0.21 (0.29)	0 (0.01)	0.19 (0.12)	0.856
KORH	3.83 (0.52)	0.04 (0.02)	0.49 (0.23)	0 (0.01)	−0.18 (0.12)	0.159
KCON	2.04 (0.34)	0.04 (0.01)	−0.06 (0.19)	0.01 (0.01)	−0.11 (0.12)	0.009∗
KBTV	2.15 (0.23)	0.02 (0.01)	−0.5 (0.22)	0.02 (0.01)	−0.2 (0.11)	0.031∗
KBDL	3.07 (0.35)	0.05 (0.02)	−0.09 (0.26)	0.02 (0.01)	0.15 (0.11)	0.011∗
KILG	3.31 (0.47)	0 (0.02)	0.21 (0.28)	0.02 (0.01)	0.16 (0.13)	0.297
KCRW	3.11 (0.47)	−0.01 (0.02)	0.33 (0.29)	0 (0.01)	0.13 (0.12)	0.885
KNXX	3.82 (0.72)	0.02 (0.02)	0.94 (0.24)	−0.01 (0.01)	0.06 (0.11)	0.23
KNHZ	2.99 (0.43)	0.05 (0.02)	0.08 (0.23)	0.02 (0.01)	0.03 (0.09)	0.019∗
KPVD	3.64 (0.76)	0.04 (0.02)	1.03 (0.23)	−0.01 (0.01)	−0.04 (0.12)	0.056
KSYR	2.72 (0.39)	0.02 (0.01)	0.38 (0.26)	−0.02 (0.01)	0.05 (0.1)	0.014∗
KABE	2.79 (0.39)	0.04 (0.02)	−0.01 (0.3)	0.02 (0.01)	0.24 (0.17)	0.075
KBDR	3.43 (0.53)	0.05 (0.02)	0.33 (0.3)	0.01 (0.01)	0.18 (0.13)	0.075
KCLE	1.98 (0.37)	0.03 (0.01)	0.06 (0.25)	0 (0.01)	0.04 (0.12)	0.049∗
KDCA	2.72 (0.64)	0.01 (0.02)	0.59 (0.27)	0 (0.01)	0.05 (0.11)	0.85
KEKN	3.09 (0.54)	0.01 (0.02)	0.51 (0.29)	0 (0.01)	0.27 (0.13)	0.873
KIPT	3.29 (0.45)	0.03 (0.02)	0.23 (0.24)	0.01 (0.01)	−0.06 (0.1)	0.127
KEWR	4.86 (0.7)	0 (0.02)	0.7 (0.36)	−0.01 (0.01)	0.41 (0.17)	0.559
KBWI	3.62 (0.71)	0.03 (0.02)	0.83 (0.26)	−0.01 (0.01)	0.01 (0.11)	0.454

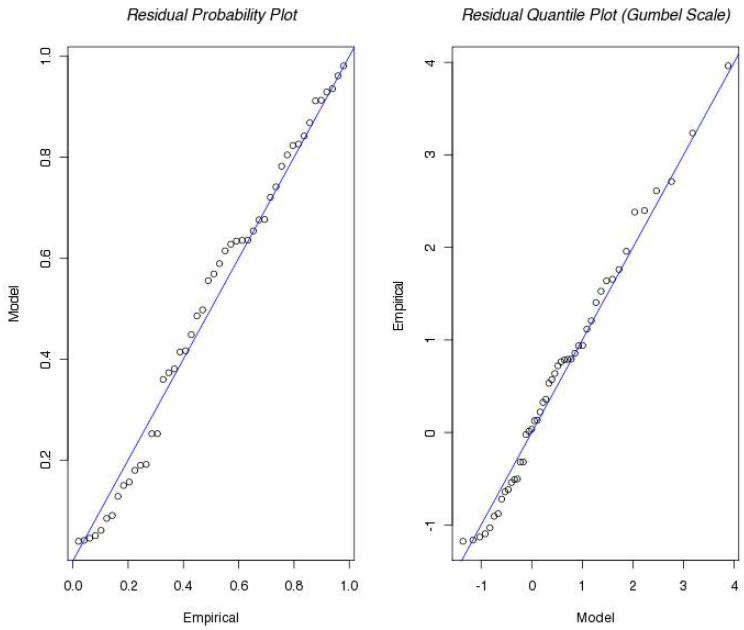

Figure 4.11: Non-stationary GEV distribution diagnostic plots for KABE.

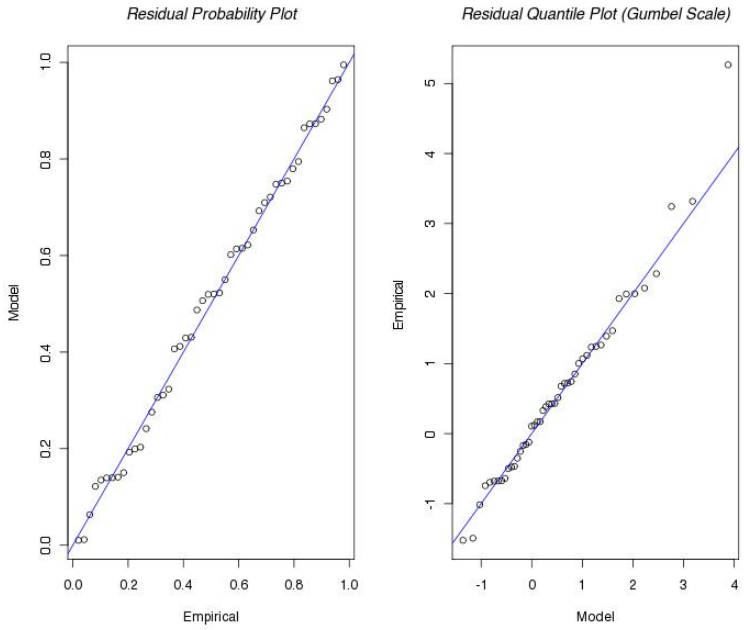

Figure 4.12: Non-stationary GEV distribution diagnostic plots for KACY.

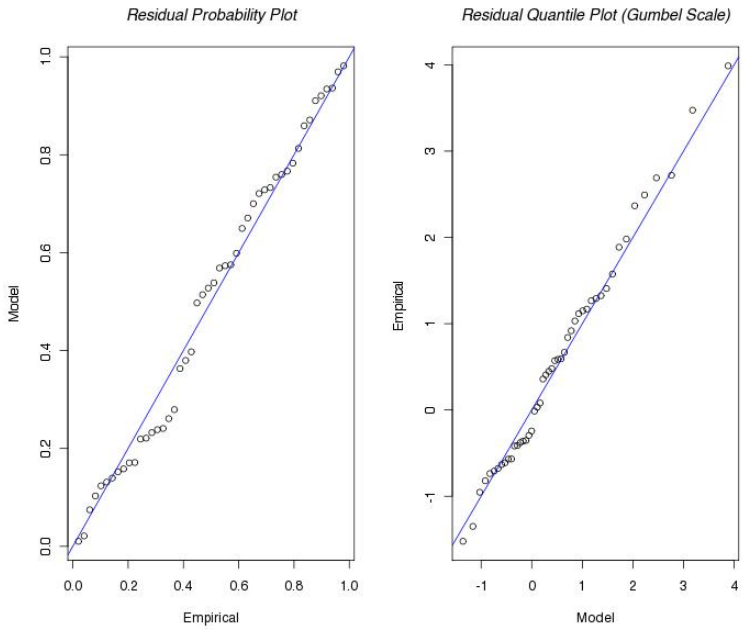

Figure 4.13: Non-stationary GEV distribution diagnostic plots for KBUF.

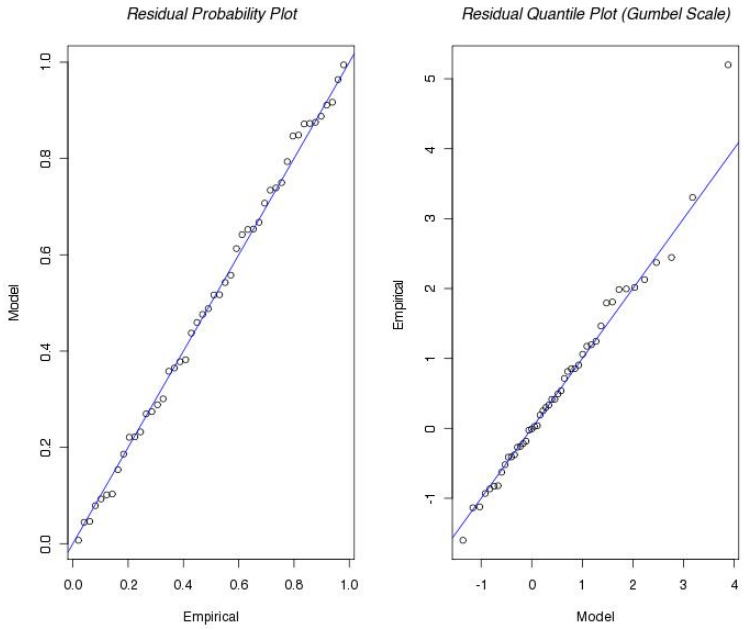

Figure 4.14: Non-stationary GEV distribution diagnostic plots for KCRW.

Table 4.4: The estimated return levels estimated for 1961 and 2008 for each station. (* - statistically significant)

	Return Level (cm)					
	From 1961 GEV parameters			From 2008 GEV parameters		
Station	2-yr	10-yr	20-yr	2-yr	10-yr	20-yr
KPIT	2.75	4.87	5.9	2.91	5.39	6.6
KALB*	2.9	5.02	5.93	4.69	7.47	8.66
KBGM	3.25	6	7.43	3.76	7.05	8.76
KITH	2.82	7.3	9.29	3.73	6.82	8.19
KLGA*	4	6.92	7.97	7.05	11.13	12.58
KPHL	3.68	7.09	8.62	4.42	8.21	9.91
KROC	2.03	3.95	4.71	3.71	6.53	7.65
KACY	3.94	6.28	7.24	3.23	8.74	10.98
KAVP*	2.79	4.65	5.44	5.18	10.75	13.09
KBOS*	3.42	6.81	8.07	6.48	10.61	12.15
KBUF	3.8	8.04	10.19	2.63	4.33	5.19
KERI	3.15	6.13	7.57	3.24	5.82	7.08
KORH	4.45	6.9	7.64	6.23	9.01	9.85
KCON*	2.42	3.98	4.49	4.77	7.79	8.79
KBTV*	2.39	3.3	3.57	3.64	5.97	6.66
KBDL*	3.47	5.61	6.6	6.4	12.19	14.87
KILG	3.78	6.74	8.13	4.5	10.83	13.82
KCRW	3.62	6.76	8.19	3.25	6.49	7.96
KNXX	4.78	9.98	12.12	5.53	8.87	10.25
KNHZ*	3.45	5.62	6.49	6.69	12.84	15.28
KPVD	4.68	9.6	11.37	6.16	8.95	9.96
KSYR*	3.28	6.17	7.35	3.92	5.34	5.92
KABE	3.22	5.86	7.24	5.79	12.51	16.01
KBDR	4.01	7.38	9	6.57	12.03	14.66
KCLE*	2.4	4.51	5.36	3.87	6.27	7.23
KDCA	3.4	7.07	8.56	4.02	7.96	9.57
KEKN	3.74	8.3	10.77	4.19	8.95	11.53
KIPT	3.78	6	6.78	5.66	9.58	10.96
KEWR	5.66	12.26	16.46	5.56	10.44	13.55
KBWI	4.49	8.85	10.53	5.53	8.8	10.06

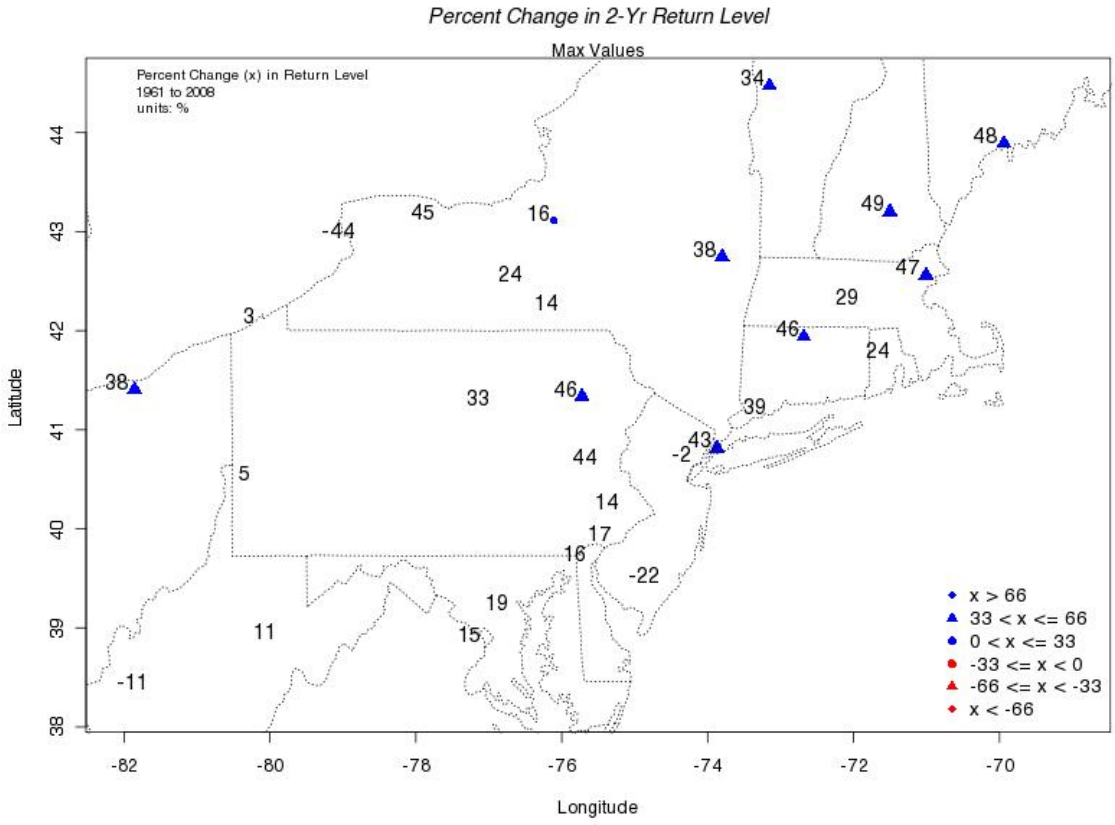

Figure 4.15: A spatial map of the differences calculated from the two sets of 2-year return levels estimated (for 1961 and for 2008) from each station's non-stationary GEV distribution fit. Stations with statistical significance are marked by symbols (triangles, diamonds, circles) next to numbers.

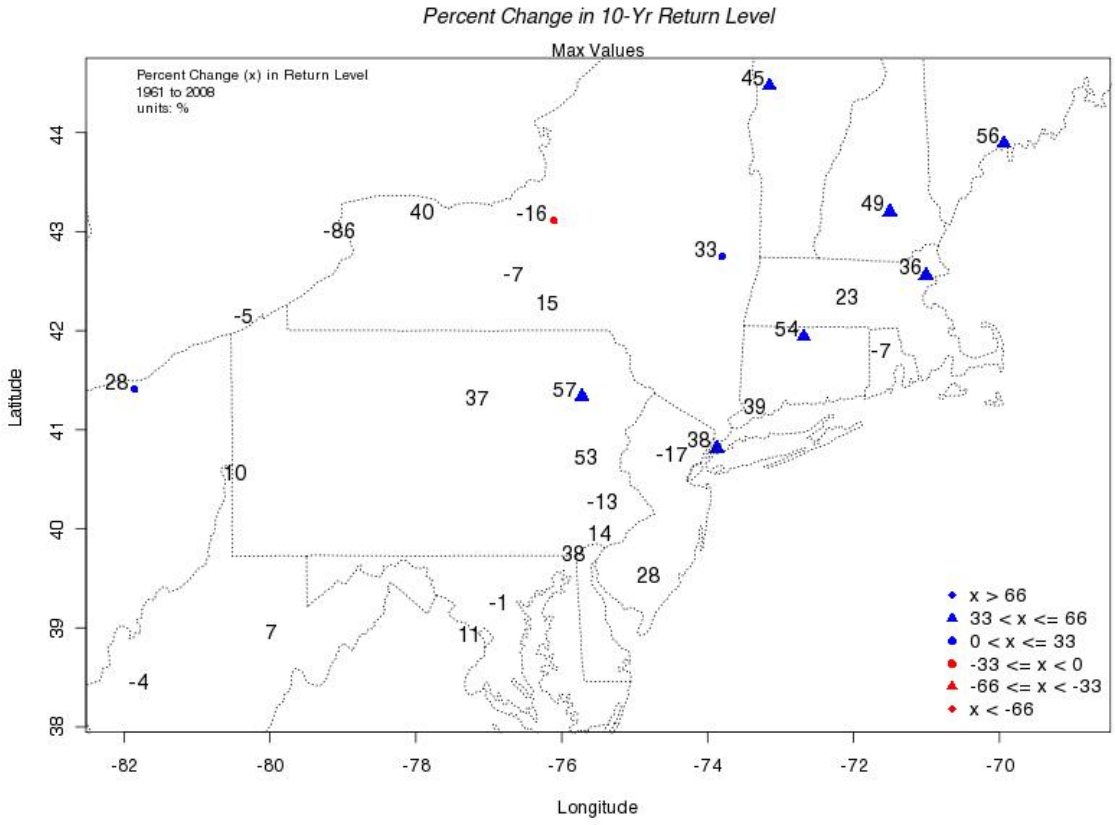

Figure 4.16: A spatial map of the differences calculated from the two sets of 10-year return levels estimated (for 1961 and for 2008) from each station's non-stationary GEV distribution fit. Stations with statistical significance are marked by symbols (triangles, diamonds, circles) next to numbers.

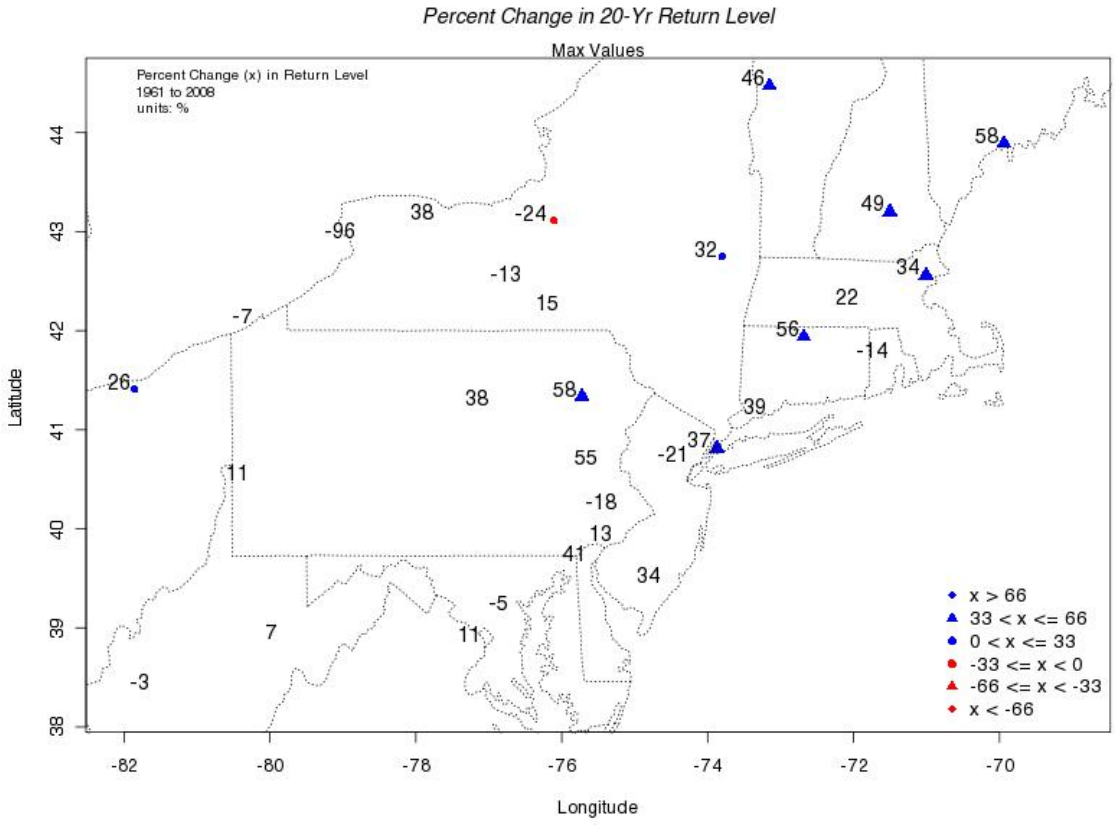

Figure 4.17: A spatial map of the differences calculated from the two sets of 20-year return levels estimated (for 1961 and for 2008) from each station's non-stationary GEV distribution fit. Stations with statistical significance are marked by symbols (triangles, diamonds, circles) next to numbers.

The differences in the 2-year, 10-year and 20-year return levels for each station were plotted spatially in Figures 4.15, 4.16, and 4.17. Of all the stations, there were only 4 stations (KACY, KBUF, KCRW, KEWR) that showed decreases in the return levels over time. Several of the stations with a statistically significant improvement of the non-stationary GEV distribution fit over the stationary GEV distribution also were some of the stations with the largest differences in the return periods from 1961 to 2008. For example, KNHZ had the largest changes in the 2-year, 10-year and 20-year return levels of 3.24 cm, 7.22 cm and 8.79 cm, respectively, from 1961 to 2008.

CHAPTER 5

GP RESULTS

5.1 Stationary GP distribution fit to cluster maxima

Stationary GP distributions were fit to the cluster maxima for each station and Table 5.1 shows the estimated scale and shape parameters with standard errors (in parentheses) from these analyses. Figures 5.1 and 5.2 show the scale and shape parameters spatially. The ranges of values for the scale and shape parameters were 1.25 cm to 2.53 cm and -0.12 to 0.16, respectively. The medians for the scale and shape parameters were 2.04 cm and -0.06, respectively. The means for the scale and shape parameters were 1.96 cm and -0.05.

Generally, the GP distribution fit well to all the stations' cluster maxima. Each had linear or nearly linear probability and quantile plots, as observed from the stations GP diagnostics. Figures 5.3, 5.4, 5.5 and 5.6 shows the stationary GP diagnostic plots for KALB, KBOS, KBUF and KIPT, respectively. The probability and quantile plots from the diagnostic plots are very linear providing support for the stationary GP distribution as a good model for the cluster maxima of these stations. The diagnostic plots for the other stations were very similar as well.

Table 5.2 shows the 2-year, 10-year and 20-year return levels for each stations cluster maxima calculated from each stations GP distribution fit. The ranges of values for the 2-year, 10-year and 20-year return levels were 3.72 cm to 7.67 cm, 5.12 cm to 11.41 cm, and 5.65 cm to 12.99 cm, respectively. The medians for 2-year, 10-year and 20-year return levels were 5.63 cm, 8.45 cm and 9.51 cm,

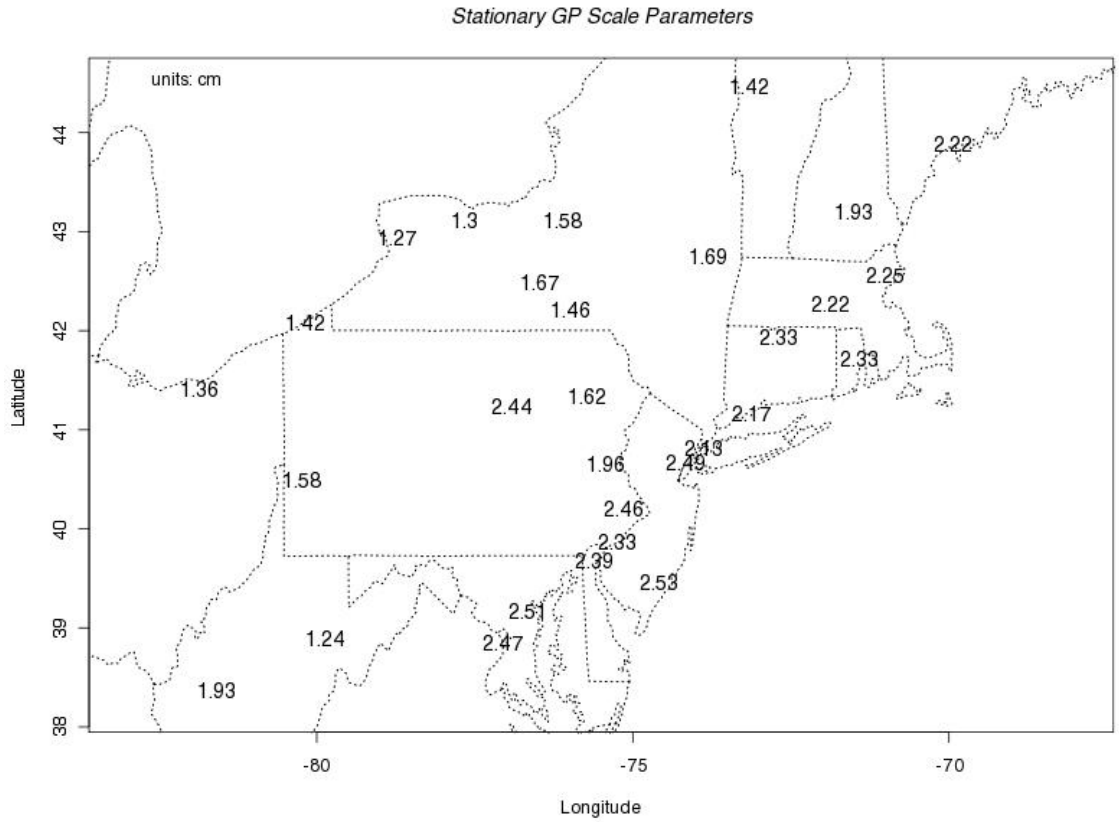

Figure 5.1: Stationary GP scale parameters spatially plotted. Values in this plot generally increase from west to east.

respectively. The means for these return levels were 5.48 cm, 8.09 cm and 9.15 cm, respectively. The spatial return level plots, Figures 5.7, 5.8, and 5.9, that the return levels for the region increase generally from the west to east.

5.2 Non-Stationary GP distribution fit to cluster maxima

Non-stationary GP distributions were fit to the cluster maxima for each station. Table 5.3 shows results from these distributions fit to each stations cluster maxima with the scale parameter changing linearly with time ($\sigma(t) = d_0 + d_1 t$) and a

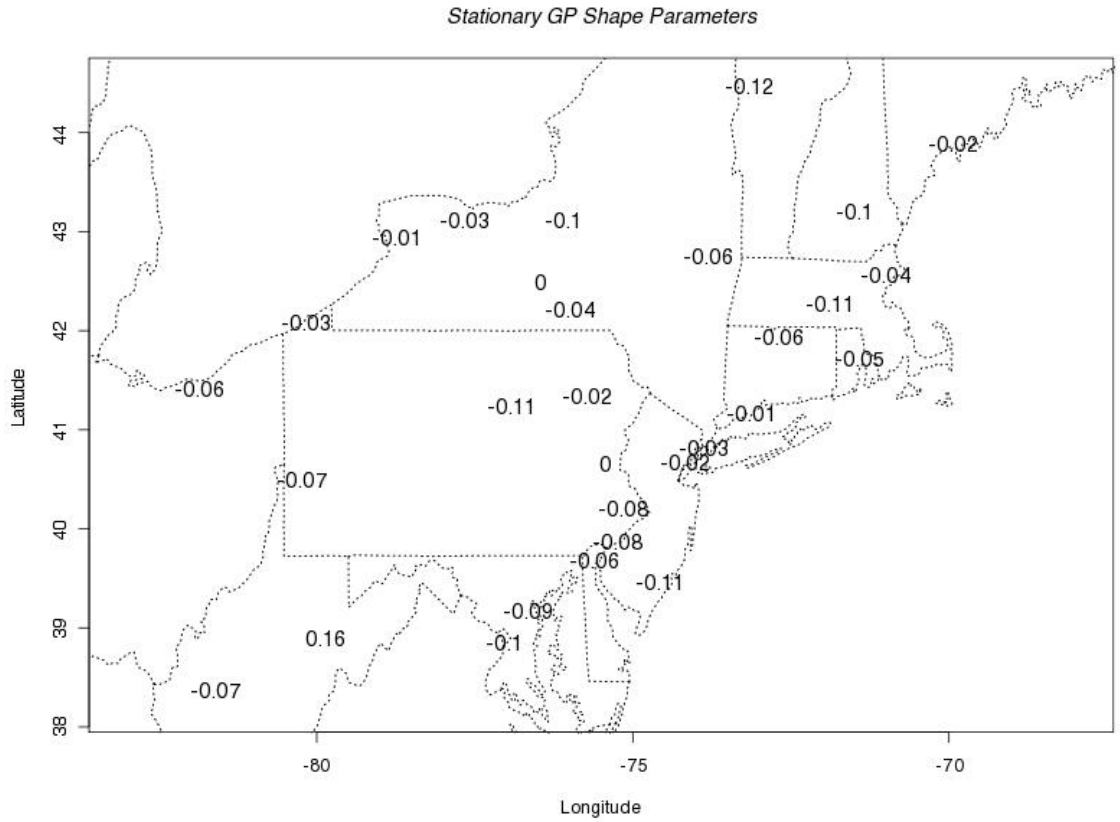

Figure 5.2: Stationary GP shape parameters spatially plotted. Most of the values in this plot were negative, but otherwise no discernible pattern existed.

constant shape parameter. The estimated scale intercept (d_0) and its slope (d_1), the shape parameter, and the standard errors for each parameter are shown for each station. The range of values for d_0 went from 0.89 cm to 2.53 cm, with a median value of 1.77 cm and mean of 1.76 cm. The range of values for d_1 went from -3.14 x 10^{-5} cm to 8.70 x 10^{-5} cm, with a median value of 3.71 x 10^{-5} cm and a mean of 3.49 x 10^{-5} cm. The shape parameter ranged from -0.17 to 0.16, with a median and mean of -0.07 and -0.06, respectively. With this analysis, 9 stations showed that the non-stationary GP distribution fit was a statistical improvement over the particular station's stationary GP distribution fit.

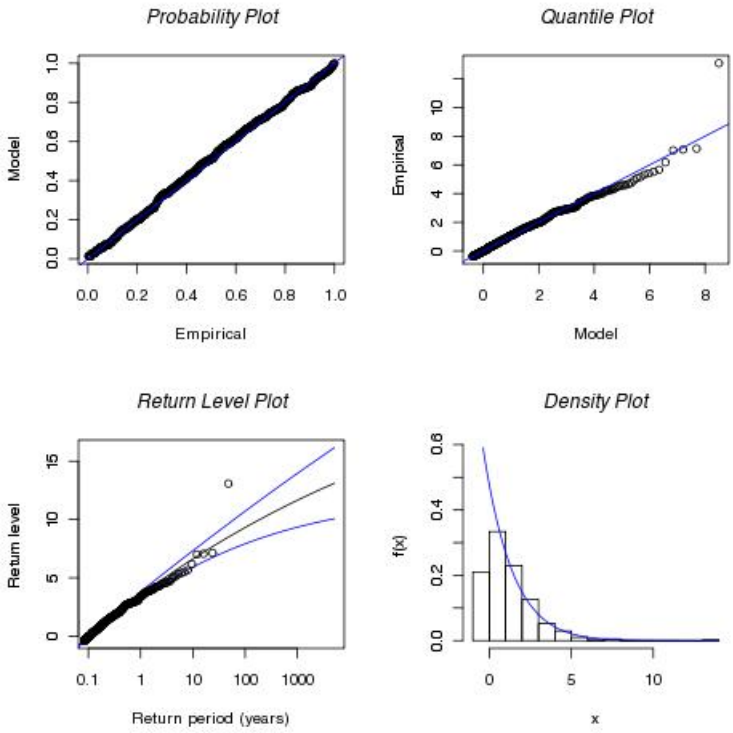

Figure 5.3: Stationary GP distribution diagnostic plots for KALB.

The non-stationary GP distribution fit very well to many of the stations cluster maxima. Most of the residual probability and quantile plots were very linear, providing confidence in the return levels produced for these stations. Figures 5.10, 5.11, 5.12 and 5.11 show the GP distribution diagnostic plots for KALB, KBTV, KBOS and KEKN, respectively. The non-stationary GP distribution fit information was used to estimate return levels for each station from estimated GP parameters for the first day of dataset (i.e. March 1st, 1961) and the last day of the dataset (i.e. October 31st, 2008).

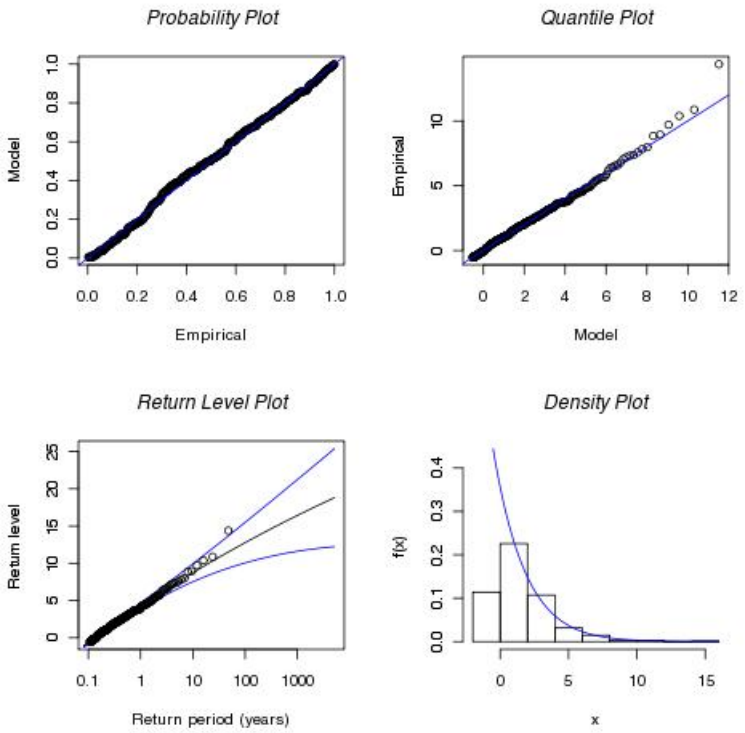

Figure 5.4: Stationary GP distribution diagnostic plots for KBOS.

Table 5.1: The table contains the estimated GP distribution parameters (scale and shape) with standard errors (in parentheses) from the stationary GP distribution fit for each station's cluster maxima.

Station	σ	ξ
KALB	1.69 (0.09)	1.69 (0.09)
KORH	2.22 (0.12)	2.22 (0.12)
KLGA	2.13 (0.11)	2.13 (0.11)
KITH	1.67 (0.11)	1.67 (0.11)
KBDL	2.33 (0.13)	2.33 (0.13)
KBDR	2.17 (0.13)	2.17 (0.13)
KPHL	2.33 (0.13)	2.33 (0.13)
KILG	2.39 (0.14)	2.39 (0.14)
KBTV	1.42 (0.07)	1.42 (0.07)
KCON	1.93 (0.12)	1.93 (0.12)
KACY	2.53 (0.19)	2.53 (0.19)
KAVP	1.62 (0.09)	1.62 (0.09)
KERI	1.42 (0.07)	1.42 (0.07)
KSYR	1.58 (0.07)	1.58 (0.07)
KEKN	1.24 (0.08)	1.24 (0.08)
KDCA	2.47 (0.17)	2.47 (0.17)
KBGM	1.46 (0.08)	1.46 (0.08)
KROC	1.3 (0.08)	1.3 (0.08)
KPVD	2.33 (0.14)	2.33 (0.14)
KNHZ	2.22 (0.14)	2.22 (0.14)
KCRW	1.93 (0.11)	1.93 (0.11)
KPIT	1.58 (0.08)	1.58 (0.08)
KBOS	2.25 (0.14)	2.25 (0.14)
KNXX	2.46 (0.13)	2.46 (0.13)
KABE	1.96 (0.12)	1.96 (0.12)
KIPT	2.44 (0.16)	2.44 (0.16)
KEWR	2.49 (0.14)	2.49 (0.14)
KBUF	1.27 (0.06)	1.27 (0.06)
KBWI	2.51 (0.15)	2.51 (0.15)
KCLE	1.36 (0.07)	1.36 (0.07)

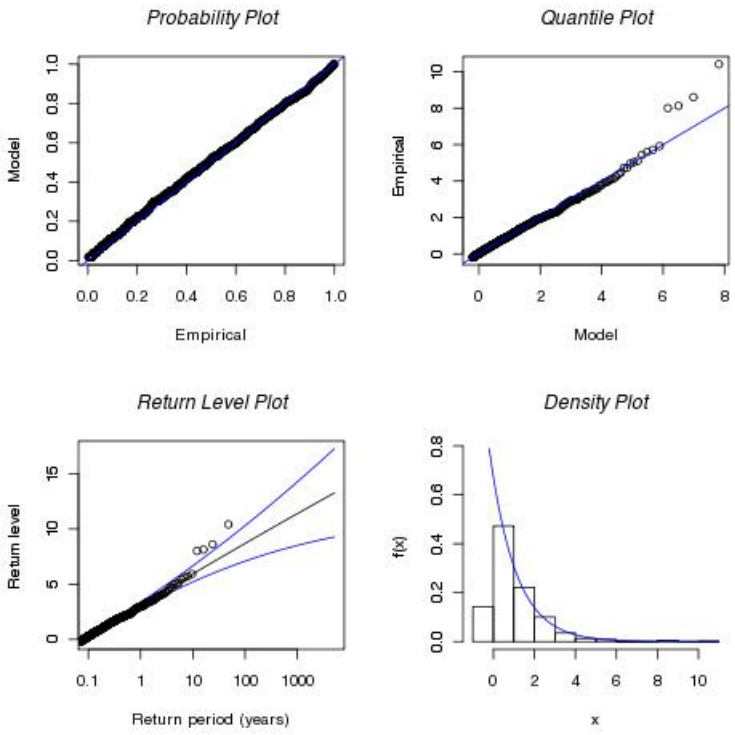

Figure 5.5: Stationary GP distribution diagnostic plots for KBUF.

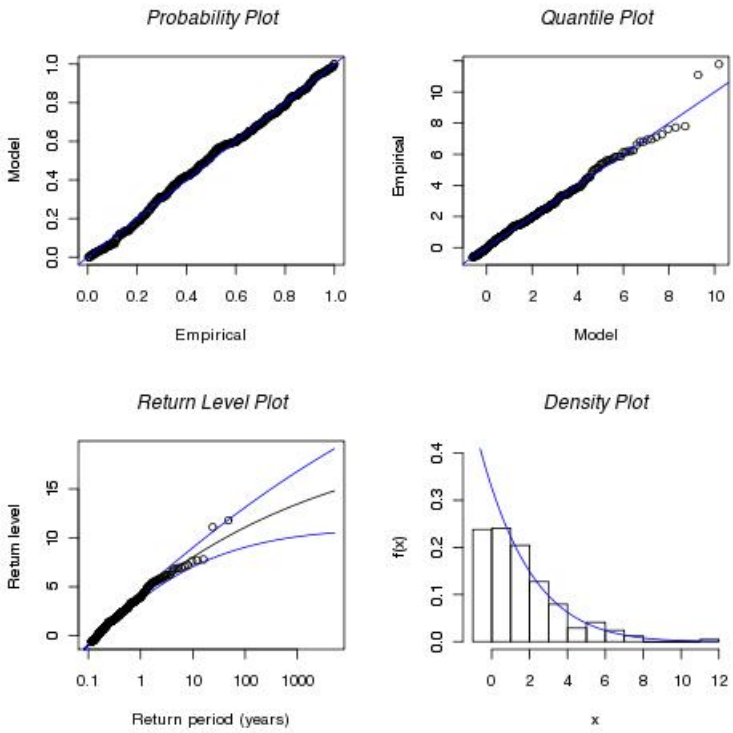

Figure 5.6: Stationary GP distribution diagnostic plots for KIPT.

Table 5.2: The table contains the 2-year, 10-year and 20-year return levels estimated from the stationary GP distribution fits for each station's cluster maxima.

Station	2-yr	10-yr	20-yr
KALB	4.87	7	7.85
KORH	6.09	8.35	9.2
KLGA	6.67	9.68	10.93
KITH	4.68	7.37	8.52
KBDL	6.47	9.46	10.67
KBDR	6.65	10.02	11.45
KPHL	6.09	8.88	9.98
KILG	6.26	9.41	10.68
KBTV	3.72	5.12	5.65
KCON	4.66	6.87	7.73
KACY	5.56	8.34	9.39
KAVP	4.96	7.38	8.4
KERI	4.4	6.45	7.3
KSYR	4.5	6.2	6.85
KEKN	5.02	8.78	10.72
KDCA	5.69	8.55	9.65
KBGM	4.44	6.47	7.3
KROC	3.78	5.66	6.44
KPVD	6.6	9.63	10.86
KNHZ	6.41	9.71	11.09
KCRW	5.06	7.48	8.44
KPIT	4.35	6.3	7.07
KBOS	6.16	9.24	10.5
KNXX	6.8	9.64	10.74
KABE	6.01	9.19	10.57
KIPT	5.99	8.63	9.63
KEWR	7.67	11.41	12.99
KBUF	4.17	6.13	6.97
KBWI	6.55	9.44	10.57
KCLE	4.06	5.75	6.43

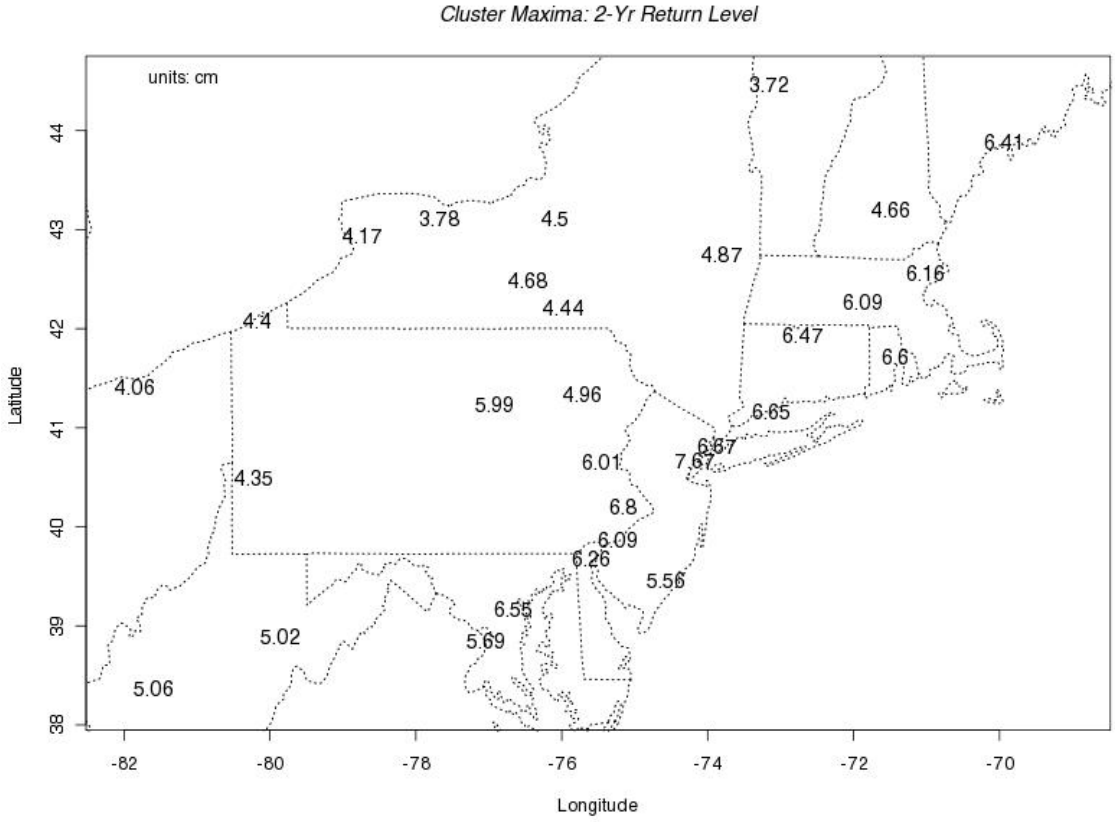

Figure 5.7: A spatial map of the 2-year return levels estimated from each station's stationary GP distribution fit. The return level values tend to increase from west to east.

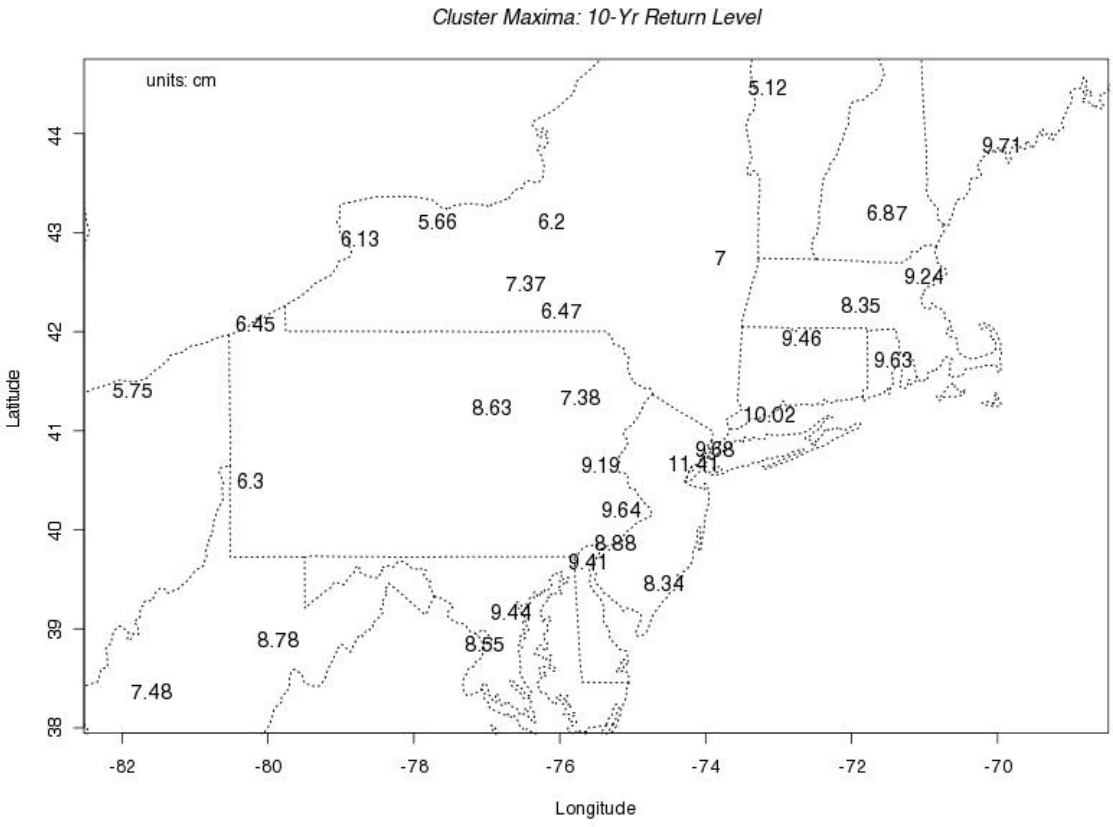

Figure 5.8: A spatial map of the 10-year return levels estimated from each station's stationary GEV distribution fit.

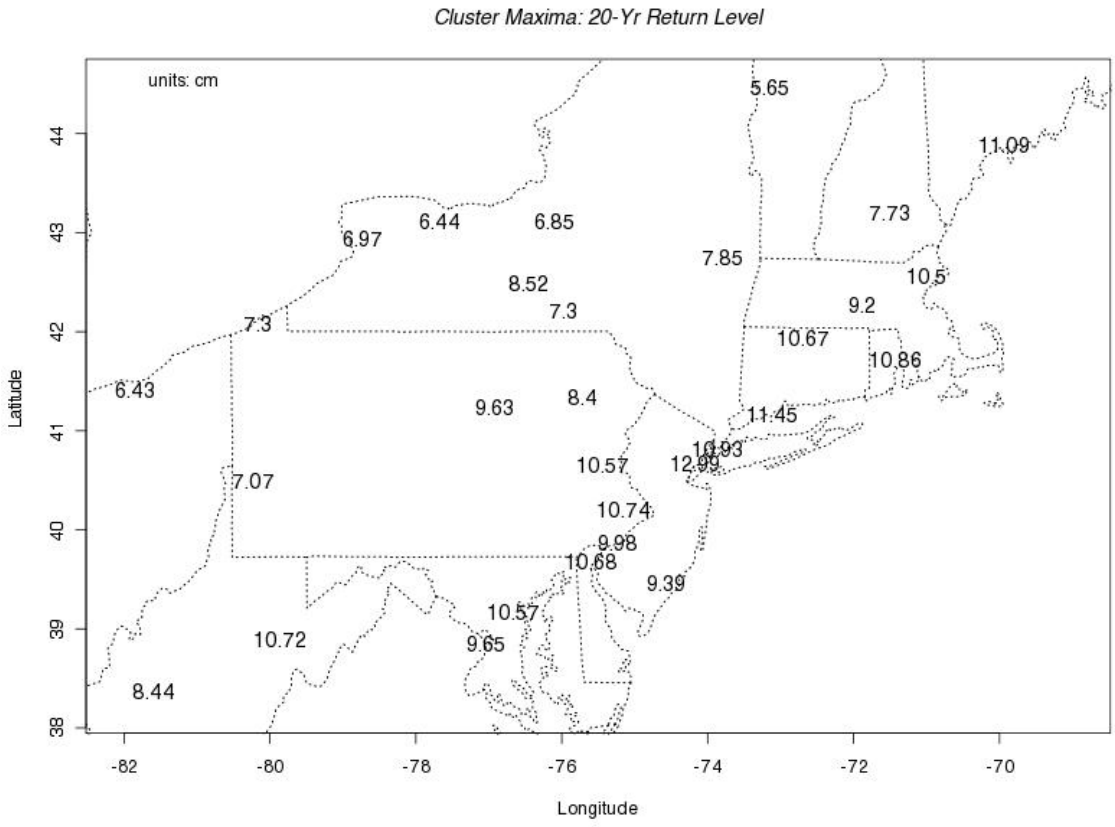

Figure 5.9: A spatial map of the 20-year return levels estimated from each station's stationary GEV distribution fit.

Table 5.3: The table contains the estimated non-stationary GP distribution parameters with standard errors. (* - statistically significant)

Station	d_0	d_1	ξ	α
KALB	1.48 (0.09)	$3.83e-05$ $(2e-06)$	−0.08 (0.03)	0.067
KORH	1.99 (0.12)	$4.22e-05$ $(2e-06)$	−0.12 (0.04)	0.083
KLGA	1.79 (0.11)	$6.13e-05$ $(2e-06)$	−0.05 (0.04)	0.013*
KITH	1.29 (0.11)	$6.5e-05$ $(2e-06)$	0.01 (0.04)	0.007*
KBDL	2.03 (0.13)	$5.25e-05$ $(2e-06)$	−0.07 (0.03)	0.086
KBDR	2.13 (0.13)	$6e-06$ $(2e-06)$	−0.01 (0.04)	0.833
KPHL	2.11 (0.13)	$4.31e-05$ $(2e-06)$	−0.09 (0.03)	0.144
KILG	2.05 (0.14)	$6.09e-05$ $(2e-06)$	−0.07 (0.04)	0.064
KBTV	1.09 (0.07)	$6.57e-05$ $(2e-06)$	−0.17 (0.03)	0*
KCON	1.59 (0.12)	$6.65e-05$ $(2e-06)$	−0.14 (0.04)	0.013*
KACY	2.42 (0.18)	$1.78e-05$ $(2e-06)$	−0.11 (0.05)	0.609
KAVP	1.31 (0.09)	$5.81e-05$ $(2e-06)$	−0.04 (0.03)	0.005*
KERI	1.32 (0.07)	$1.85e-05$ $(2e-06)$	−0.03 (0.03)	0.336
KSYR	1.39 (0.07)	$3.09e-05$ $(2e-06)$	−0.09 (0.02)	0.083
KEKN	1.24 (0.08)	$4e-07$ $(2e-06)$	0.16 (0.05)	0.979
KDCA	2.46 (0.17)	$2.9e-06$ $(2e-06)$	−0.1 (0.04)	0.928
KBGM	1.34 (0.08)	$2.01e-05$ $(2e-06)$	−0.04 (0.03)	0.218
KROC	0.89 (0.07)	$6.77e-05$ $(2e-06)$	−0.03 (0.04)	0*
KPVD	2.13 (0.14)	$3.08e-05$ $(2e-06)$	−0.05 (0.04)	0.268
KNHZ	1.75 (0.13)	$8.69e-05$ $(2e-06)$	−0.05 (0.04)	0.006*
KCRW	2.15 (0.11)	$-3.14e-05$ $(2e-06)$	−0.08 (0.03)	0.185
KPIT	1.54 (0.08)	$7.6e-06$ $(2e-06)$	−0.07 (0.02)	0.698
KBOS	1.89 (0.14)	$6.53e-05$ $(2e-06)$	−0.06 (0.04)	0.028*
KNXX	2.33 (0.13)	$2.26e-05$ $(2e-06)$	−0.08 (0.03)	0.431
KABE	1.67 (0.11)	$5.21e-05$ $(2e-06)$	−0.01 (0.04)	0.06
KIPT	2.16 (0.16)	$5.2e-05$ $(2e-06)$	−0.12 (0.04)	0.112
KEWR	2.53 (0.14)	$-5.8e-06$ $(2e-06)$	−0.02 (0.03)	0.847
KBUF	1.34 (0.06)	$-1.16e-05$ $(2e-06)$	−0.01 (0.03)	0.458
KBWI	2.33 (0.15)	$2.69e-05$ $(2e-06)$	−0.08 (0.04)	0.381
KCLE	1.16 (0.07)	$3.59e-05$ $(2e-06)$	−0.07 (0.03)	0.02*

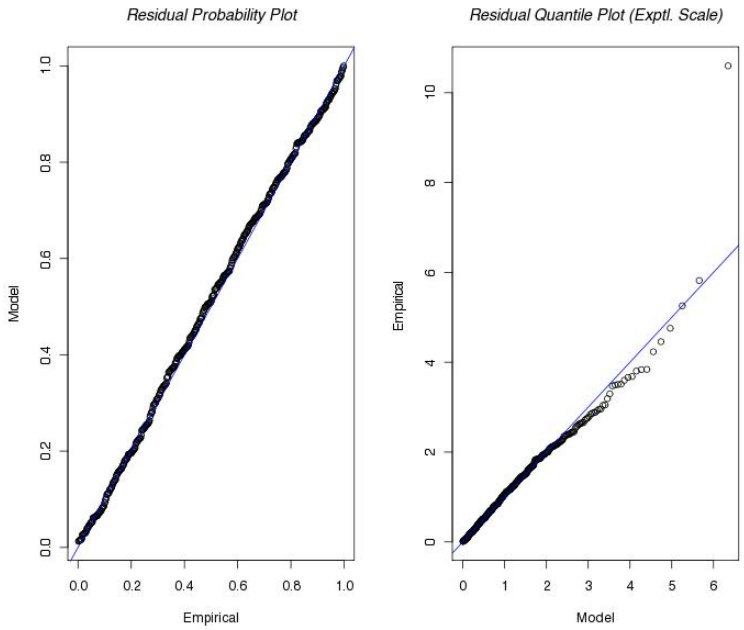

Figure 5.10: Non-stationary GP distribution diagnostic plots for KALB.

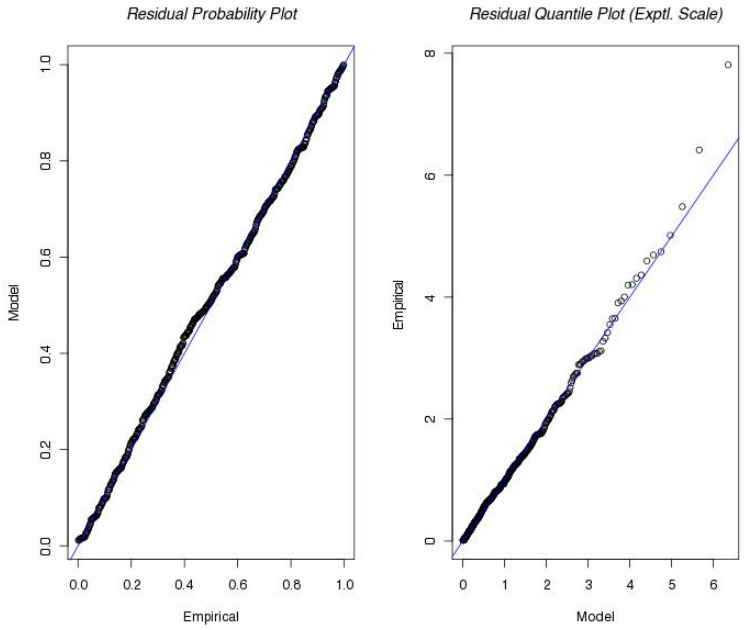

Figure 5.11: Non-stationary GP distribution diagnostic plots for KBTV.

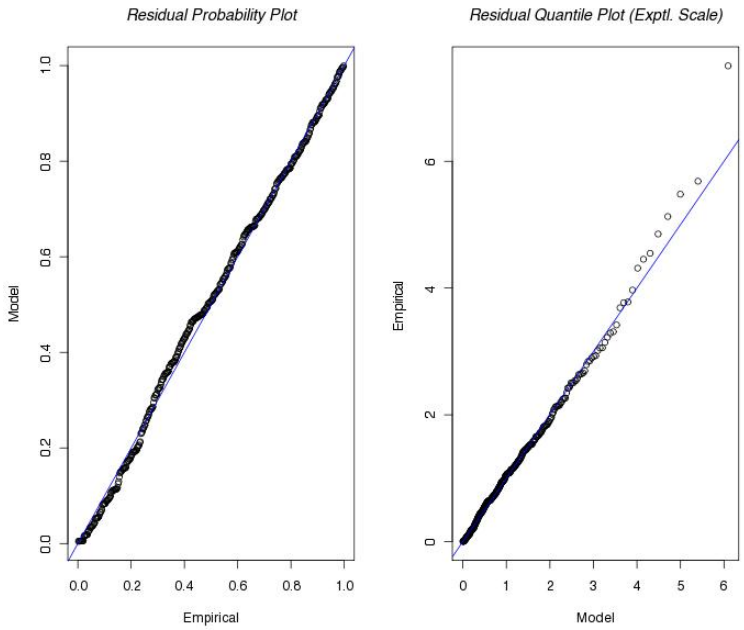

Figure 5.12: Non-stationary GP distribution diagnostic plots for KBOS.

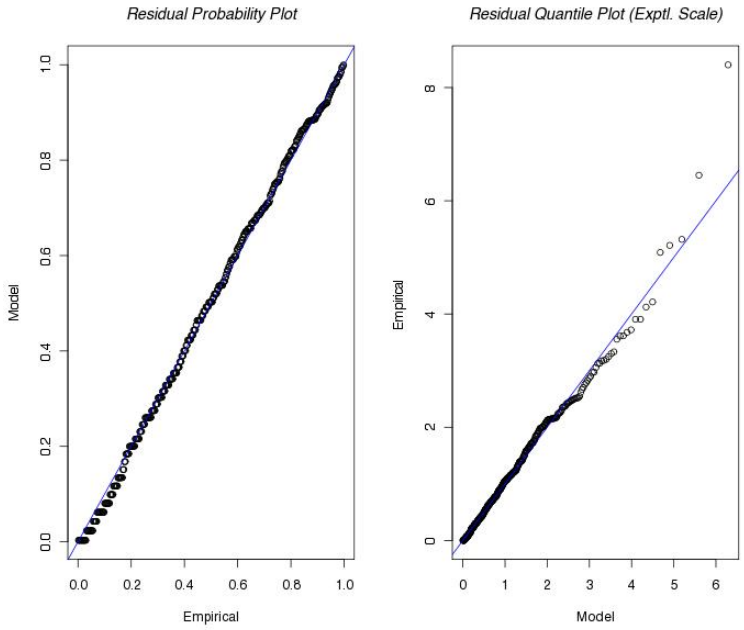

Figure 5.13: Non-stationary GP distribution diagnostic plots for KEKN.

Table 5.4: Table contains 2-year, 10-year, and 20-year return levels estimated from the non-stationary GP distribution parameters. (* - statistically significant)

	Return Level (cm)					
	From 1961 GP parameters			From 2008 GP parameters		
Station	2-yr	10-yr	20-yr	2-yr	10-yr	20-yr
KALB	4.17	5.94	6.64	5.44	7.75	8.66
KORH	5.39	7.36	8.1	6.74	9.2	10.13
KLGA*	5.45	7.8	8.76	7.65	10.95	12.29
KITH*	3.66	5.78	6.7	5.82	9.21	10.67
KBDL	5.53	8.02	9.01	7.21	10.46	11.74
KBDR	6.54	9.84	11.25	6.75	10.17	11.62
KPHL	5.42	7.85	8.79	6.72	9.74	10.91
KILG	5.29	7.87	8.89	7.14	10.61	11.99
KBTV*	2.69	3.6	3.92	4.59	6.14	6.69
KCON*	3.64	5.23	5.81	5.43	7.79	8.66
KACY	5.33	8	9.01	5.79	8.69	9.79
KAVP*	3.88	5.69	6.44	5.91	8.67	9.8
KERI	4.07	5.95	6.74	4.74	6.94	7.85
KSYR	3.99	5.53	6.12	5.04	6.97	7.72
KEKN	5.01	8.77	10.71	5.03	8.8	10.75
KDCA	5.65	8.48	9.58	5.72	8.6	9.71
KBGM	4.07	5.92	6.68	4.79	6.97	7.86
KROC*	2.59	3.85	4.38	4.89	7.29	8.28
KPVD	6.08	8.9	10.04	7.11	10.41	11.75
KNHZ*	4.88	7.26	8.22	7.73	11.49	13.02
KCRW	5.54	8.12	9.13	4.59	6.73	7.56
KPIT	4.22	6.08	6.82	4.46	6.44	7.22
KBOS*	5.06	7.49	8.47	7.11	10.53	11.91
KNXX	6.43	9.11	10.16	7.16	10.15	11.31
KABE	5.02	7.59	8.69	6.86	10.38	11.87
KIPT	5.18	7.4	8.22	6.65	9.49	10.55
KEWR	7.78	11.57	13.16	7.57	11.26	12.81
KBUF	4.39	6.43	7.29	3.94	5.78	6.56
KBWI	6.12	8.86	9.93	6.95	10.06	11.27
KCLE*	3.39	4.77	5.32	4.63	6.51	7.25

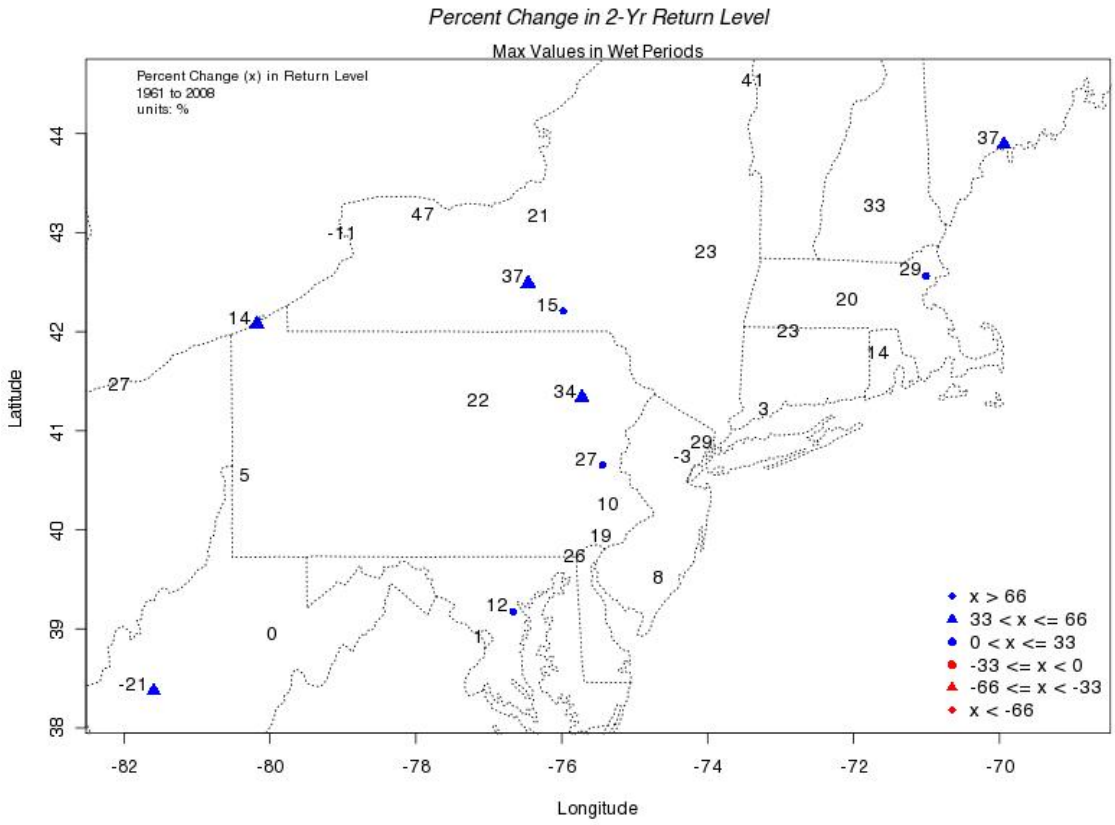

Figure 5.14: A spatial map of the percent change in the estimated 2-year return levels from 1961 to 2008 for each station's non-stationary GP distribution fit. Stations with statistical significance are marked by symbols (triangles, diamonds, circles) next to numbers.

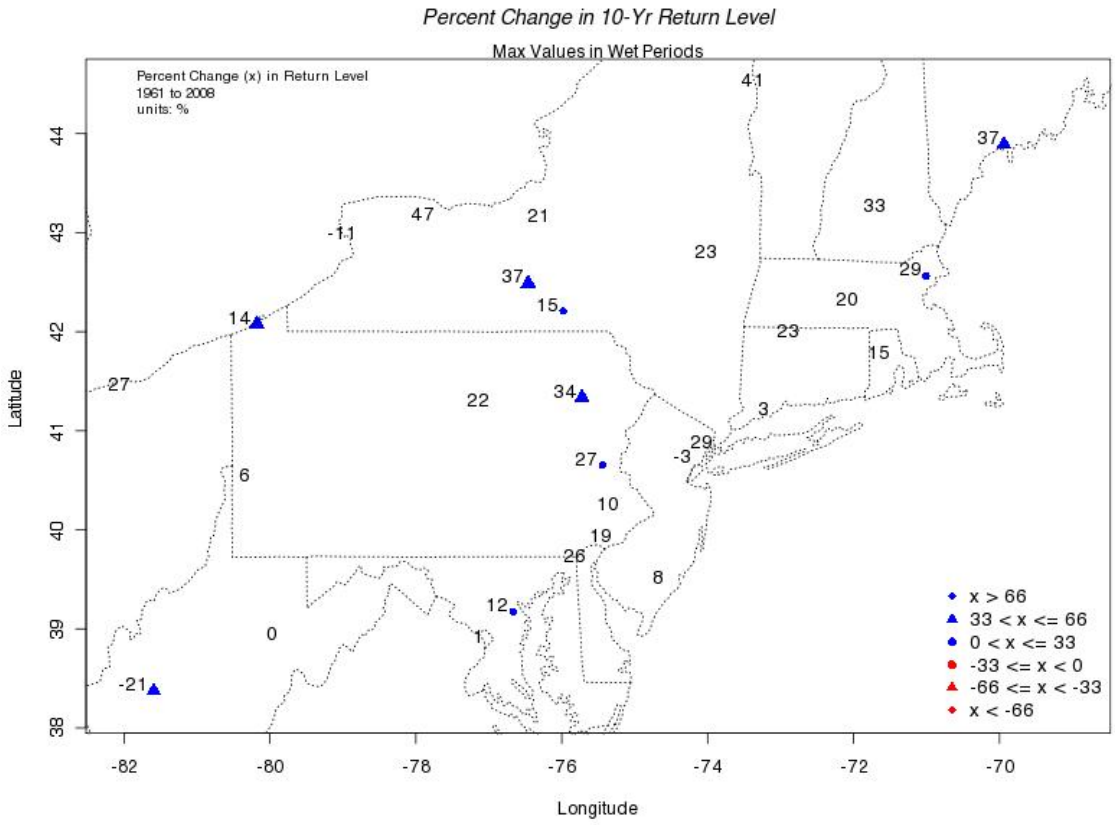

Figure 5.15: A spatial map of the percent change in the estimated 10-year return levels from 1961 to 2008 for each station's non-stationary GP distribution fit. Stations with statistical significance are marked by symbols (triangles, diamonds, circles) next to numbers.

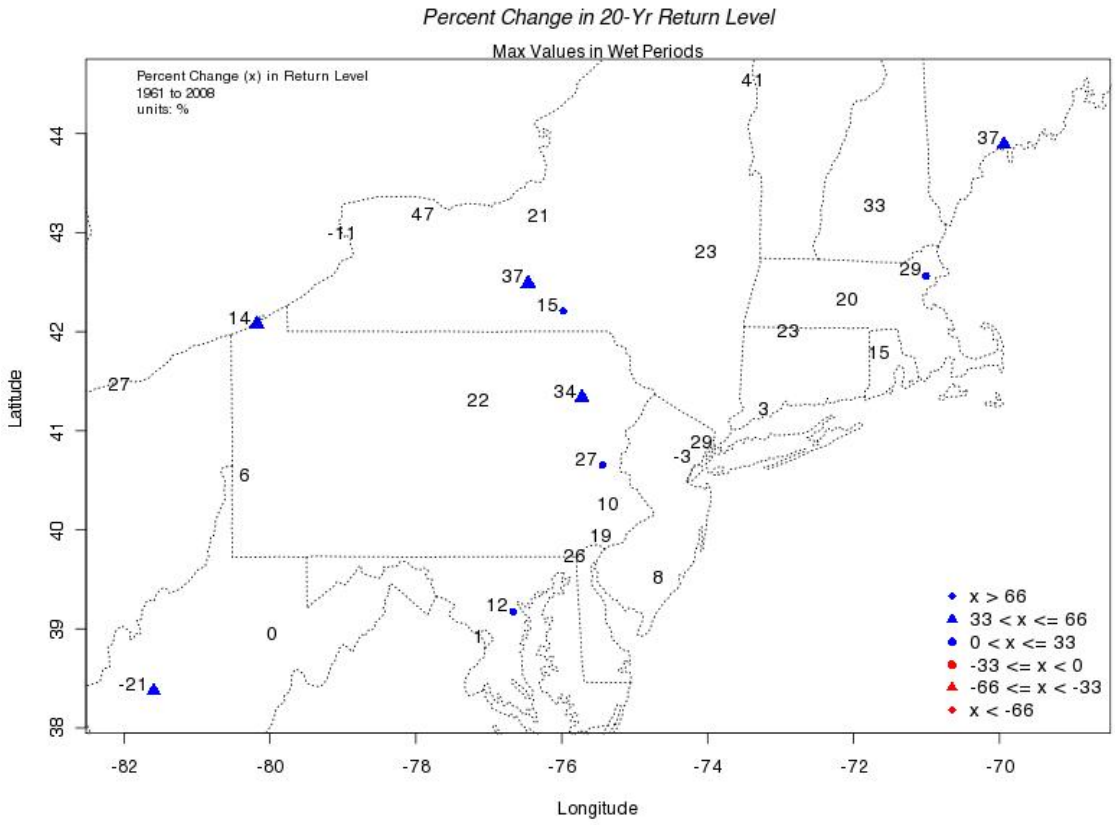

Figure 5.16: A spatial map of the percent change in the estimated 20-year return levels from 1961 to 2008 for each station's non-stationary GP distribution fit. Stations with statistical significance are marked by symbols (triangles, diamonds, circles) next to numbers

Table 5.4 shows the 2-year, 10-year and 20-year return levels for the first day of 1961 and the last day of 2008 for each station's cluster maxima calculated from each station's non-stationary GP distribution fit. A total of 27 individual stations showed an increase in the 2-year, 10-year and 20-year estimated return levels from 1961 to 2008. For example, KITH saw an increase in the estimated return levels of 2.16 cm, where the 1961 2-year return level was estimated to be 3.66 cm but with the 2008 GP parameters, it was estimated to be 5.82 cm. KBTV's 1961 10-year return level was estimated to be 3.60 cm, but in 2008 it was estimated to be 6.14 cm. As well, KBOS's 1961 20-year return level was estimated to be 8.47 cm, but in 2008 it was estimated to be 11.91 cm.

CHAPTER 6

DURATION GEV RESULTS

6.1 Stationary GEV distribution fit to Wet Period Duration Block Maxima

As mentioned in the methods section, stationary GEV distributions were fit to the wet period duration block maxima of each station. Table 6.1 shows the estimated GEV location, scale and shape parameters with standard errors (in parentheses) for each stations GEV distribution fit. Note that the GEV parameters for KEKN were excluded from this analysis due to a poor GEV distribution fit. The ranges of values for the location, scale and shape parameters were 11.68 days to 21.52 days, 3.39 days to 9.46 days and -0.42 to 0.14, respectively. The medians of the location, scale and shape parameters were 15.04 days, 5.68 days and -0.05, respectively. The means for the location, scale and shape parameters were 15.62 days, 5.75 days and -0.07, respectively. The spatial plots of the location, scale and shape parameters are shown in Figures 6.1, 6.2, and 6.3.

Generally, the stationary GEV distributions fit well to the each stations block maxima. Diagnostic plots produced from the stationary GEV distribution fits for KALB, KABE, KBUF and KBWI are shown in Figures 6.4, 6.5, 6.6, and 6.7 as examples of this. The probability and quantile plots for these stations were very linear, with only a few outliers. This was the case for the rest of the stations in the block maxima analysis except for KEKN. The stationary GEV distribution fit information was used to estimate return levels for each station. Table 6.2 shows the 2-year, 10-year and 20-year return levels for each stations block maxima

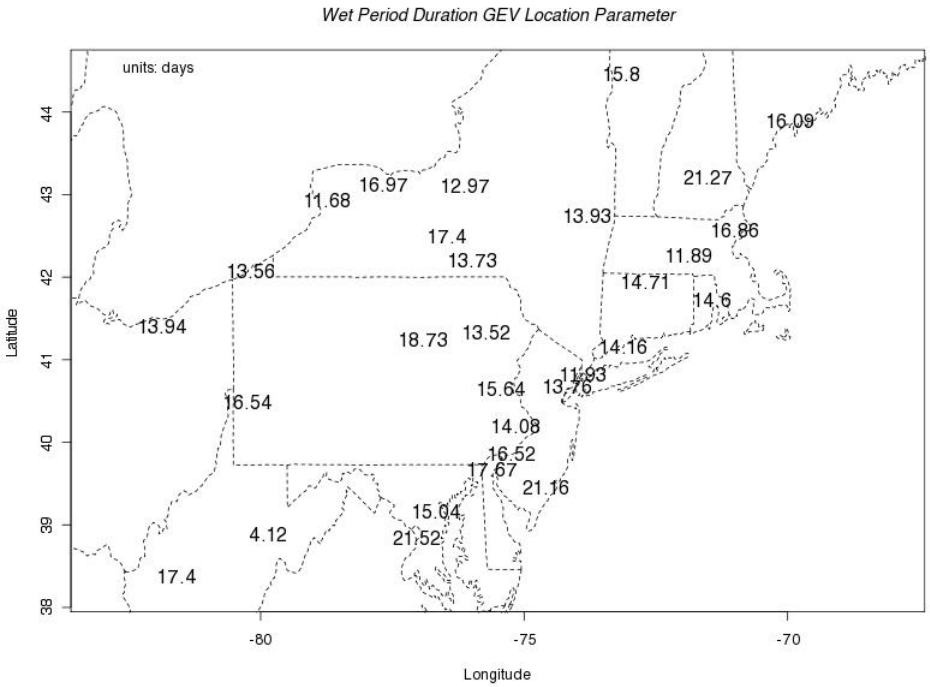

Figure 6.1: Stationary GEV location parameters spatial plot. There is no particular pattern with the location parameter.

calculated from the each stations GEV distribution fit.

The stationary GEV distribution fit information was used to estimate return levels for each station. Table 6.2 shows the 2-year, 10-year and 20-year return levels for each stations wet period duration block maxima calculated from the each stations GEV distribution fit. The ranges of values for the 2-year, 10-year and 20-year return levels were 12.89 days to 24.73 days, 18.19 days to 44.99 days and 19.86 days to 53.79 days, respectively. The medians for the 2-year, 10-year and 20-year return levels were 16.91 days, 27.15 days and 30.75 days, respectively. The means for these return levels were 17.71 days, 27.74 days and 31.35 days, respectively. The 2-year, 10-year and 20-year return levels are shown spatially in Figures 6.8, 6.9 and 6.10.

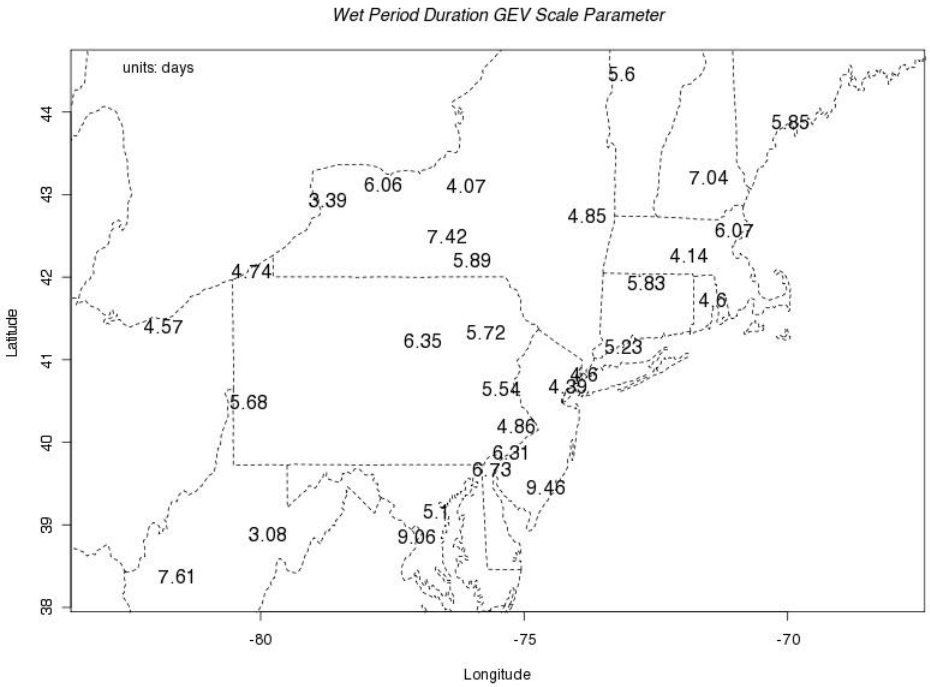

Figure 6.2: Stationary GEV scale parameters spatial plot. There is no particular pattern with the scale parameter.

6.2 Stationary GEV distribution fit to Dry Period Duration Block Maxima

Stationary GEV distributions were fit to the dry period duration block maxima of each station as well. Table 6.3 shows the estimated GEV location, scale and shape parameters with standard errors (in parentheses) for each stations GEV distribution fit. Spatial plots were also produced for location, scale and shape parameters, as shown in Figures 6.11, 6.12, and 6.13. As in the case of the wet duration, KEKN dry period duration GEV results were excluded due to a poor GEV fit. The ranges of values for the location, scale and shape parameters were 17.05 days to 30.41 days, 7.66 days to 32.15 days and -0.16 to 0.56, respectively. The medians of the location, scale and shape parameters were 23.49 days, 19.17

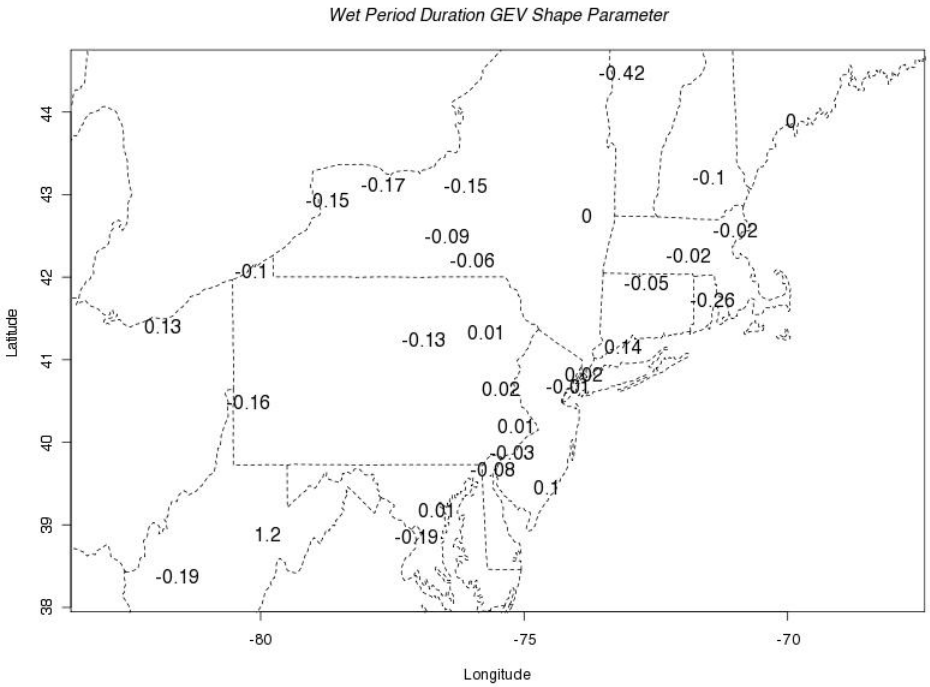

Figure 6.3: Stationary GEV shape parameters spatial plot. There is no particular pattern with the shape parameter.

days and 0.05, respectively. The means for the location, scale and shape parameters were 23.60 days, 18.39 days and 0.10, respectively.

Generally, the stationary GEV distributions fit well to the each stations dry period block maxima. Diagnostic plots produced from the stationary GEV distribution fits for KALB, KABE, KBUF and KBWI are shown in Figures 6.15, 6.15, 6.16 and 6.17 as examples of this. The probability and quantile plots for these stations were very linear, with only a few outliers. This was the case for the majority of stations in the block maxima analysis. The stationary GEV distribution fit information was used to estimate return levels for each station. Table 6.2 shows the 2-year, 10-year and 20-year return levels for each stations block maxima calculated from the each stations GEV distribution fit.

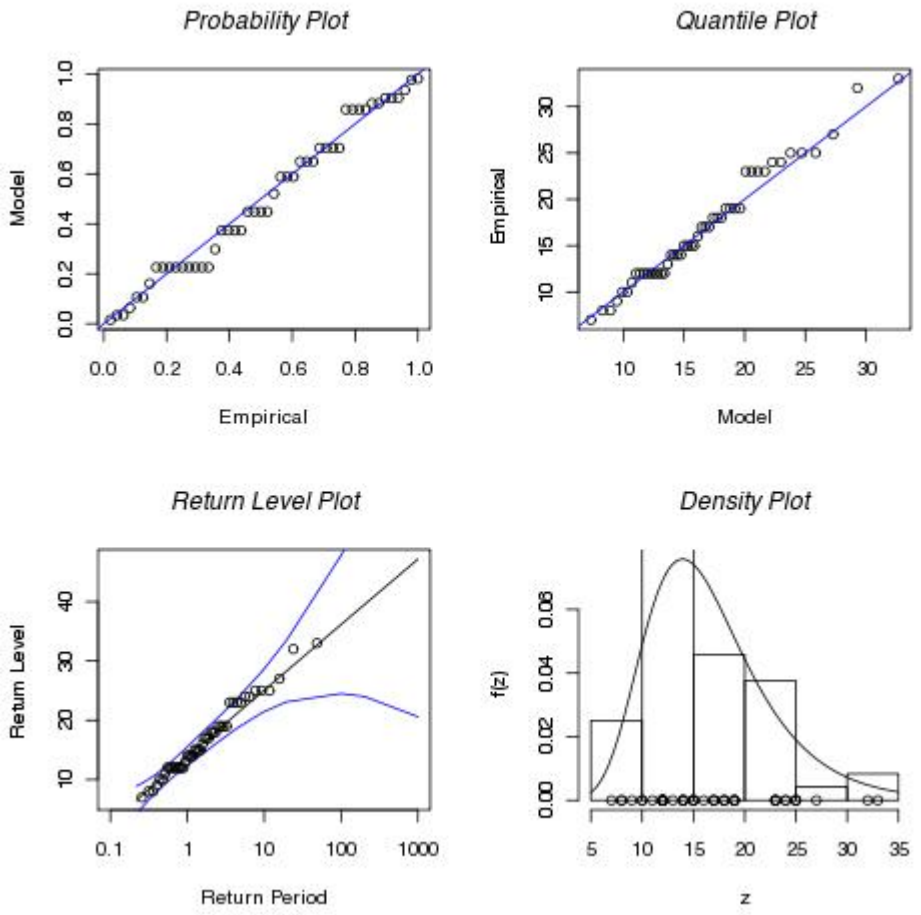

Figure 6.4: Stationary wet period duration GEV distribution diagnostic plots for KALB.

The stationary GEV distribution fit information was used to estimate return levels for each station. Table 6.2 shows the 2-year, 10-year and 20-year return levels for each stations dry period duration block maxima calculated from the each stations GEV distribution fit. The ranges of values for the 2-year, 10-year and 20-year return levels were 19.83 days to 30.61 days, 33.25 days to 73.68 days and 38.02 to 89.32, respectively. The median values were 30.49 days, 72.60 days and 93.30, respectively. The medians were 30.61 days, 73.68 days and 89.32.

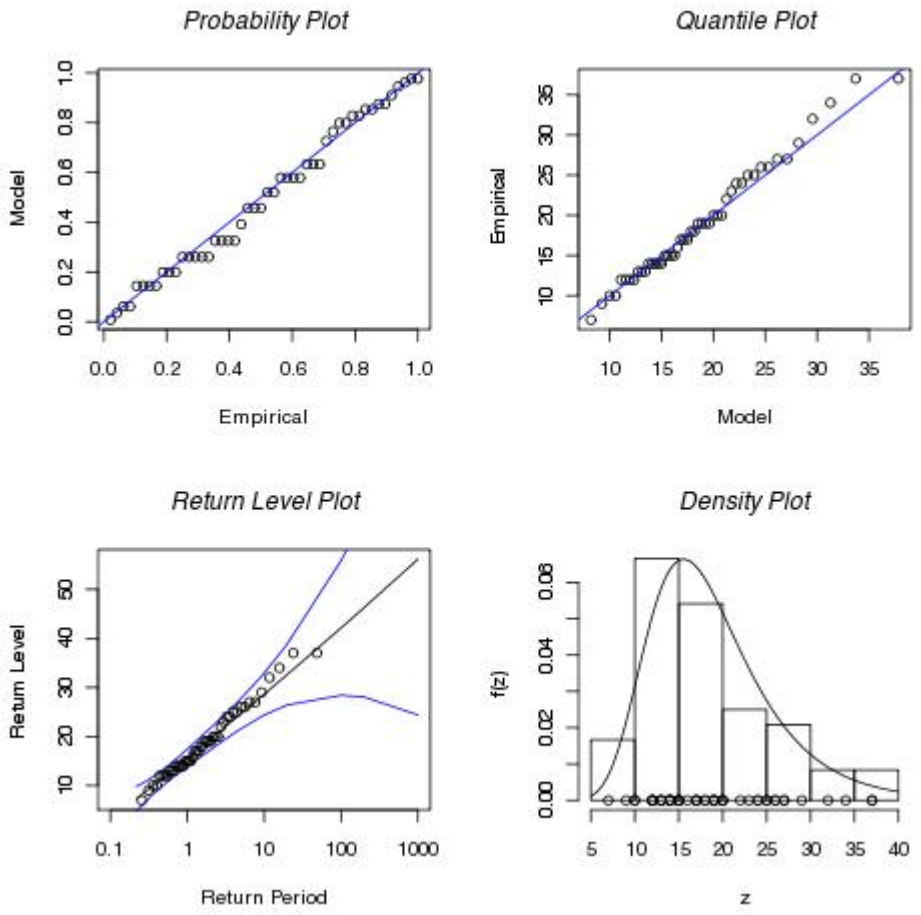

Figure 6.5: Stationary wet period duration GEV distribution diagnostic plots for KABE.

6.3 Non-stationary GEV Wet Period Duration Block Maxima

Non-stationary GEV distributions were fit to each stations wet period block maxima duration and the parameter results of these analyses are shown in table 6.5. For the non-stationary GEV distributions, the location parameter was modeled to change linearly with time ($\mu(t) = b_0 + b_1 t$) and the scale parameter was modeled to change log-normally with time $\ln(\sigma(t) = c_0 + c_1 t)$. Specifically, the estimated location intercept (b_0) and its slope (b_1), the log-normally transformed

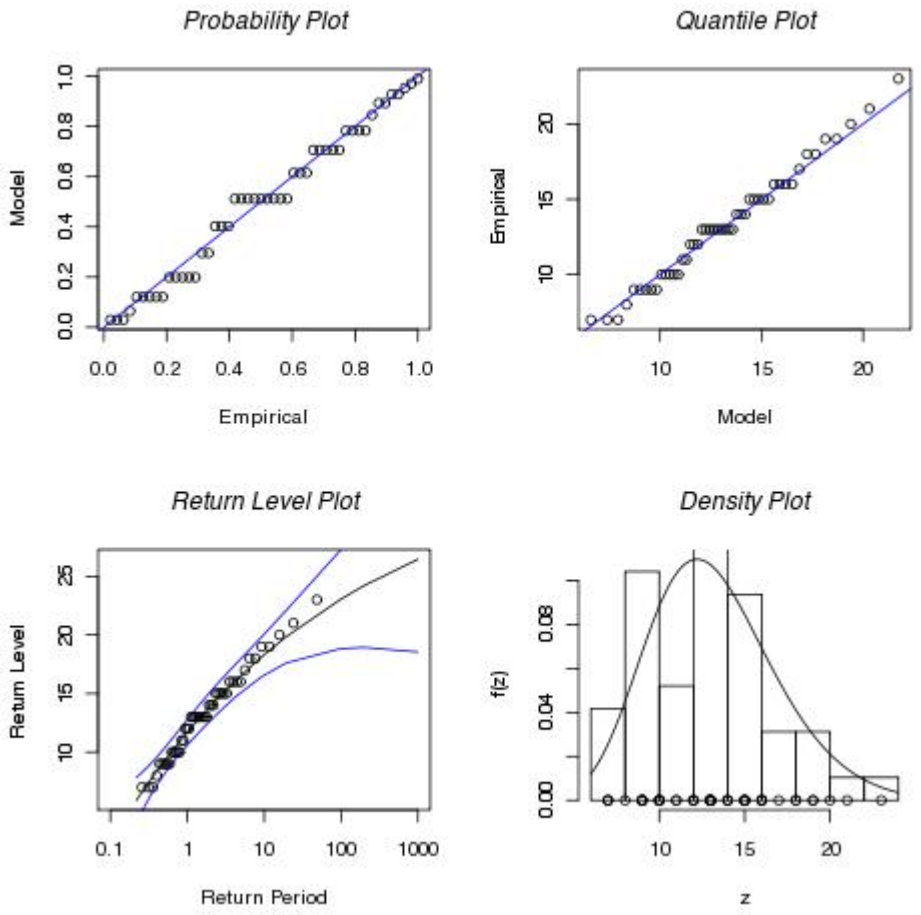

Figure 6.6: Stationary wet period duration GEV distribution diagnostic plots for KBUF.

scale intercept (c_0) and its slope (c_1), and the shape parameters with standard errors are shown for each station. Table 6.5 also shows the p-value results from a likelihood ratio test (LRT) performed to test the statistical significance of the non-stationary GEV distribution fit over the stationary GEV fit for each station.

From the analysis, there were only 3 stations with a non-stationary GEV distribution fit that was a statistical improvement over its stationary partner. These stations were KPIT, KNXX, and KAVP, all of which are spread out across the region of analysis. There were also 24 stations within this analysis that had neg-

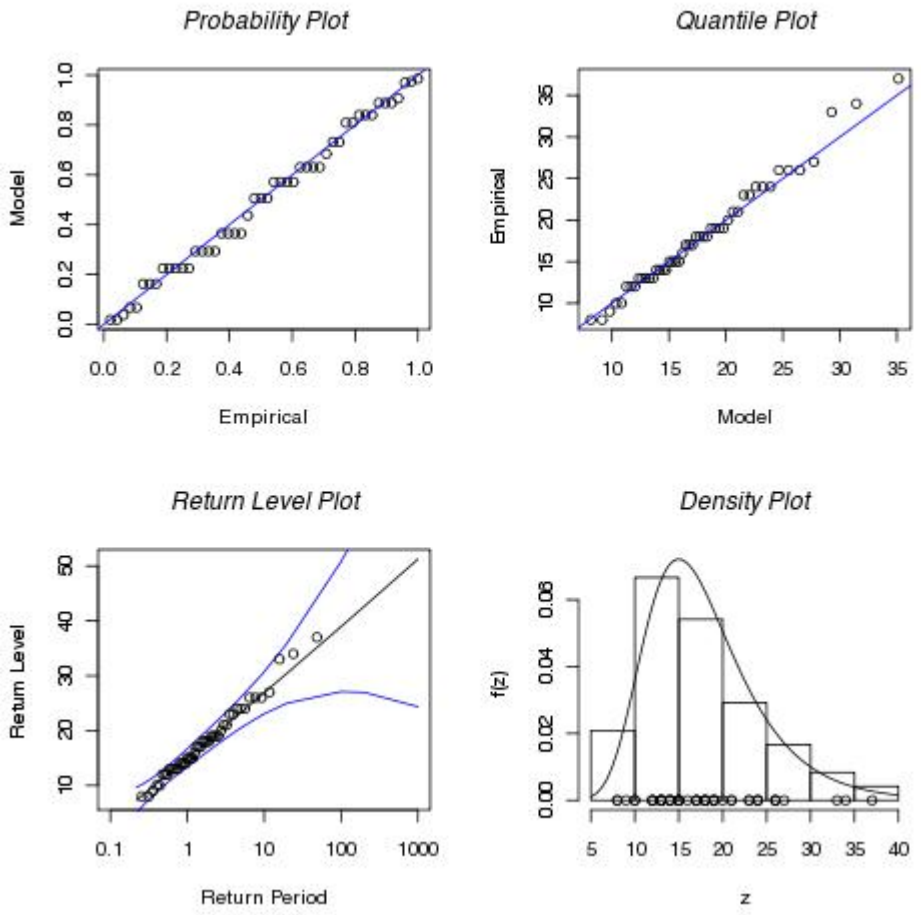

Figure 6.7: Stationary wet period duration GEV distribution diagnostic plots for KBWI.

ative shape values, signifying a bounded right tail of the GEV distribution for each of these stations.

In terms of the location trend parameter, b_1, there were a total of 11 stations that had positive values for this signifying a positive trend in the location parameter. There were 18 stations having negative values thus signifying negative trends. The highest positive trend value was roughly 0.10 days from KCON. The lowest negative trend value came from KPIT with -0.17 days. In terms of the scale trend parameter, c_1, noting that values in Table 6.5 are the log trans-

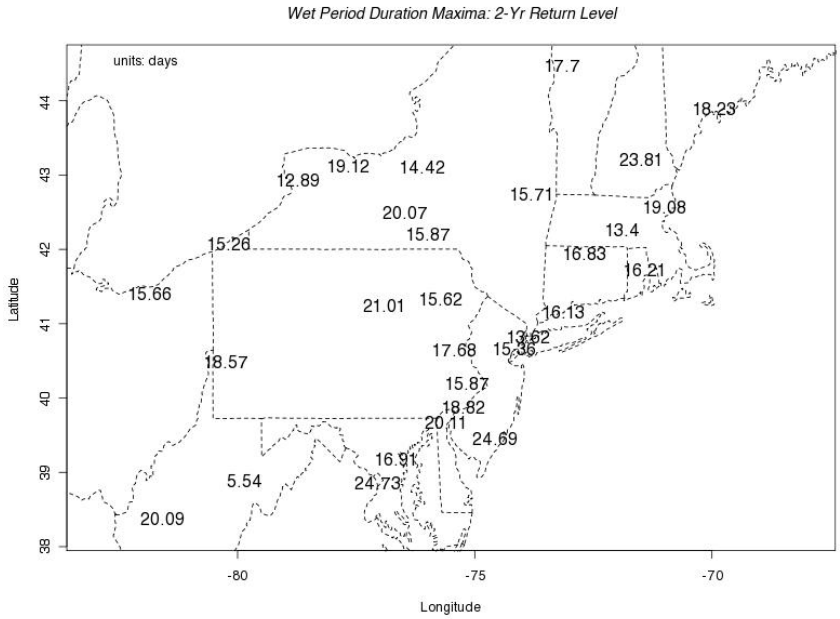

Figure 6.8: A spatial map of the 2-year return levels estimated from each stations GEV distribution fit.

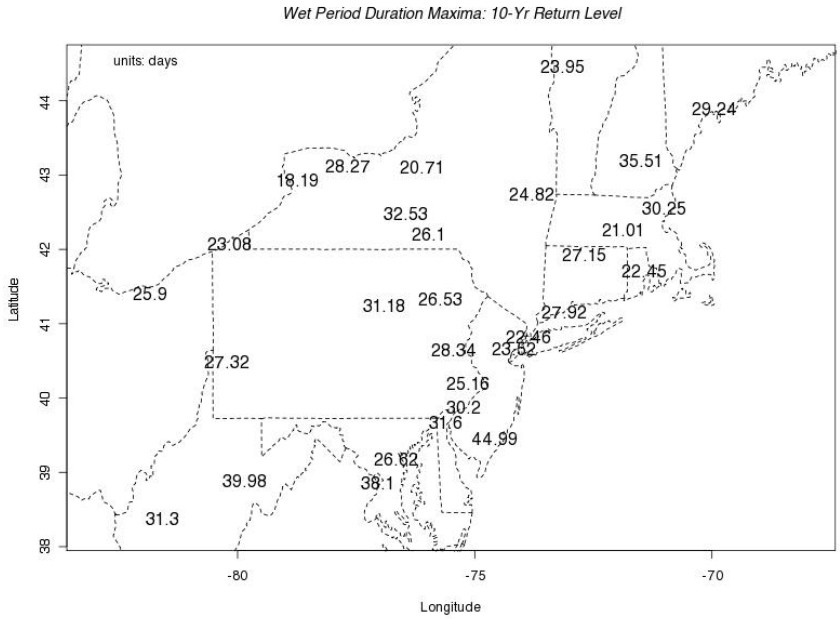

Figure 6.9: A spatial map of the 10-year return levels estimated from each stations GEV distribution fit.

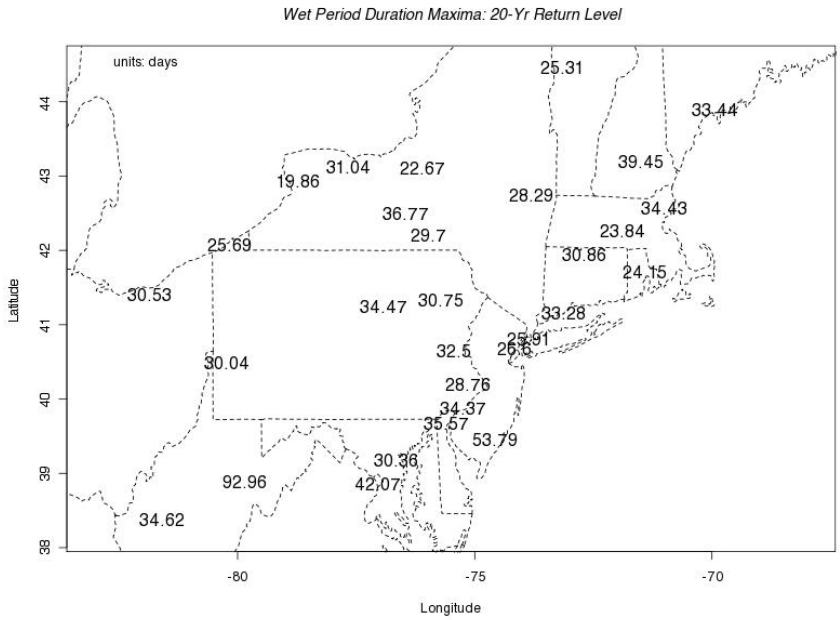

Figure 6.10: A spatial map of the 20-year return levels estimated from each stations GEV distribution fit.

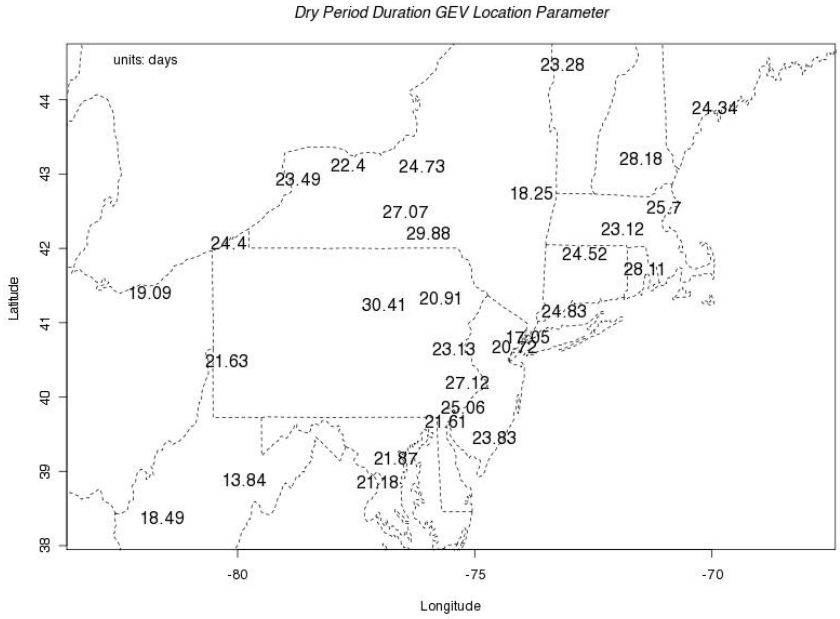

Figure 6.11: Stationary GEV location parameters spatial plot for dry periods maxima duration. There is no particular pattern with the location parameter.

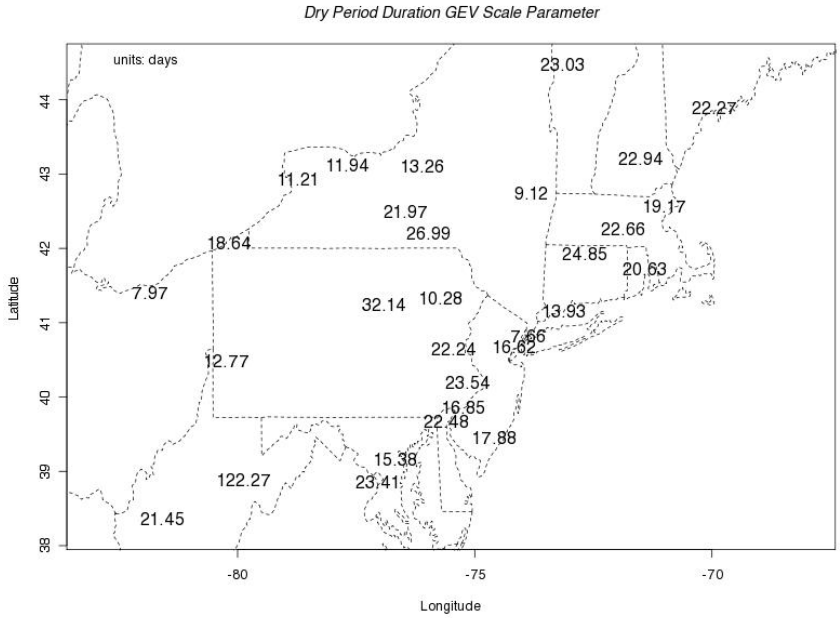

Figure 6.12: Stationary GEV scale parameters spatial plot for dry periods maxima duration. There is no particular pattern with the location parameter.

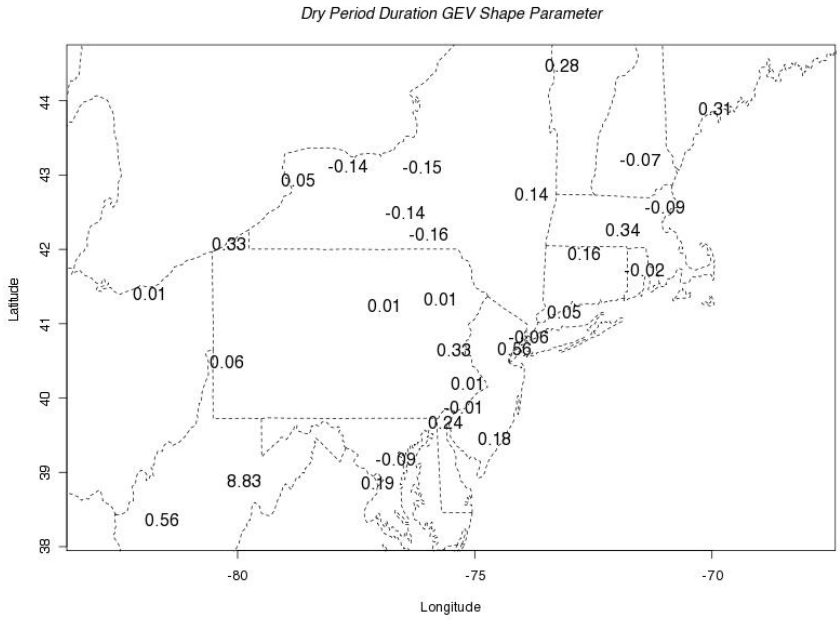

Figure 6.13: Stationary GEV shape parameters spatial plot for dry periods maxima duration. There is no particular pattern with the location parameter.

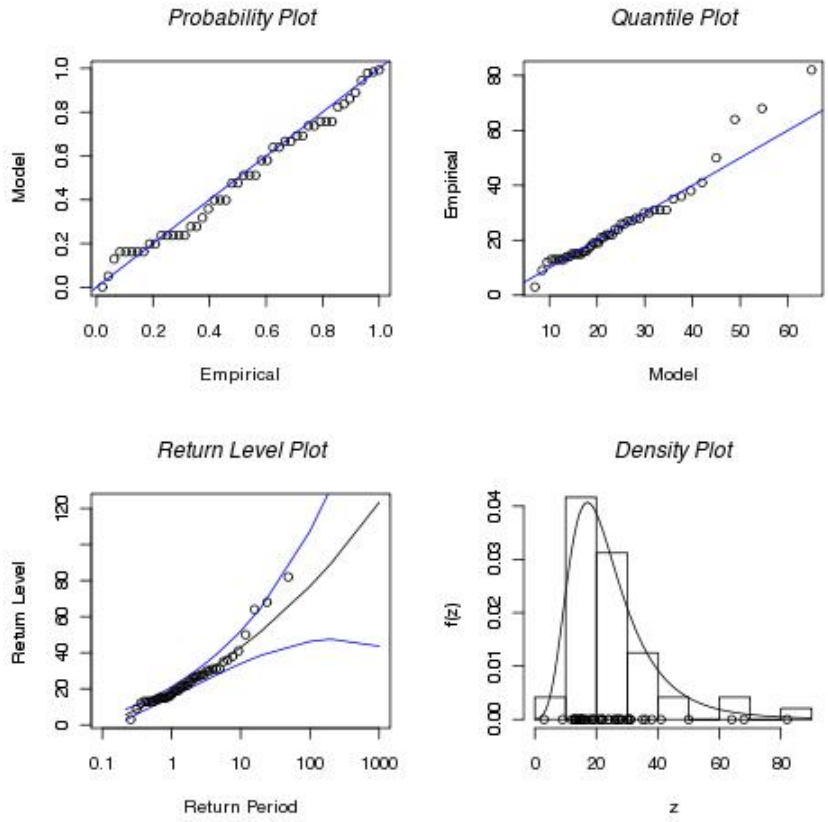

Figure 6.14: Stationary dry period duration GEV distribution diagnostic plots for KACY.

formed values, there were 10 stations with positive values and 19 stations with negative values. But generally these values did not vary much from each other. In terms of the shape parameters, which was assumed to be constant with time, there were a total of 25 stations with negative shape parameter values, meaning that most of the stations in the analysis for the wet period duration, follows a type III GEV distribution, which has a bounded tail. This type of distribution is known as a Weibull distribution.

The location parameter and its trend, the scale parameter and its trend, and the shape parameters were used to obtain 2-year, 10-year and 20-year return

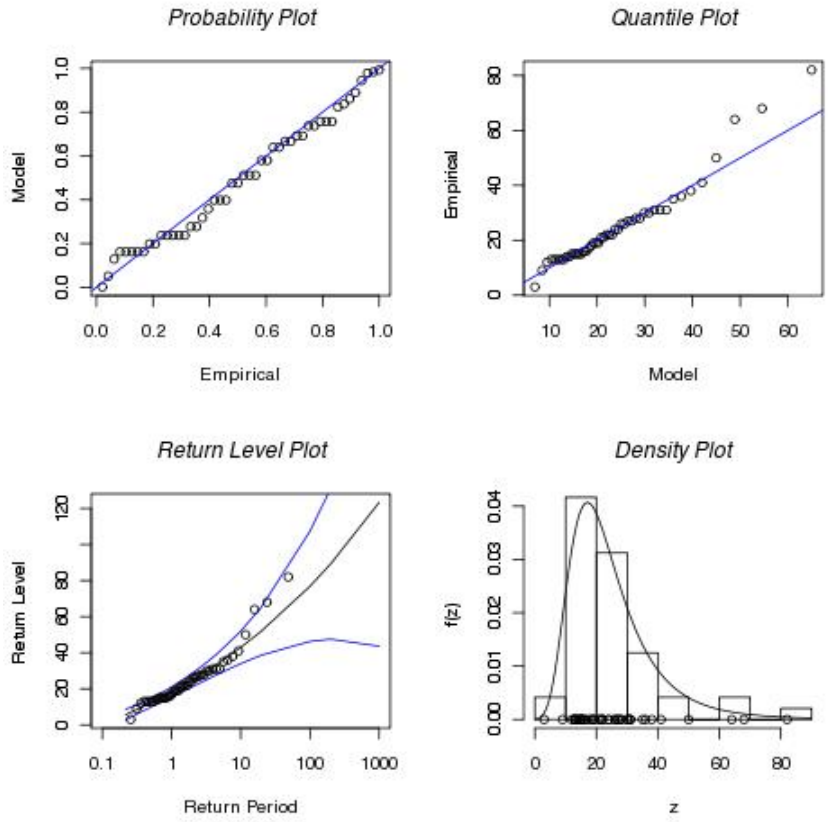

Figure 6.15: Stationary dry period duration GEV distribution diagnostic plots for KBDR.

periods for each station of interest in this study.

The diagnostic plot for KCON, KWBI, KPIT and KROC are shown in Figures in 6.18, 6.19, 6.20 and 6.21. These diagnostic plots show that the non-stationary GEV distributions was a good fit to the wet period duration data for most of the stations in the study.

The non-stationary GEV distribution fit information was used to estimate 2 sets of the 2-year, 10-year and 20-year return levels; the first set produced from the stations 1961 estimated GEV parameters, and the second produced from the stations 2008 estimated GEV parameters. This was done to observe how the

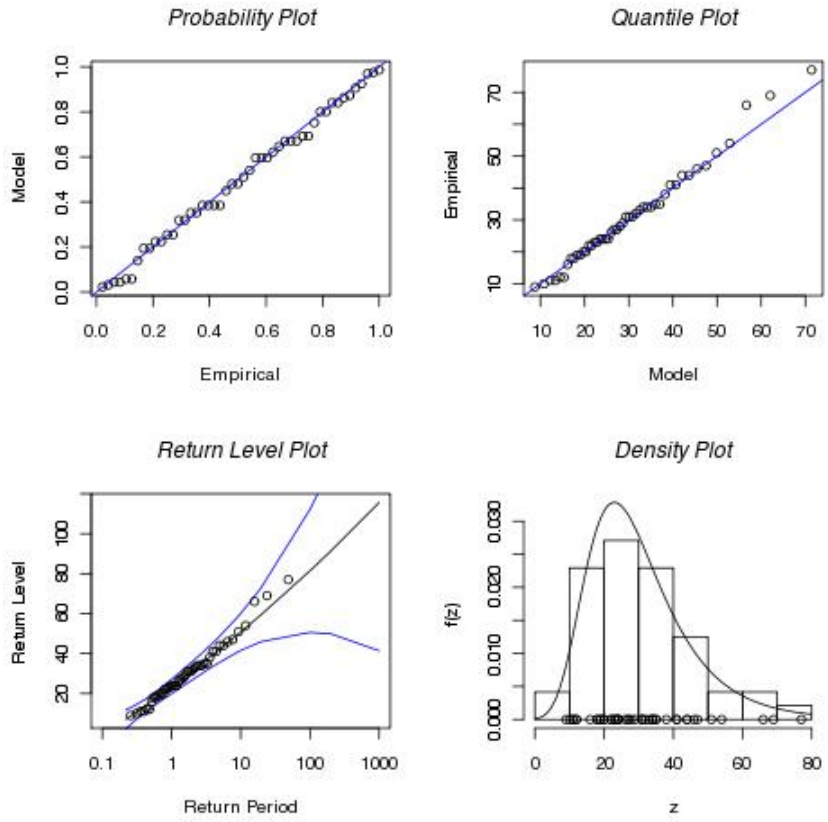

Figure 6.16: Stationary dry period duration GEV distribution diagnostic plots for KLGA.

estimated return levels changed through time and is shown in Table 6.6. The differences in the 2-year, 10-year and 20-year return levels for each station were plotted spatially in figures 6.22, 6.23 and 6.24. For either the 2-year, 10-year or 20-year return levels, there were between 18 and 19 stations that showed a decrease in at least one of these return levels. There were between 10 and 11 stations that showed an increase in one of these return levels over time. There were a total of 14 stations that showed an increase in all of the stations 2-year, 10-year and 20-year return levels (KALB, KLGA, KBDR, KPHL, KACY, KERI, KBGM, KPIT, KNXX, KABE, KEWR, KBUF, KBWI, KCLE). There were a total of 7 stations that showed a decrease in all of its return levels (KORH, KBDL,

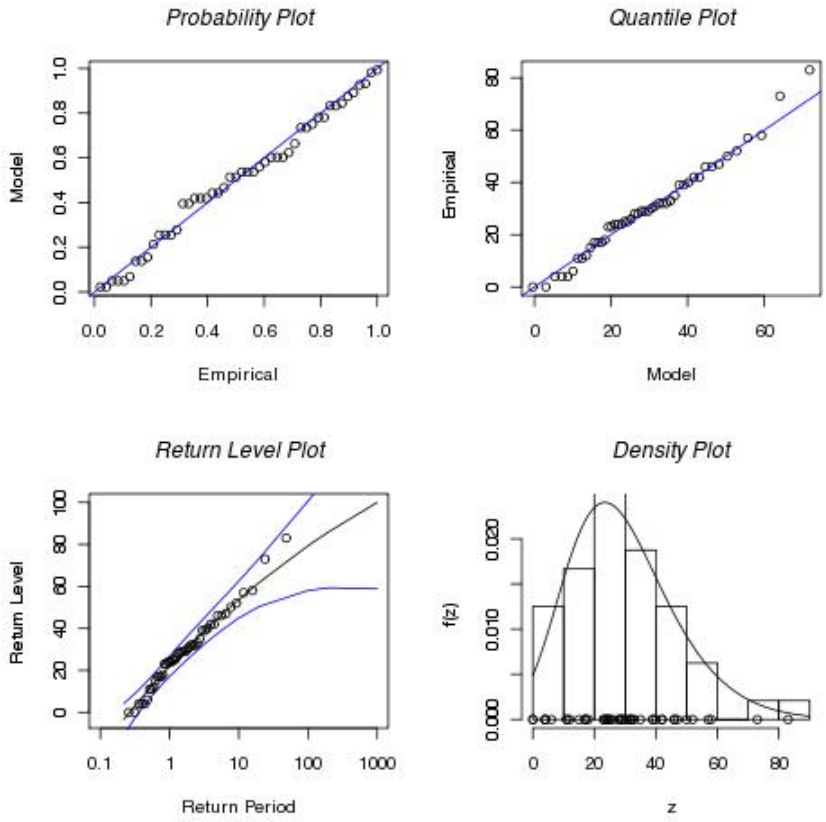

Figure 6.17: Stationary dry period duration GEV distribution diagnostic plots for KBDR.

KCON, KDCA, KROC, KNHZ, KBOS). For the three stations with a statistically significant non-stationary GEV distribution fits, two of the stations were shown to have decreases in return levels from 1961 to 2008.

6.4 Non-stationary GEV Dry Period Duration Block Maxima

As was the case for the max duration wet period data, non-stationary GEV distributions were fit to each station's dry period block maxima duration and the parameter results of these analyses are shown in Table 6.7. Table 6.7 also shows

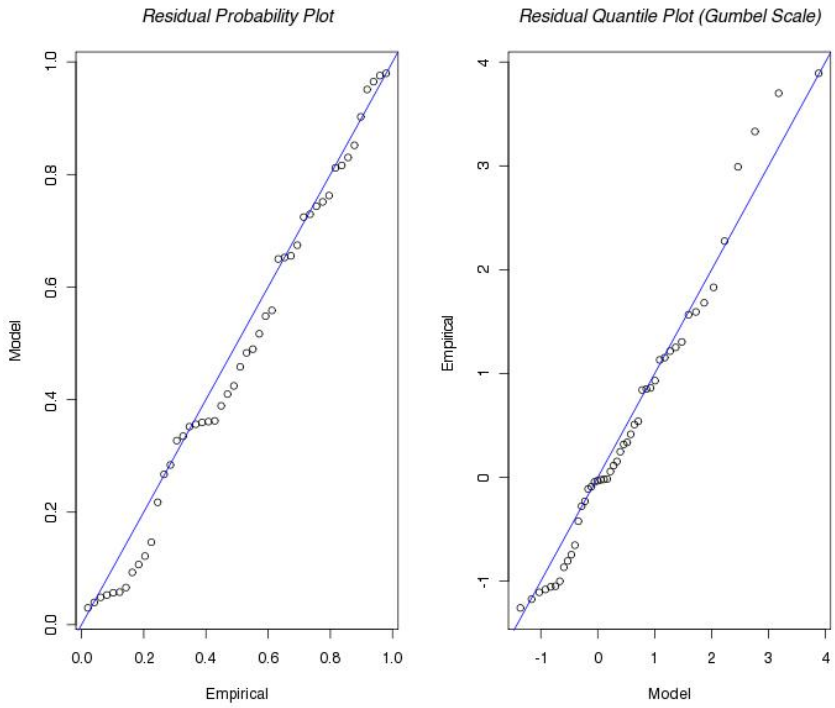

Figure 6.18: Non-stationary GEV distribution diagnostic plots for KCON.

the p-value results from a likelihood ratio test (LRT) performed to test the statistical significance of the non-stationary GEV distribution fit over the stationary GEV fit for each station.

From the analysis, for many of the stations dry period duration block maxima, the non-stationary GEV distribution did not fit well to this data. Due to poor fits, several stations non-stationary GEV results were excluded from this analysis. The table below shows those stations with reasonable fits. Of those in the table below, only one (KBWI) had a non-stationary GEV distribution that was a statistically significant improvement over its stationary counterpart.

The non-stationary GEV distribution fit information was used to estimate 2 sets of the 2-year, 10-year and 20-year return levels; the first set produced from

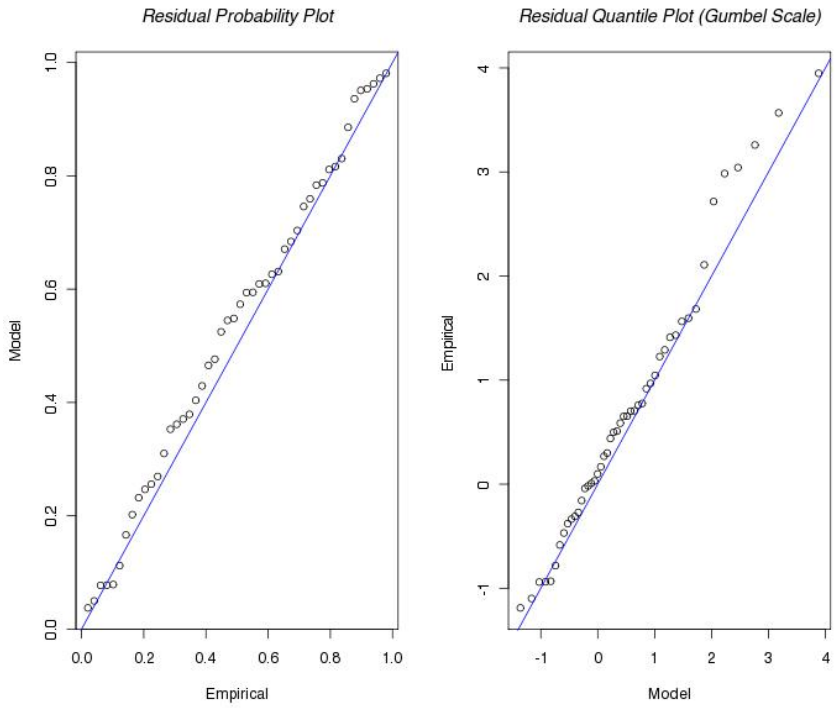

Figure 6.19: Non-stationary GEV distribution diagnostic plots for KBWI.

the stations' 1961 estimated GEV parameters, and the second produced from the stations' 2008 estimated GEV parameters. This was done to observe how the estimated return levels changed through time and is shown in Table 6.8. The differences in the 2-year, 10-year and 20-year return levels for each station were plotted spatially in Figures 6.25, 6.26 and 6.25. Of the 14 stations with reasonable non-stationary GEV distribution fits, 12 stations showed a decrease in the 2-year, 10-year and 20-year return level from 1961 to 2008. KBWI, which was the lone station with a statistically significant non-stationary GEV distribution fit, showed an increase in the 2-year, 10-year and 20-year return levels.

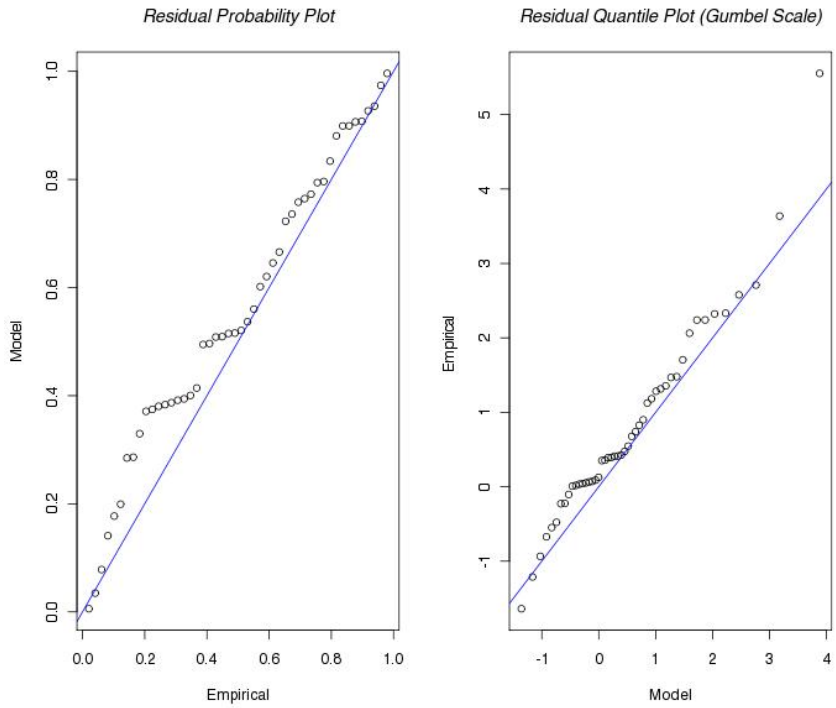

Figure 6.20: Non-stationary GEV distribution diagnostic plots for KPIT.

Table 6.1: The estimated GEV distribution parameters with standard errors (in parentheses) from the stationary GEV distribution fit to each stations wet period duration block maxima. The values were rounded to 2 decimals.

Station	μ	σ	ξ
KALB	13.93(0.81)	4.85(0.6)	0(0.13)
KORH	11.89(0.69)	4.14(0.51)	−0.02(0.13)
KLGA	11.93(0.74)	4.6(0.54)	0.02(0.1)
KITH	17.4(1.26)	7.42(0.94)	−0.09(0.14)
KBDL	14.71(0.96)	5.83(0.7)	−0.05(0.12)
KBDR	14.16(0.85)	5.23(0.65)	0.14(0.11)
KPHL	16.52(1.02)	6.31(0.73)	−0.03(0.11)
KILG	17.67(1.09)	6.73(0.78)	−0.08(0.11)
KBTV	15.8(0.92)	5.6(0.73)	−0.42(0.14)
KCON	21.27(1.16)	7.04(0.84)	−0.1(0.12)
KACY	21.16(1.61)	9.46(1.24)	0.1(0.14)
KAVP	13.52(0.93)	5.72(0.68)	0.01(0.11)
KERI	13.56(0.77)	4.74(0.55)	−0.1(0.11)
KSYR	12.97(0.66)	4.07(0.48)	−0.15(0.11)
KEKN	4.12(0.49)	3.08(0.75)	1.2(0.2)
KDCA	21.52(1.45)	9.06(1.03)	−0.19(0.09)
KBGM	13.73(0.97)	5.89(0.7)	−0.06(0.11)
KROC	16.97(0.99)	6.06(0.71)	−0.17(0.11)
KPVD	14.6(0.76)	4.6(0.56)	−0.26(0.13)
KNHZ	16.09(0.96)	5.85(0.7)	0(0.12)
KCRW	17.4(1.27)	7.61(0.93)	−0.19(0.13)
KPIT	16.54(0.91)	5.68(0.65)	−0.16(0.1)
KBOS	16.86(1)	6.07(0.72)	−0.02(0.12)
KNXX	14.08(0.78)	4.86(0.56)	0.01(0.09)
KABE	15.64(0.92)	5.54(0.68)	0.02(0.12)
KIPT	18.73(1.04)	6.35(0.75)	−0.13(0.12)
KEWR	13.76(0.7)	4.39(0.5)	−0.01(0.09)
KBUF	11.68(0.55)	3.39(0.4)	−0.15(0.11)
KBWI	15.04(0.84)	5.1(0.62)	0.01(0.12)
KCLE	13.94(0.79)	4.57(0.62)	0.13(0.16)

Table 6.2: The 2-year, 10-year and 20-year return levels estimated from the GEV distribution fit to each stations wet period duration block maxima.

	Return Level (cm)		
Station	2-yr	10-yr	20-yr
KALB	15.71	24.82	28.29
KORH	13.4	21.01	23.84
KLGA	13.62	22.46	25.91
KITH	20.07	32.53	36.77
KBDL	16.83	27.15	30.86
KBDR	16.13	27.92	33.28
KPHL	18.82	30.2	34.37
KILG	20.11	31.6	35.57
KBTV	17.7	23.95	25.31
KCON	23.81	35.51	39.45
KACY	24.69	44.99	53.79
KAVP	15.62	26.53	30.75
KERI	15.26	23.08	25.69
KSYR	14.42	20.71	22.67
KEKN	5.54	39.98	92.96
KDCA	24.73	38.1	42.07
KBGM	15.87	26.1	29.7
KROC	19.12	28.27	31.04
KPVD	16.21	22.45	24.15
KNHZ	18.23	29.24	33.44
KCRW	20.09	31.3	34.62
KPIT	18.57	27.32	30.04
KBOS	19.08	30.25	34.43
KNXX	15.87	25.16	28.76
KABE	17.68	28.34	32.5
KIPT	21.01	31.18	34.47
KEWR	15.36	23.52	26.6
KBUF	12.89	18.19	19.86
KBWI	16.91	26.62	30.36
KCLE	15.66	25.9	30.53

Table 6.3: The estimated GEV distribution parameters with standard errors (in parentheses) from the stationary GEV distribution fit to each stations dry period duration block maxima. The values were rounded to 2 decimals.

Station	μ	σ	ξ
KALB	18.25(1.45)	9.12(1.09)	0.14(0.09)
KORH	23.12(4.07)	22.66(3.54)	0.34(0.19)
KLGA	17.05(1.24)	7.66(0.89)	−0.06(0.11)
KITH	27.07(3.63)	21.97(2.63)	−0.14(0.12)
KBDL	24.52(4.81)	24.85(3.98)	0.16(0.22)
KBDR	24.83(2.29)	13.93(1.7)	0.05(0.12)
KPHL	25.06(2.75)	16.85(2.01)	−0.01(0.11)
KILG	21.61(4.19)	22.48(3.52)	0.24(0.2)
KBTV	23.28(4.34)	23.03(3.7)	0.28(0.21)
KCON	28.18(3.86)	22.94(2.86)	−0.07(0.13)
KACY	23.83(2.97)	17.88(2.35)	0.18(0.13)
KAVP	20.91(1.72)	10.28(1.29)	0.01(0.13)
KERI	24.4(3.31)	18.64(2.87)	0.33(0.18)
KSYR	24.73(2.13)	13.26(1.49)	−0.15(0.09)
KEKN	13.84(0)	122.27(0)	8.83(0)
KDCA	21.18(4.42)	23.41(3.66)	0.19(0.21)
KBGM	29.88(5.03)	26.99(4.06)	−0.16(0.2)
KROC	22.4(1.98)	11.94(1.44)	−0.14(0.12)
KPVD	28.11(3.33)	20.63(2.39)	−0.02(0.1)
KNHZ	24.34(3.72)	22.27(3.15)	0.31(0.14)
KCRW	18.49(3.98)	21.45(3.88)	0.56(0.22)
KPIT	21.63(2.03)	12.77(1.46)	0.06(0.09)
KBOS	25.7(3.08)	19.17(2.18)	−0.09(0.09)
KNXX	27.12(4.32)	23.54(3.41)	0.01(0.19)
KABE	23.13(3.89)	22.24(3.38)	0.33(0.17)
KIPT	30.41(6.17)	32.14(4.99)	0.01(0.22)
KEWR	20.72(2.98)	16.62(2.93)	0.56(0.2)
KBUF	23.49(1.85)	11.21(1.38)	0.05(0.12)
KBWI	21.87(2.48)	15.38(1.75)	−0.09(0.1)
KCLE	19.09(1.3)	7.97(0.95)	0.01(0.11)

Table 6.4: The 2-year, 10-year and 20-year return levels estimated from the GEV distribution fit to each stations dry period duration block maxima.

	Return Level (cm)		
Station	2-yr	10-yr	20-yr
KALB	21.68	42.29	51.69
KORH	31.96	99.26	138.49
KLGA	19.83	33.25	38.02
KITH	34.92	69.38	80.3
KBDL	33.9	91.93	119.19
KBDR	29.98	57.83	69.12
KPHL	31.23	62.6	74.44
KILG	30.22	88.61	118.84
KBTV	32.16	95.36	129.73
KCON	36.48	75.72	89.32
KACY	30.61	73.62	94.38
KAVP	24.69	44.19	51.69
KERI	31.66	86.58	118.38
KSYR	29.46	50.18	56.71
KDCA	30.07	87.3	115.35
KBGM	39.48	80.74	93.45
KROC	26.67	45.54	51.57
KPVD	35.64	73.68	87.9
KNHZ	32.99	96.96	133.18
KCRW	27.21	114.85	181.36
KPIT	26.36	52.4	63.16
KBOS	32.61	64.69	75.56
KNXX	35.76	80.57	97.88
KABE	31.8	97.75	136.14
KIPT	42.23	103.91	127.92
KEWR	27.48	95.7	147.69
KBUF	27.63	50.16	59.33
KBWI	27.41	53.05	61.71
KCLE	22.01	37.26	43.17

Table 6.5: The estimated non-stationary GEV distribution parameters with standard errors in parentheses are shown for each station's max duration for wet periods. (* - statistical significance)

Station	b_0	b_1	c_0	c_1	ξ	α
KALB	14.36(3.36)	0.09(0.1)	2.62(0.27)	−0.02(0.01)	0.14(0.13)	0.144
KORH	78.91(0)	−3.09(0)	10.87(0)	−0.41(0)	6.92(0)	0*
KLGA	18.44(2.47)	−0.06(0.08)	2.12(0.21)	0(0.01)	−0.04(0.11)	0.755
KITH	36.21(8.13)	−0.21(0.26)	3.31(0.21)	−0.01(0.01)	−0.19(0.12)	0.402
KBDL	34.14(0)	24.76(0)	4.19(0)	0.07(0)	−4.16(0)	0*
KBDR	20.75(5.43)	0.09(0.19)	2.68(0.34)	0(0.01)	0.02(0.15)	0.173
KPHL	22.13(6.37)	0.11(0.27)	2.83(0.23)	0.01(0.01)	−0.19(0.11)	0.083
KILG	48.61(0)	−2.64(0)	11.61(NaN)	−0.72(0)	6.86(0)	0*
KBTV	52.38(0)	−2.97(0)	13.8(0)	−0.68(0)	8.92(0)	0*
KCON	42.77(8.81)	−0.45(0.26)	3.45(0.25)	−0.01(0.01)	−0.13(0.13)	0.865
KACY	37.48(11.14)	−0.38(0.33)	3.3(0.42)	−0.01(0.01)	0.17(0.14)	0.062
KAVP	25.18(3.78)	−0.15(0.12)	2.57(0.24)	−0.01(0.01)	−0.01(0.12)	0.453
KERI	45.07(25.13)	−0.48(0.65)	3.6(0.87)	−0.01(0.02)	0.29(0.23)	0.001*
KSYR	25.01(5.3)	−0.01(0.17)	2.94(0.26)	−0.01(0.01)	−0.28(0.12)	0.202
KDCA	44.32(0)	−2.51(0)	12.67(NaN)	−0.73(0)	7.83(0)	0*
KBGM	38.06(9.23)	−0.28(0.31)	3.32(0.21)	0(0.01)	−0.2(0.19)	0.962
KROC	28.29(4.08)	−0.21(0.14)	2.6(0.21)	0(0.01)	−0.21(0.14)	0.252
KPVD	31.19(6.67)	−0.1(0.24)	3.03(0.24)	0(0.01)	−0.03(0.1)	0.946
KNHZ	48.13(0)	2.78(0)	7.82(0)	−0.3(0)	−7.06(0)	0*
KCRW	39.44(0)	−2.75(0)	12.69(0)	−0.92(0)	13.65(0)	0*
KPIT	20.83(NaN)	−0.07(NaN)	3.06(NaN)	−0.02(NaN)	−0.09(NaN)	0.356
KBOS	30.19(6.07)	−0.22(0.2)	2.98(0.21)	0(0.01)	−0.07(0.09)	0.318
KNXX	7.54(8.09)	0.59(0.29)	3.1(0.35)	0(0.01)	0.24(0.22)	0.257
KABE	53.06(0)	−2.12(0)	15.32(0)	−0.68(0)	6.84(0)	0*
KIPT	41.4(0)	−2.58(0)	12.89(0)	−0.92(0)	12.91(0)	0*
KEWR	50.29(0)	−2.03(0)	14.71(0)	−0.64(0)	8.1(0)	0*
KBUF	22.77(3.46)	0.03(0.12)	2.37(0.24)	0(0.01)	0.05(0.12)	0.962
KBWI	14.18(6.39)	0.24(0.24)	2.44(0.28)	0.01(0.01)	−0.07(0.14)	0.038*
KCLE	23.43(3.21)	−0.11(0.11)	2.24(0.28)	0(0.01)	−0.04(0.13)	0.088

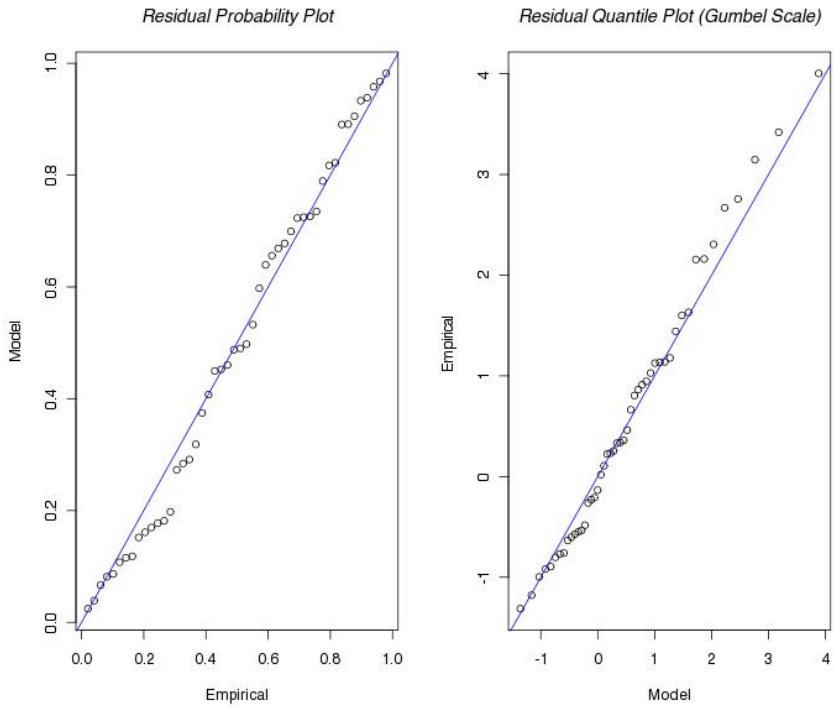

Figure 6.21: Non-stationary GEV distribution diagnostic plots for KROC.

Table 6.6: The estimated return levels of 1961 and 2008 for each station's max duration of wet periods. (* - statistical significants)

	Return Level (cm)					
	From 1961 GEV parameters			From 2008 GEV parameters		
Station	2-yr	10-yr	20-yr	2-yr	10-yr	20-yr
KALB	17.36	28.24	32.27	14.26	21.38	24.01
KORH	12.72	19.54	22.12	14.05	22.62	25.86
KLGA	15.65	25.41	29.2	11.7	19.35	22.32
KITH	18.89	32.8	37.67	21.02	32.44	36.44
KBDL	16.29	26.78	30.56	17.35	27.52	31.18
KBDR	18.57	31.76	37.71	13.86	23.79	28.27
KPHL	20.28	31.69	35.87	17.38	28.61	32.72
KILG	20.37	30.76	34.36	19.86	32.49	36.86
KBTV	18.62	23.89	25.11	16.48	24.14	25.92
KCON	21.35	30.92	34	26.62	39.55	43.71
KACY	30.86	57.32	67.29	21.36	34.16	38.98
KAVP*	19.52	32.35	37.08	12.21	20.02	22.9
KERI	15.78	24.07	26.82	14.78	22.06	24.47
KSYR	13.82	22.7	25.44	15.19	19.18	20.41
KDCA	23.37	33.84	36.94	26.78	42.76	47.5
KBGM	16.06	30.3	35.49	15.41	22.61	25.23
KROC	17.69	26.2	28.72	20.68	30.03	32.8
KPVD	15.58	24.31	26.83	16.66	21.07	22.34
KNHZ	17.92	28.81	32.97	18.53	29.65	33.89
KCRW	22.42	31.59	34.19	18.8	31.85	35.55
KPIT*	22.55	30.85	33.48	14.58	22.59	25.14
KBOS	18.89	30.09	34.27	19.28	30.41	34.57
KNXX*	19.85	30.77	34.87	12.34	18.87	21.32
KABE	20.72	32.86	37.42	14.95	23.22	26.33
KIPT	22.17	30.55	33.3	19.81	31.97	35.97
KEWR	17.13	26.09	29.45	13.69	20.77	23.43
KBUF	13.99	19.02	20.64	11.72	17.21	18.98
KBWI	18.43	28.36	32.19	15.44	24.73	28.31
KCLE	17.29	27.77	32.56	14.03	23.81	28.27

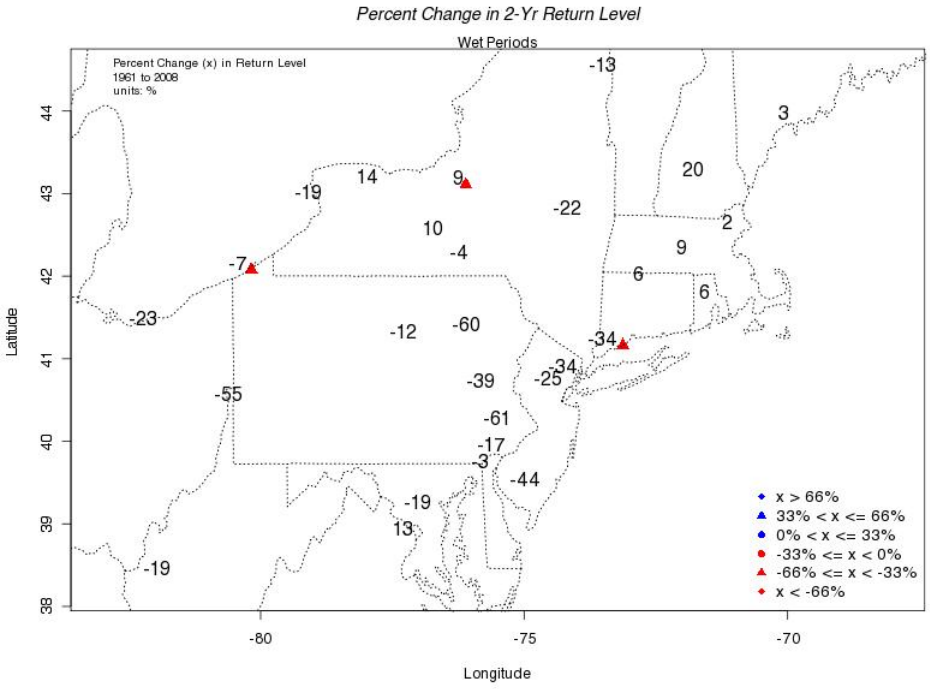

Figure 6.22: Surface plots showing the percent change in the 2-year return levels for each stations wet period duration maxima in the analyses. 19 stations showed a decrease in the 2-year return levels. Symbols (triangles, diamonds, squares) represent station's with statistical significance.

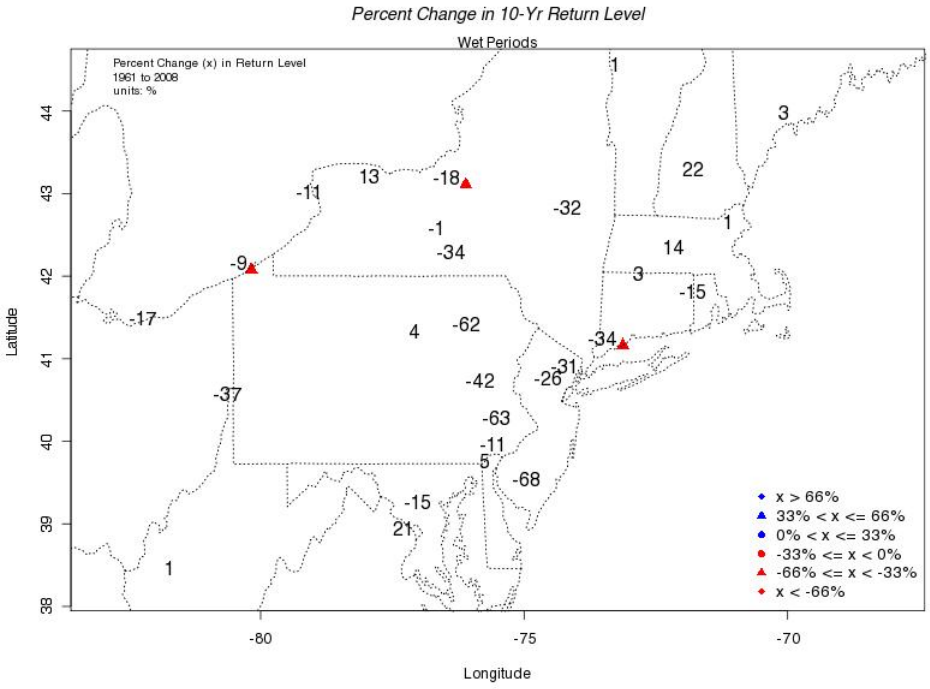

Figure 6.23: Surface plots showing the percent change in the 10-year return levels for each stations wet period duration maxima in the analyses. 18 stations showed a decrease in the 10-year return levels. Symbols (triangles, diamonds, squares) represent station's with statistical significance.

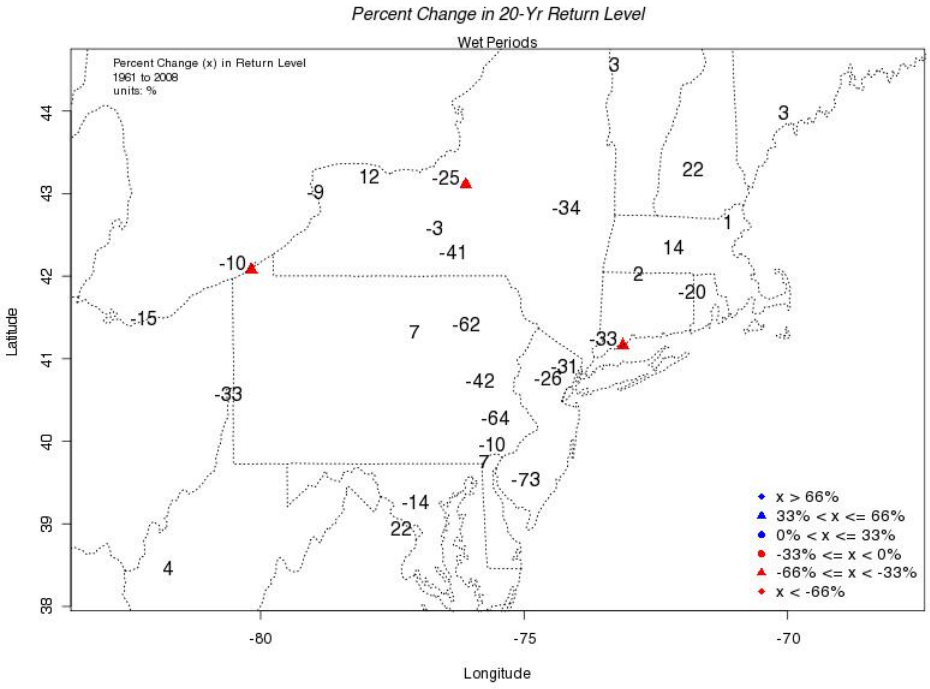

Figure 6.24: Surface plots showing the percent change in the 20-year return levels for each stations wet period duration maxima in the analyses. At least 18 stations showed a decrease in the 20-year return levels. Symbols (triangles, diamonds, squares) represent station's with statistical significance.

Table 6.7: The estimated non-stationary max dry period duration GEV distribution parameters with standard errors in parentheses are shown for each station.

Station	b_0	b_1	c_0	c_1	ξ	α
KALB	14.36(3.36)	0.09(0.1)	2.62(0.27)	−0.02(0.01)	0.14(0.13)	0.144
KLGA	18.44(2.47)	−0.06(0.08)	2.12(0.21)	0(0.01)	−0.04(0.11)	0.755
KITH	36.21(8.13)	−0.21(0.26)	3.31(0.21)	−0.01(0.01)	−0.19(0.12)	0.402
KBDR	20.75(5.43)	0.09(0.19)	2.68(0.34)	0(0.01)	0.02(0.15)	0.173
KPHL	22.13(6.37)	0.11(0.27)	2.83(0.23)	0.01(0.01)	−0.19(0.11)	0.083
KCON	42.77(8.81)	−0.45(0.26)	3.45(0.25)	−0.01(0.01)	−0.13(0.13)	0.865
KACY	37.48(11.14)	−0.38(0.33)	3.3(0.42)	−0.01(0.01)	0.17(0.14)	0.062
KAVP	25.18(3.78)	−0.15(0.12)	2.57(0.24)	−0.01(0.01)	−0.01(0.12)	0.453
KSYR	25.01(5.3)	−0.01(0.17)	2.94(0.26)	−0.01(0.01)	−0.28(0.12)	0.202
KBGM	38.06(9.23)	−0.28(0.31)	3.32(0.21)	0(0.01)	−0.2(0.19)	0.962
KROC	28.29(4.08)	−0.21(0.14)	2.6(0.21)	0(0.01)	−0.21(0.14)	0.252
KPVD	31.19(6.67)	−0.1(0.24)	3.03(0.24)	0(0.01)	−0.03(0.1)	0.946
KBOS	30.19(6.07)	−0.22(0.2)	2.98(0.21)	0(0.01)	−0.07(0.09)	0.318
KBUF	22.77(3.46)	0.03(0.12)	2.37(0.24)	0(0.01)	0.05(0.12)	0.962
KBWI	14.18(6.39)	0.24(0.24)	2.44(0.28)	0.01(0.01)	−0.07(0.14)	0.038*
KCLE	23.43(3.21)	−0.11(0.11)	2.24(0.28)	0(0.01)	−0.04(0.13)	0.088

Table 6.8: The estimated return levels from 1961 and 2008 for the max durations for dry periods for each station. (* - statistical significance)

	Return Level (cm)					
	From 1961 GEV parameters			From 2008 GEV parameters		
Station	2-yr	10-yr	20-yr	2-yr	10-yr	20-yr
KALB	19.54	50.31	64.42	20.72	32.59	38.03
KLGA	21.41	36.27	41.67	18.18	30.51	34.99
KITH	45.66	86.04	98.07	32.9	61.35	69.81
KBDR	26.22	54.48	65.54	30.92	62.38	74.7
KPHL	28.34	53.85	61.46	37.27	79.49	92.08
KCON	53.45	103.17	119.23	27.45	56.36	65.71
KACY	47.21	110.51	140.62	25.06	62.1	79.73
KAVP	29.79	53.83	62.85	21.1	36.19	41.85
KSYR	31.54	56.33	62.85	27.91	41.49	45.05
KBGM	47.59	88.18	100.13	34.44	74.35	86.1
KROC	32.82	52.29	57.96	22.02	37.65	42.2
KPVD	38.65	76.43	90.4	33.92	72.19	86.34
KBOS	37.05	70.62	82.27	25.87	55.61	65.93
KBUF	26.77	48.28	56.99	28.55	51.96	61.45
KBWI*	18.64	38.68	45.67	34.22	74.18	88.12
KCLE	26.75	43.64	49.79	21.35	36.33	41.78

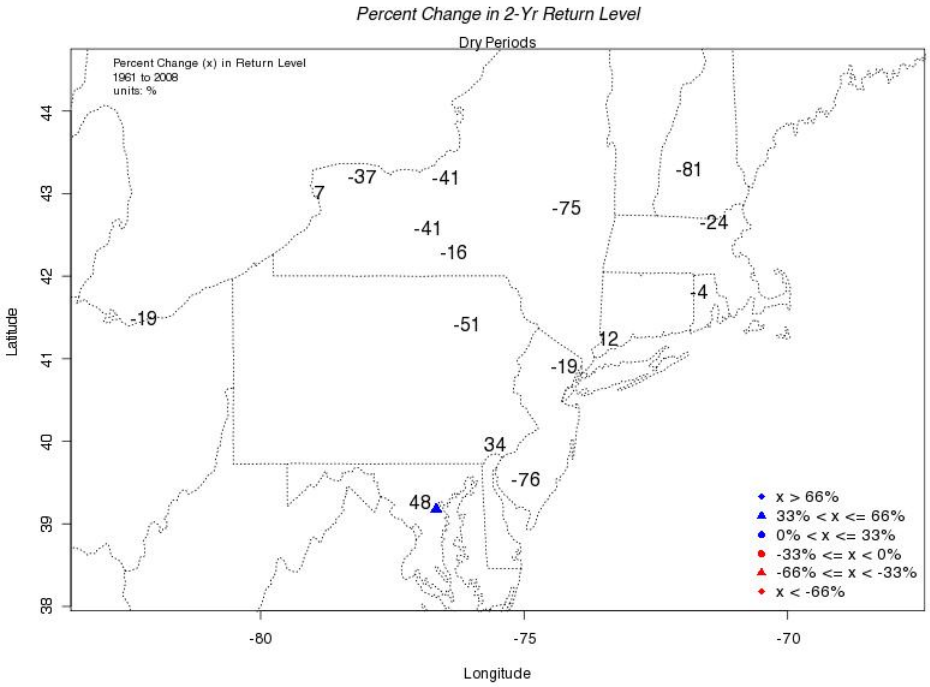

Figure 6.25: Surface plots showing the percent change in the 2-year return levels for each stations wet period duration maxima in the analyses. 12 stations showed a decrease in the 2-year return levels.

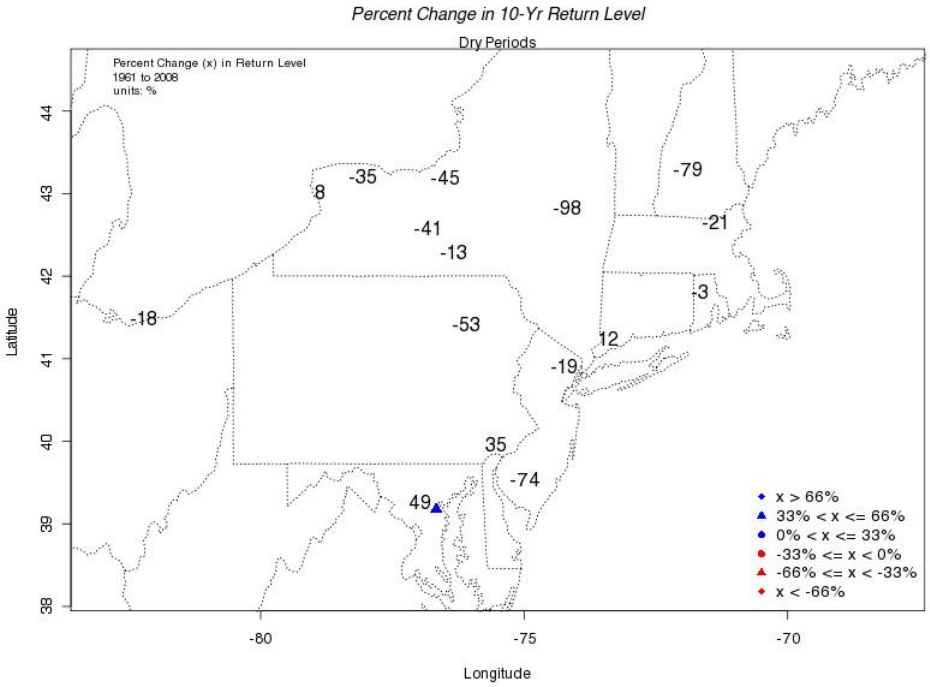

Figure 6.26: Surface plots showing the percent change in the 10-year return levels for each stations wet period duration maxima in the analyses. 12 stations showed a decrease in the 10-year return levels.

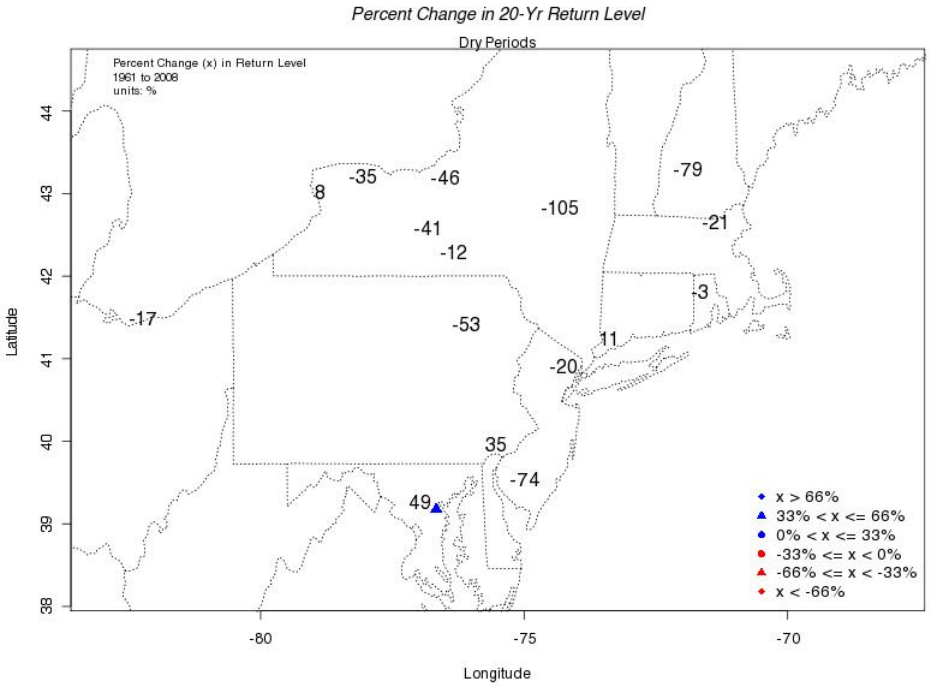

Figure 6.27: Surface plots showing the percent change in the 20-year return levels for each stations dry period duration maxima in the analyses. 12 stations showed a decrease in the 20-year return levels.

This was done to observe how the estimated return levels changed through time and is shown in Table 6.8. The differences in the 2-year, 10-year and 20-year return levels for each station were plotted spatially in Figures 6.25, 6.26 and 6.25. Of the 14 stations with reasonable non-stationary GEV distribution fits, 12 stations showed a decrease in the 2-year, 10-year and 20-year return level from 1961 to 2008. KBWI, which was the lone station with a statistically significant non-stationary GEV distribution fit, showed an increase in the 2-year, 10-year and 20-year return levels.

CHAPTER 7

DISCUSSION

In this research almost every characteristic of wet periods and dry periods were analyzed.

Overall, the GEV distribution fit very well to each station's block maxima. The location, scale and shape perimeters were obtained for each station and we were able to get an understanding of the characteristics for these parameters across the Northeast. One of the most important findings from this study was that largest location and scale parameter values were located closer to and along the eastern seaboard. This may be due to the respective stations being located close to a large water body, in this case, the Atlantic Ocean. In terms of the stationary shape parameters, there was no discernible pattern, except that most of the values for the parameter were positive (22 out of 30), meaning most stations have unbounded tails and fit into the type III category of GEV distributions. We were able to use this parameter information to calculate return levels and return periods under a stationary climate regime. The largest return levels were located along the east coast as well.

We also learned that non-stationary GEV distributions fit very well to the block maxima data. From this, we were able to estimate how the return levels for a particular station might change over time. Most stations showed an increase in return levels over the time period study. Using a likelihood ratio test, we were also able to show that 10 of 30 stations in the study had a non-stationary GEV fit that was a statistical improvement over its stationary counterpart. Most of these particular stations were located closest to the east coast.

The block maxima results suggests that there may have been an increase in the intensity of wet periods over time (intensity measured by the block maxima values). This could indirectly be supported by work performed by Karl and Knight (1998) which found that there is a tendency for more 1-day and multi-day heavy precipitation events in the United States and other countries.

We were not able to do the same for the block minima data due to the nature of the data (the minimum value occurred to often in the data set). Still, other characteristics of dry periods were analyzed to get an understanding of these events.

For wet periods, we were able to fit stationary GP distributions to each station's cluster maxima in the study. Generally, the GP distribution fit well to each stations data. One key finding from this analysis was that scale parameters showed significant spatial variability. No set pattern could be determined from this analysis. This finding can be supported by Dai et al. (1998) which found that there is considerable variability of drought and excess wetness in United States. Another key finding was that most of the shape parameters were positive. This means that for this study the GP distributions had unbounded tails. This falls in line with what's been seen typically for tail shapes for rainfall and streamflow, as examples (Katz, 2010). We were able to use the parameters from each station GP fit to estimate return levels from return periods of interest. Return levels generally increased from west to east as well. This is likely again due in part to the influence Atlantic Ocean.

Non-stationary GP distributions were successful fit to the each station's cluster maxima. The findings showed that most stations had small increases in return levels from 1961 to 2008. Most of the stations' increases were not statisti-

cally significant. This would lead one to believe a stationary climate environment might be best to use as a frame work when analyzing this data. As in the case of the block minima, cluster minima were could not be analyzed with the GP distribution because of the nature of the data.

The duration of wet periods using a stationary and non-stationary GEV distribution we analyzed as well. The stationary GEV distribution fit well to each stations duration data. A key finding here is that there wasnt a spatial pattern discernible for the GEV parameters. The non-stationary GEV distribution fit well to each stations wet period duration data but there were only three stations that showed a statistical significance over its stationary counter part. Based on our study, this would mean that the duration of wet periods may not necessarily be changing over time. This was same for analyzing dry period durations.

Groisman and Knight (2008) found significant increases in the occurrence of dry periods, but based on our definition of wet periods and dry periods and the subsequent analysis, we were not able to find much of a significant change in the duration of these events.

As for the number of wet periods or dry periods per year, there was no significant changes in these over time.

CHAPTER 8

CONCLUSION

The goal of this research was to understand the occurrence of dry periods and wet periods in the northeastern United States over a 48 year period, from 1961 to 2008, along with expanding upon the work of Groisman and Knight (2008). From this study, we learned that there has not been a statistically significant change in the occurrence or duration of dry periods and wet periods in Northeast United States. As for intensity, measured by a station's block maxima, most stations showed an increase in the return levels over time, and some showed statistically significant increases. This result in particular suggests that there may have been a slight wetting trend across the Northeast over the period of study. It also showed that there may have a slight increase in the extremes of the wet periods over time.

Groisman and Knight (2008) found significant increases in the occurrence of dry periods, but based on our definition of wet periods and dry periods, we were not able to find much of a significant change in the occurrence or duration of these events.

Due to the nature of the minima data, further work is needed to analyze the intensity of dry periods. This would involve investigating new ways to measure both wet and dry periods. Only linear and lognormal trends were used in this analysis to estimate how return levels for the characteristics of dry periods and wet periods would change over time. To provide further analysis into possible changes in characteristic, fitting the data to more complicated trend lines such as the El Nino Southern Oscillation and North Atlantic Oscillation Indices could be very useful and beneficial. Also, in this study, the precipitation data was

assumed to not have any statistical changes of frequency during an individual year. Further work would also involve analyzing and accounting for how the frequency of precipitation may change during a year for each station, and how that may impact wet periods and dry periods.

CHAPTER 9

APPENDIX

9.1 Maximum Likelihood Estimation

For every value in the domain of a parameter for a statistical distribution, variations of that distribution exist and attach probabilities (or probability densities) to some observed data of interest. The range of values for a parameter depends on the distribution the parameter was obtained from and the data being analyzed. For example, for the GEV distribution, the domain of the location parameter μ is: (-∞, ∞). Any value in this domain can be used to attach probabilities to observed data, but any and every parameter value may not produce a reasonable or good statistical distribution fit to the observed data.

A method used to obtain the best possible parameters for a statistical distribution fit to some observed data is maximum likelihood estimation (MLE). MLE involves maximizing the likelihood, or log-likelihood, function for a statistical distribution to obtain parameters that, when used for the statistical distribution, best match to the empirical probability of the observed data. The parameters for the GEV (μ, σ, ξ) and GP (σ, ξ) distributions, for both stationary and non-stationary cases, were obtained using MLE.

The likelihood function is a function where the probability assigned to observed data changes depending on the value of the parameters. For some examples, it is possible to obtain the MLE parameters explicitly usually by differentiating the log-likelihood function and equating it to zero (Coles, 2001). In more complicated examples, it is usually necessary to apply numerical techniques to

maximize the log-likelihood function, as was the case in this study. Often the log-likelihood function is used for this instead of the likelihood function because it can be more convenient to work with (Coles, 2001).

The log-likelihood function for the stationary GEV distribution when $\xi \neq 0$ is shown in equation 9.1.

$$l(\mu, \sigma, \xi) = -mlog(\sigma) - (1 + \frac{1}{\xi})\Sigma log[1 + \xi\frac{(z_i - \mu)}{\sigma}] - \Sigma[1 + \xi\frac{(z_i - \mu)}{\Sigma}]^{\frac{-1}{z_i}} \quad (9.1)$$

The log-likelihood function is valid provided that $1 + \xi(z_i - \mu)/\sigma > 0$, for every block maxima from the first to last (i.e. for i =1,..., m). z_i in this equation represents is the value of the i^{th} block maxima.

$$l(\mu, \sigma) = -mlog(\sigma) - \Sigma log[\frac{(z_i - \mu)}{\sigma}] - \Sigma exp - [\frac{(z_i - \mu)}{\sigma}] \quad (9.2)$$

The log-likelihood function for the stationary GEV distribution when $\xi = 0$ is shown in equation 9.2.

For the non-stationary GEV distribution, μ, σ, ξ in the log-likelihood function are replaced with μ(t), σ(t), ξ(t) in equations 9.1 and 9.2.

The log likelihood function for the stationary GP distribution when $\xi \neq 0$ is shown in equation 9.3.

$$l(\sigma, \xi) = -klog(\sigma) - (1 + \frac{1}{\xi})\Sigma log(1 - \frac{\xi y_i}{\sigma}) \quad (9.3)$$

provided that $(1 - \sigma y_i/\sigma) > 0$ for every cluster maxima from the first to last

(i.e. for i =1,..., k). y_i is the value of the i^{th} cluster maxima.

The log-likelihood function for the stationary GP distribution when $\xi = 0$ is shown in equation 9.4.

$$l(\sigma, \xi) = -klog(\sigma) - (\frac{1}{\sigma})\Sigma log(y_i) \tag{9.4}$$

For the non-stationary GP distribution, σ and ξ in the log-likelihood function are replaced with σ(t), ξ(t) in equation 9.3 and equation 9.4.

These equations have been built into the extRemes Toolkit and numerical methods from the toolkit and R programming environment are used to maximize the necessary equation or equations to find the MLE parameter estimates.

9.2 Return Periods and Return Levels

The concepts of return level and return period are commonly used to convey information about the likelihood of rare or extreme events. The return level is defined as the level that is expected to be exceeded, on average, once every equal number of time points (the time point can be hours, days, years, etc.). The equal number of time points is called the return period (T) and is defined as the expected time interval between exceedances of a particular return level. The return period is mathematically defined as T = 1/p, where p is the probability of the return level being exceeded. For example, p = 0.01 for some yearly data would correspond to a return period T = (1/0.01) or 100 years. The return period, return level, and probability are all connected through a statistical distribution. Using the inverse of the statistical distribution function of interest will

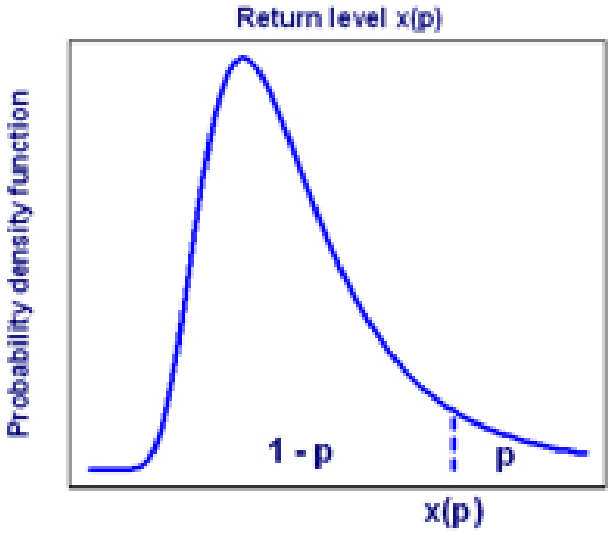

Figure 9.1: A generic probability density function for a statistical distribution with return level (X) and its associated probability (p) from Katz, 2008. The area to the right of the return level represents the probability (p) of X being exceeded. 1/p gives the return period.

allow for calculating return levels from given return periods and probabilities.

As mentioned earlier in the methods section, the Block Maxima approach was used to fit a stationary and non-stationary GEV distribution to the block maxima and minima for each station. To calculate return levels for the block maxima and minima for each station, the inverse of the GEV distribution function was used. The inverse function for the GEV distribution, with $\xi \neq 0$ and $\xi = 0$, is shown in equation 9.5 and equation 9.6, respectively. For this study, the inverse function where $\xi \neq 0$ was used. z_P in equation 9.5 and equation 9.6 represents the estimated return level, measured in years, for a given probability (p) of exceedence.

$$z_p = \mu - \frac{\sigma}{\xi}[1 - [-log(1-p)]^{-\xi}] \tag{9.5}$$

$$z_p = \mu - \sigma log[-log(1-p)] \tag{9.6}$$

The 2-year, 10-year, and 20-year return levels were of interest because they were within the range of years of the data (only 48 years of data) for the stationary and non-stationary GEV distribution fits. For the stationary case, the estimated GEV parameters for each stations block maxima and minima were inserted in to the GEV inverse function. For each stations GEV stationary parameter estimates, the probabilities of 0.50, 0.10, and 0.05, corresponding to the 2-year, 10-year, and 20-year return periods (T = 1/p), were used in the inverse function to obtain the return levels for these return periods. For the non-stationary case, the GEV non-stationary parameter estimates for 1961, the first year, and 2008, the last year, were used to obtain the 2-year, 10-year, and 20-year return levels at the first year and the last year. Having the estimated return levels at the first year and the last year will give prospective on how these levels may have changed through time.

Similar steps were taken to obtain the return levels for the cluster maxima and minima to which stationary and non-stationary GP distributions were fit from the POT approach. The inverse function of the GP distribution was used and an approximation of this function for a large threshold is shown below. Because the GP distribution was fit to one value in each cluster, y_P in 9.7 represents the estimated m-cluster return level for threshold excesses associated with a given a probability (p) of exceedence, with m being the number of clusters. In other words, the return period (T) is measured in terms of the number of clusters observed, for example, the 20-cluster return level. Probability p is still obtained by inverting the return period, p = 1/T.

$$y_p = \frac{\sigma}{\xi}[(1-p)^{-\xi} - 1] \tag{9.7}$$

The 2-year, 10-year and 20-year return levels were of interest for the stationary and non-stationary GP distribution fits as well. For this, first, the average number of cluster maxima and minima per year for each station were obtained. For example, if the average number of cluster maxima per year for a station was 5, then a 10-cluster return level would represent an estimated 2-year return level, a 50-cluster return level would represent a 10-year return level, and a 100-cluster return level would correspond to a 20 year return level.

For the stationary case, the estimated GP parameters for each stations cluster maxima and minima were inserted in to the GP inverse function. The probabilities for the estimated 2-year, 10-year, and 20-year return periods were used in the inverse function to obtain the return levels for these return periods. For the non-stationary case, the GP estimated parameters for the first day of 1961 and the last day of 2008, were used to obtain the 2-year, 10-year, and 20-year return levels at the beginning and end the data. As in the non-stationary GEV case, having the estimated return levels at the beginning of the first year and end of the last year will give prospective on how these levels may have changed through time.

9.3 R Programming Environment and the extRemes Toolkit

R is a free software language and environment for statistical computing and graphics. It is an integral suite of software facilities for data manipulation, calculation, and graphical display. The term environment is intended to characterize

it as a fully planned and coherent system, rather than an incremental accretion of very specific and inflexible tools. (Source: http://www.r-project.org) The extRemes Toolkit (extRemes) is designed to facilitate the use of extreme value theory (EVT) in applications oriented toward weather and climate problems that involve extremes, such as the high temperature over a fixed time period. The development of the toolkit is motivated by the continued use of traditional statistical distributions (normal, lognormal, gamma,) in situations where extreme value theory is applicable. The language R was chosen in conjunction with a Tcl/Tk graphical user interface (GUI) as a platform for extRemes to be used.

BIBLIOGRAPHY

[1] K. M. Andreadis, E. A. Clark, A. W. Wood, A. F. Hamlet, and D. P. Lettenmaier, *Twentieth-Century Drought in the Conterminous United States*, Journal of Hydrometeorology (2000)

[2] S. Coles, *An Introduction to Statistical Modeling of Extreme Values*, Springer-Verlag (2001)

[3] A.T. DeGaetano, K. L. Eggeslton and W. W. Knapp, *Daily Evapotranspiration and Soil Moisture Estimates for the Northeastern United States*, Northeast Regional Climate Center, Cornell University, RR 94-1, January (1994)

[4] A. Dai, K. E. Trenberth and Taotao Qian, *A Global Dataset of Palmer Drought Severity Index for 1870–2002: Relationship with Soil Moisture and Effects of Surface Warming*, Journal of Hydrometeorology (2004)

[5] D. R. Easterling, J. L. Evans, P. Ya. Groisman, T. R. Karl, K. E. Kunkel, P. Ambenie, *Observed Variability and Trends in Extreme Climate Events: A Brief Review* Bulletin of the American Meteorological Society (2000)

[6] D. R. Easterling, G. A. Meehl, C. Parmesan, S. A. Changnon, T. R. Karl, L. O. Mearns, *Climate Extremes: Observations, Modeling, and Impacts* Science **289** (2000)

[7] E. Gilleland and R. W. Katz, *New Software to Analyze How Extremes Change Over Time*, EOS Transactions **92(2)** (2011)

[8] P. Ya Groisman and R. W. Knight, *Prolonged Dry Episodes over the Conterminous United States: New Tendencies Emerging during the Last 40 Years*, Journal of Climate (2007)

[9] P. Ya Groisman, R. W. Knight, D. R. Easterling, T. R. Karl, G. C. Hegerl, and V. N. Razuvaev, *Trends in intense precipitation in the climate record*, Journal of Climate **18** (2005), 1326-1350

[10] T. A. Howell and S. R. Evett, *The Penman-Monteith Method*, USDA-Agricultural Research Service, Conservation Production Research Laboratory (2004)

[11] T. R. Karl and R. W. Knight, *Secular trends of precipitation amount, frequency,*

and intensity in the United States, Bulletin of the American Meteorological Society **79** (1998), 1107-1119

[12] R. W. Katz, *Extreme value analysis for climate time series*, Extreme Events in Climate and Weather - An Interdisciplinary Workshop, Banff, Alberta (2010) http://www.isse.ucar.edu/staff/katz/docs/pdf/banffrwk.pdf

[13] D. A. Miller and R. A. White, *A Conterminous United States Multilayer Soil Characteristics Dataset for Regional Climate and Hydrology Modeling* Earth Interactions **2** (1998)

[14] L. A. Richards, W. R. Gardner and G. Ogata, *Physical Processes Determining Water Loss from Soil*, Soil Science Society Proceedings (1995)

[15] R Development Core Team, *R: A Language and Environment for Statistical Computing*, R Foundation for Statistical Computing (2009)

[16] B. Sun and P. Ya Groisman, *Variations in low cloud cover over the United States during the second half of the twentieth*, Journal of Climate **17** (2004), 1883-1888

[17] D. A. Wilhite, *Drought as a natural hazard: Concepts and definitions*, Soil Science Society Proceedings(1995)

[18] C. A. Woodhouse and J. T. Overpeck, *2000 Years of Drought Variability in the Central United States*, Bulletin of the American Meteorological Society **12** (1998)